Waste-to-Resource Preparation of Geopolymers Containing Glass Foams Derived from Hazardous Glass Waste

Ph.D. Dissertation

by
Al-Saudi Sarah Kareem Mohammed
(MSc in Materials Engineering)

Antal Kerpely Doctoral School of Materials Science and Technology

Hungary, Miskolc

2025

Waste-to-Resource Preparation of Geopolymers Containing Glass Foam Derived from Hazardous Glass Waste

A PhD dissertation submitted to Antal Kerpely Doctoral School of Materials Science and Technology for the degree of Doctor of Philosophy in the subject of Materials Science and Technology

by
Al-Saudi Sarah Kareem Mohammed
(MSc in Materials Engineering)

Supervisor:
Dr. Róbert Géber, Associate Professor

Head of the Doctoral School:
Prof. Dr. Valéria Mertinger, DSc.

Institute of Energy-, Ceramics, and Polymer Technology

Faculty of Materials and Chemical Engineering

University of Miskolc

Hungary, 2025

ACKNOWLEDGEMENTS

Al-Saudi Sarah Kareem Mohammed

2025

Supervisor's recommendation

Al-Saudi Sarah Kareem Mohammed started her PhD studies in February 2021, then in a different research topic with a different supervisor. As her supervisor passed away in February 2022, a change of supervisor and research topic was required. This meant that she only had 3 years to complete her new research topic. The process of acquiring knowledge about the new topic, conducting a review of the literature, and developing materials, in addition to conducting standard tests for the material systems produced, was also time-consuming.

Al-Saudi Sarah Kareem Mohammed carried out her research on "***Waste-to-resource preparation of geopolymers containing glass foams derived from hazardous glass waste***". Her experiments involved the production of glass foams from heavy metal-containing glass (*CRT glass*) extracted from electronic waste, using the foaming technique at different temperatures and embedding it in a special binder (*geopolymer*). Geopolymers are novel silicate-based binders that can be used as alternatives to traditional cementitious building materials such as concrete.

The research work involved embedding the glass foams produced as so-called lightweight aggregates in a geopolymer matrix, thus achieving several objectives at the same time. On the one hand, by mixing the two material systems, a structural material (*so-called lightweight geopolymer concrete*) was produced that can be used as a thermally insulating element in the building industry. In this way, the product developed contributes to the construction of low-energy buildings. A significant role of the geopolymer binder is to prevent heavy metals and alkaline earth metals (*mainly lead, barium and their compounds*) in the glass foam from leaching into the environment. By encapsulating these hazardous substances, the disposal of CRT glass in landfills can be reduced. The PhD research investigates both the practical applicability of lightweight geopolymer concrete and the materials science aspects of the interaction between the two material systems (*glass foam-geopolymer*).

The Candidate has consistently demonstrated independence and enthusiasm in her research endeavours. She has presented her research findings at numerous national and international conferences and has also published in scientific journals. In this way, she has fulfilled the publication requirements of the Antal Kerpely Doctoral School of Materials Science and Technology.

As the supervisor of the thesis, I hereby recommend its acceptance and the award of the PhD degree.

Miskolc, 10th April 2025   **Róbert Géber**

Ethical Use of Artificial Intelligence in Dissertation Preparation

 "I declare that during the preparation of the thesis, I did not use the services of artificial intelligence, except for grammatical and stylistic corrections".

Al-Saudi Sarah Kareem Mohammed

List of Abbreviations

2θ	Diffraction Angles
Adj MS	Adjusted Mean Square
Adj SS	Adjusted Sum of Squares
ANOVA	Analysis of variance
ASTM	American Society for Testing and Materials
CRT	Cathode Ray Tubes
CRT-GW	Cathode Ray Tubes Glass Waste
DF	Degrees of Freedom
EN	Europäische Norm (*European standards*)
FGA	Foam Glass Aggregate
FTIR	Fourier Transform Infrared Spectroscopy
GP	Geopolymer
HE	Height Expansion
L/S	Liquid-to-Solid ratio
LWGP	Lightweight Geopolymer
LWGP-FGA	Lightweight Geopolymer with Foam Glass Aggregate
M	Molarity
MK	Metakaolin
MK-GP	Metakaolin-based Geopolymer Binder
OPC	Ordinary Portland Cement
P_0	Apparent Porosity
PSD	Particle Size Distribution
SEM	Scanning Electron Microscope
Seq SS	Sequential Sum of Squares
UCS	Uniaxial Compressive Strength
Vol %	Volume Percentage
VS	Volume Shrinkage
WA	Water Absorption
wt.%	Weight Percentage
XRD	X-Ray Diffraction
XRF	X-Ray Fluorescence spectrometer

List of units

g/cm^3	Gram per Cubic Centimetre
mg/L	Milligram per Liter
MPa	Newton per square millimetre
rpm	Revolutions Per Minute
W/m·K	Watts per meter Kelvin

Table of Contents

List of Figures

List of Tables

Chapter One/Introduction and Literature Review

1.1 Introduction

As regulations to protect the environment become stricter, more and more people are interested in using green and environmentally friendly materials [1, 2]. For the construction of new buildings, the maintenance of buildings, and technical infrastructure, the construction industry requires a significant amount of natural aggregates and cement. However, the extensive use of these natural resources is causing a gradual depletion of the Earth's reserves, potentially leading to environmental degradation. Researchers are dedicated to discovering and developing new environmentally beneficial materials. These materials are either derived from waste materials or created through methods that reduce the emission of polluting gases. Glass waste represents a significant amount of solid waste. According to the EU Action Plan, the recycling rate for glass waste must reach at least 85 % by 2030 [3]. In this respect, producing foam glass represents an excellent opportunity to recycle large amounts of glass waste. It is well known that foam glass, produced by mixing waste glass powder with a foaming agent and then heating the mixture above the softening point of the glass, is used as a thermal and acoustic insulation material in construction and road building. The number of studies on the development of glass foam has increased in the last decade. Researchers investigated the use of glass waste from various sources, such as bottles, cathode-ray tube (CRT), flat glass, etc., for this purpose. According to the United Nations Environment Programme, the cathode ray tube glass waste (CRT-GW) reaches 50 million tons annually [4]. In recent years, cement production has increased extraordinarily worldwide. It is the third-largest contributor to anthropogenic CO_2 (carbon dioxide) emissions. Each one ton of calcium carbonate used in cement production generates 0.44 tons of CO_2. Figure 1. shows the CO_2 emissions of the global cement industry by region from 1990 to 2019 [5,6]. The construction industry will face future challenges in adopting alternative building materials to replace cement. Geopolymers (GPs) are currently being introduced to fully substitute ordinary Portland cement (OPC) in concrete production [6,7]. GP is the name given to this innovative binder material. In terms of the environment, the main advantage of geopolymer is that it can reduce CO_2 emissions into the atmosphere by about 80-90% compared to OPC and lower energy consumption during production [7,8]. GP is an inorganic polymeric material obtained by mixing a dry solid (aluminosilicate) with an alkaline solution and possibly other ingredients [9]. GP exhibits good properties such as chemical resistance, high-

temperature strength, chloride penetration resistance, and freeze-thaw cycle resistance [9,10].
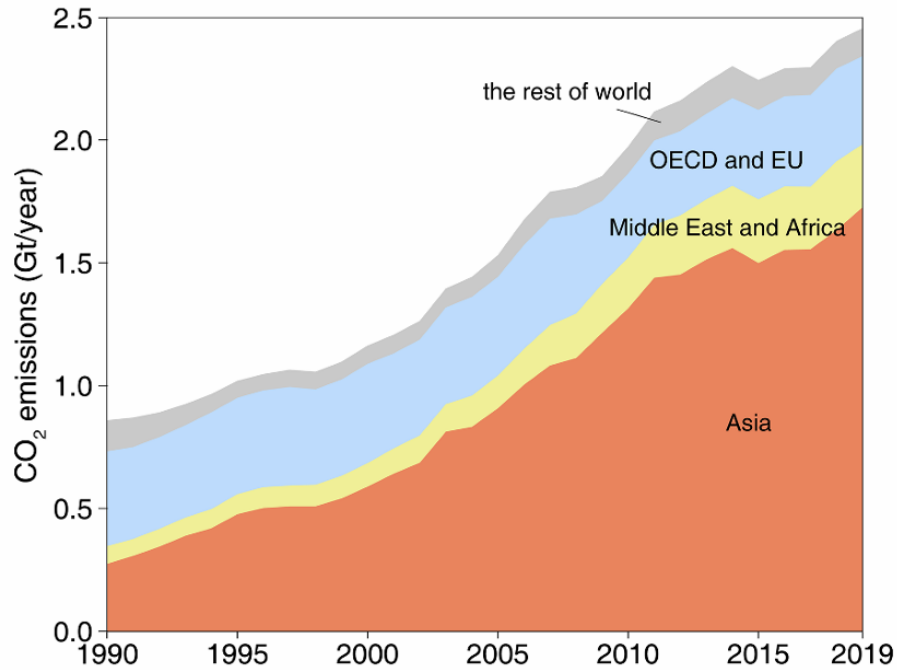
Figure 1. The amount of CO_2 emissions from cement production in different regions for the past three decades (1Gt=10^9 tons) [5]

The construction industry will face future challenges in adopting alternative building materials to replace cement. Geopolymers (GPs) are currently being introduced to fully substitute ordinary Portland cement in concrete production [6,7]. GP is the name given to this innovative binder material. In terms of the environment, the main advantage of geopolymer is that it can reduce CO_2 emissions into the atmosphere by about 80-90% compared to OPC and lower energy consumption during production [7,9]. GP is an inorganic polymeric material obtained by mixing a dry solid (aluminosilicate) with an alkaline solution and possibly other ingredients [8]. GP exhibits good properties such as chemical resistance, high-temperature strength, chloride penetration resistance, and freeze-thaw cycle resistance [9,10].

Energy consumption has become a pressing global issue due to its significant environmental and economic impacts. It has been projected that global energy consumption will increase by 50% by 2050 [11]. Developing countries are expected to account for 80% of this rise in energy demand. Additionally, the building sector is anticipated to consume 40% of the total global energy consumption, as shown in Figure 2. [12].
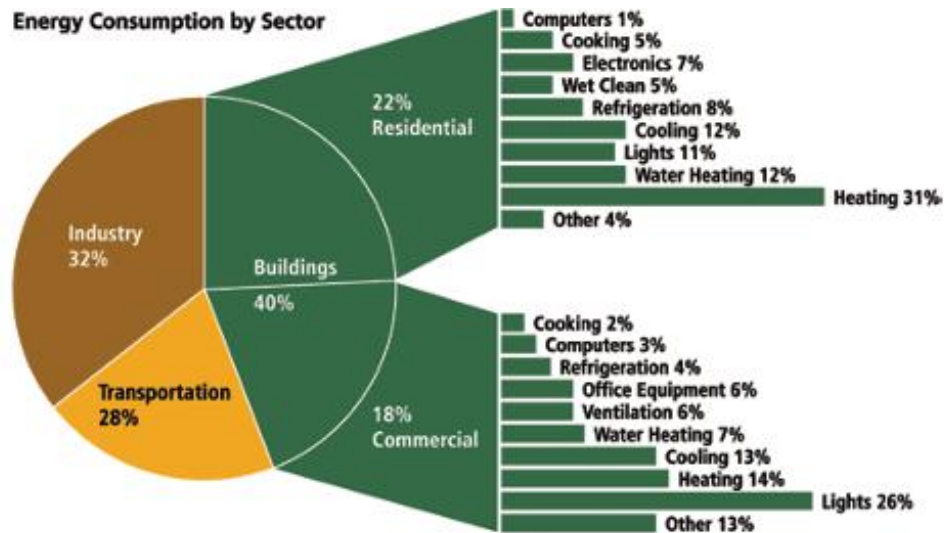
Figure 2. Global energy consumption in different sectors [12]

Lightweight geopolymers (LWGPs) have emerged as a revolutionary class of materials that promise significant advancements in sustainable construction. When formulated as lightweight materials, geopolymers not only reduce the structural weight of buildings but also offer superior thermal insulation and fire resistance [13]. These properties contribute to lower energy consumption in heating and cooling buildings, further amplifying their environmental benefits. When FGA is used as a lightweight aggregate made from glass waste, making lightweight geopolymers will be a key component in the transition towards more sustainable and energy-efficient construction practices.

1.2 Theoretical background and literature overview

Theoretical background and literature concerning the production process and the influencing factors associated with lightweight structures, foam glass aggregates, and geopolymer binders.

1.2.1 Lightweight structure

Lightweight structure, a promising structural material, possesses numerous advantages. These include diminished dead load on structures, enhanced thermal and sound insulation characteristics, ease of handling and transport, and reduced construction expenses. Consequently, it finds diverse applications, such as flooring in steel-framed buildings, parking structures, bridge decks, girders with specified density concrete, lightweight prestressed concrete, etc. [14].

The properties of the lightweight concrete structures have approximately ranges: bulk density of 0.3-2 g/cm³, compressive strength ranging from 1-60 MPa, and thermal

conductivity ranging from 0.2-1.0 W/m·K. These values can be contrasted with normal concrete values, which typically range around 2.1-2.5 g/cm³ for bulk density, 15-100 MPa for compressive strength, and 1.6-1.9 W/m·K for thermal conductivity [15, 16]. Lightweight concretes are classified into three types: 1) No-fines concrete, 2) aerated and foam concrete, and 3) lightweight aggregate concrete, as shown in Figure 3.
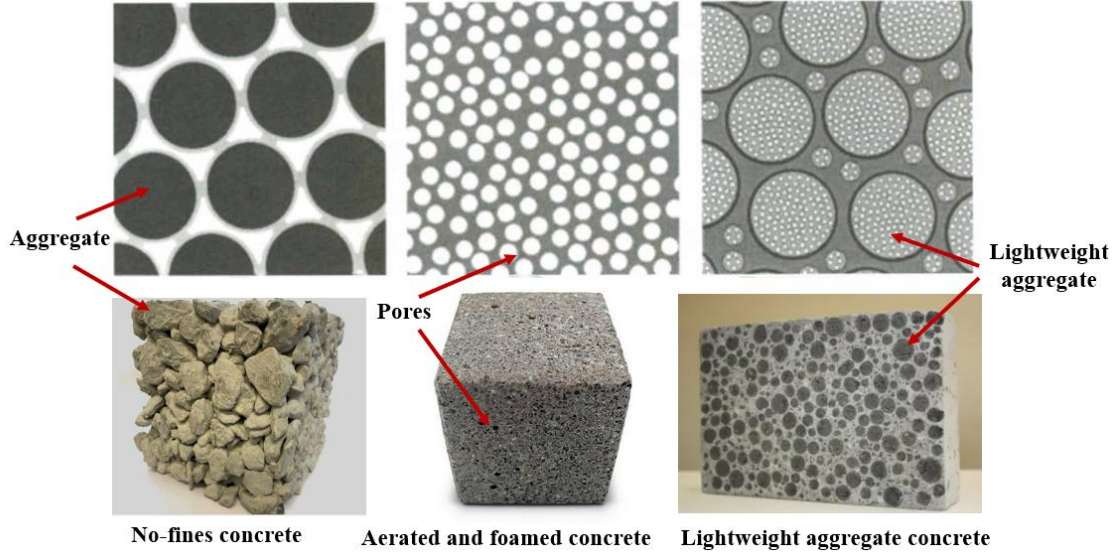
Figure 3. Lightweight concrete types [15] [17]

No-fines concrete structure is made from a coarse aggregate and a small percentage of a cement binder without fine aggregate. The aggregate-to-cement ratio is in the range of 3 to 6, in which each coarse aggregate particle is coated with a cement binder layer with a thickness reaching 1.3 mm. The cement binder bonds the grains together and leaves a void between them. These voids lead to the production of porous, open-textured concrete with decreased density, strength, and shrinkage. The properties of this concrete depend on the aggregate type and size, and the aggregate-to-cement ratios. There are two kinds of aggregate: normal and lightweight aggregate used to get low concrete density [17, 18].

The aggregate size range used in this concrete type is 7 to 75 mm and must contain <10 wt.% of undersized particles but no less than 5 mm. The aggregate should not have sharp edges leading to an increase in the likelihood of crushing under load [18]. In Table 1.**,** a range of common properties of no-fines concrete created with various aggregate types is displayed.

Table 1. Typical properties of no-fines concrete made with different aggregate types [16, 17].

Typical properties	Normal weight aggregate	Lightweight aggregate
Aggregate/cement ratio (% mass)	6-10	3-8
Water/cement ratio (% mass)	0.38-0.45	0.38-0.45
Air dry density (g/cm³)	1.2- 1.9	0.8-1.4
Cube strength (MPa)	20-40	3-7

There are many applications of no-fine aggregate concrete structures, such as pavement construction, underwater construction, rapid construction, refractory applications, green construction, void filling, and lightweight construction [17].

Aerated and foam concrete has a low-density value, reaching 0.4 g/cm^3 due to voids between the cement binder. There are two principal methods for the production: aerating and foaming. The aerating method generated hydrogen gas by adding 0.2 wt.% of aluminium reacted with Ca(OH)$_2$ and alkalis. The gas disperses in the mixture to increase volume and reduce the density. This type of concrete is cured in steam at normal atmospheric pressure or in steam under high pressure at 180 °C inside an autoclave [16]. The foaming method produces pre-formed foam that can be blended with other components. This concrete type possesses a porosity exceeding 25 vol%, with pore diameters ranging from 0.1 to 1 mm [16, 19]. The aerated and foam concrete applications as insulation provide excellent thermal and acoustic insulation for walls, floors, and roofs in both residential and commercial buildings due to their lightweight nature, which reduces structural load and allows for faster construction [19].

Lightweight aggregate concrete is made with a lightweight aggregate, and historical structures created by using this type are shown in Figure 4., from the 3rd millennium B.C. The application was found in ancient Babylon, where natural lightweight aggregates with volcanic origin (such as pumice, scoria, etc.) were utilized. The Greeks and Romans practiced in their construction projects. Many of these impressive ancient structures, like the St. Sophia Cathedral, also called Hagia Sophia, in Istanbul, Turkey, still stand today, and the Pantheon, a Roman temple constructed in A.D. 118. [20].

| Babylon, Iraq | Istanbul, Turkey | Roman |
| Built-in the 3rd millennium B.C | Built-in 4th century | Built- in A.D. 118 |

Figure 4. Historical structures constructed using lightweight aggregate [21].

Lightweight aggregate concretes, utilized in diverse applications based on their properties, are classified into three groups according to ASTM C330 and C332 standards. These classifications, detailed in Table 2., are based on specific properties and intended applications.

Table 2. Classification of the LWC according to ASTM C 330 [21].

LWC groups	Density range (g/cm³)	Compressive strength range (MPa)	Thermal conductivity (W/m·K)
Structural	1.440 to 1.840 (equilibrium)	>17	not specified
Structural/insulating	0.720 to 1.440 (equilibrium)	3.4 to 17	0.45-1.05 (oven-dry)
Insulating	0.240 to 0.800 (oven-dry)	0.7 to 3.4	0.065-0.22 (oven dry)
Equilibrium: Density for LWC after 28-day exposure to the relative humidity of 50 ± 5% and a temperature of 23 ± 2 ℃. *Oven-dry: the density of LWC after being put in an oven (110 ± 5 ℃) for some time engaged to the density change by lower than 0.5% for 24 hours.*			

1.2.2 Lightweight aggregate

Lightweight aggregate is typically described as any aggregate with a bulk density of under 1.2 g/cm³ and a uniaxial compressive strength of more than 1 MPa [10, 11, 22]. The advantages of lightweight aggregates are:

- Reduced weight is their ability to reduce the overall weight of structures.

- Improved insulation can enhance the insulation properties of materials, making them suitable for applications where thermal efficiency is important.

- Ease of handling due to their lower density and light weight.

The use of lightweight aggregates allows for more design flexibility, as architects and engineers can explore innovative and efficient structural solutions [23-25].

Lightweight aggregate is classified into two main categories based on natural and artificial sources: **natural lightweight aggregates** are porous volcanic stones like scoria, pumice, light sand, etc., and **waste natural materials** like oil palm shells.

Figure 5. shows the different types of natural lightweight aggregates [26, 27].

Pumice   Black slag   Oil palm shell

Figure 5. Types of natural lightweight aggregates [26], [27].

Artificial lightweight aggregates are made from clay and industrial waste materials, including glass waste, fly ash, slag, etc. The process of manufacturing lightweight aggregates depends on the types of raw materials. Generally, it includes the following steps: preparing the mixture by adding foaming agents or additives, forming pellets (pelletizing), and sintering by subjecting the pellets to a heating process at high temperatures, causing them to expand and become porous. This process can be carried out in rotary kilns or other types of furnaces, and these pellets to cooled to form the final aggregate product.

Chung et al. [28] used three types of artificial lightweight aggregates: expanded clay, expanded glass, and foamed glass to prepare lightweight concrete. Figure 6. shows the lightweight aggregate samples.

(a) Expanded clay

(b) Expanded glass

(c) Foamed glass
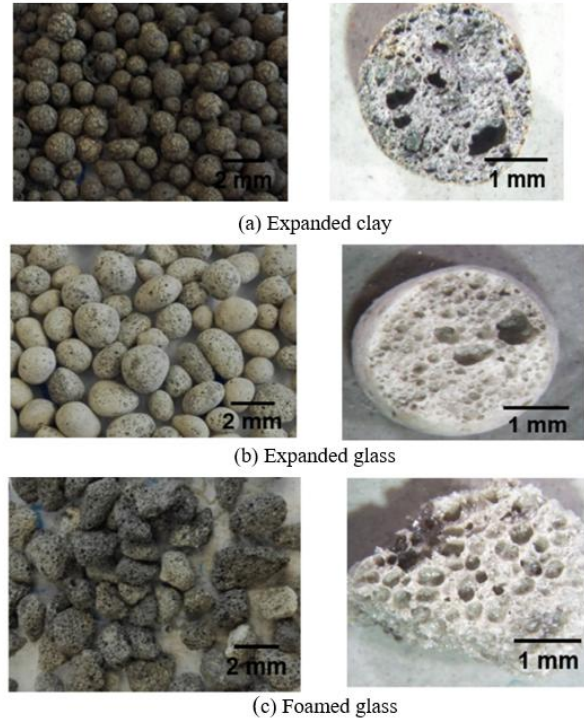
Figure 6. Types of artificial lightweight aggregates [28].

Expanded clay was produced from clay sintering at 1200 °C in a rotary kiln, creating a product with small pores. The expanded glass was made from waste glass sintering at 900 °C in a rotary kiln, the pellets had a smooth surface and closed pores with a shell. The foamed glass was created by heating a mixture of waste powdered glass and a foaming agent to 1000 °C, resulting in a cellular structure in the aggregates.

1.2.3 Foam glass aggregate

Foam glass aggregate (FGA) is produced from over 98 wt.% waste glass and less than 2 wt.% foaming agents, playing an important role in waste management technology. The problem of waste glass involves the difficulty of managing and recycling substantial amounts of discarded glass, which frequently ends up in landfills, contributing to environmental pollution and resource depletion [29]. Recycling waste glass into new glass products is often prohibitively expensive due to high processing costs. However, repurposing waste glass into valuable products like foam glass aggregate offers a more cost-effective and environmentally friendly solution. The advantages of FGA can be utilized in many types of civil engineering

structures, providing thermal insulation and frost protection, reducing vertical and lateral earth pressures, and enhancing slope stability, as shown in Figure 7. [30].

Figure 7. Foam glass aggregate applications: a) insulation of ground-contact slabs, (b) slab insulation during building refurbishment, (c) insulation of intermediate slabs in refurbishments, and (d) base and insulation layer for heated underground garage ramps [30].

Since the 1930s, several patents have been issued for various methods of manufacturing foam glass [32]. The most used method, glass cullet, is introduced into a ball mill for grinding into a fine powder, typically ranging from 100 to 500 μm. This fine glass powder is then combined with a foaming agent and heated to a foaming temperature between 700 – 900 °C, depending on the glass and foaming agent composition [33, 34]. Figure 8. illustrates the process flow diagram for converting waste glass cullet into foam glass.
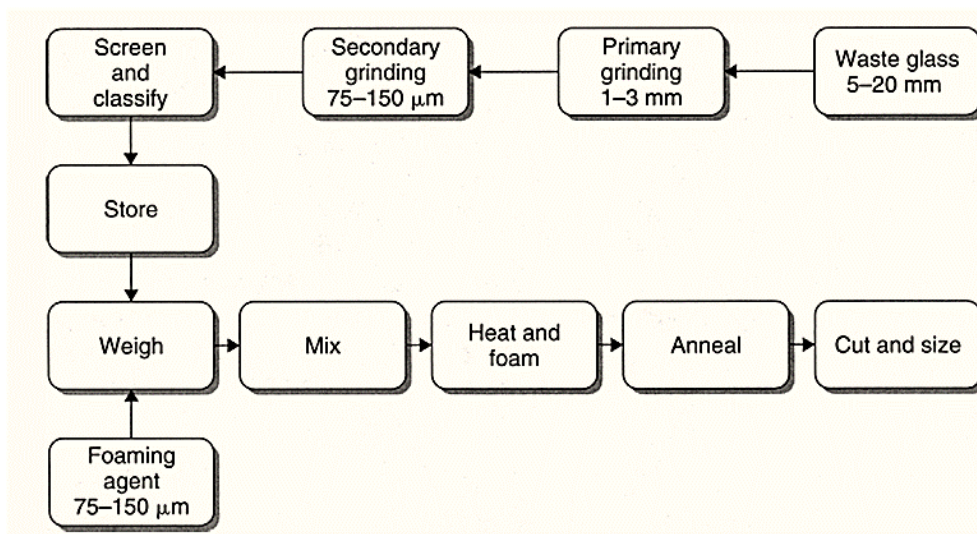
Figure 8. Process flow diagram for the production of foam glass [33].

The principle behind the foam glass production process is that during the heating process the glass powder is softened at a temperature of up to 600 °C, meaning glass transforms into a viscous liquid. During this phase, the foaming agent decomposes or reacts (depending on the type), releasing a gas that forms bubbles within the softened glass. The glass must maintain sufficient viscosity to prevent the gas bubbles from rising and escaping through the liquid mass. This ensures the bubbles remain in place throughout the foaming heat cycle. [11, 35]. Figure 9. shows the foaming mechanism in the foam glass during heating.
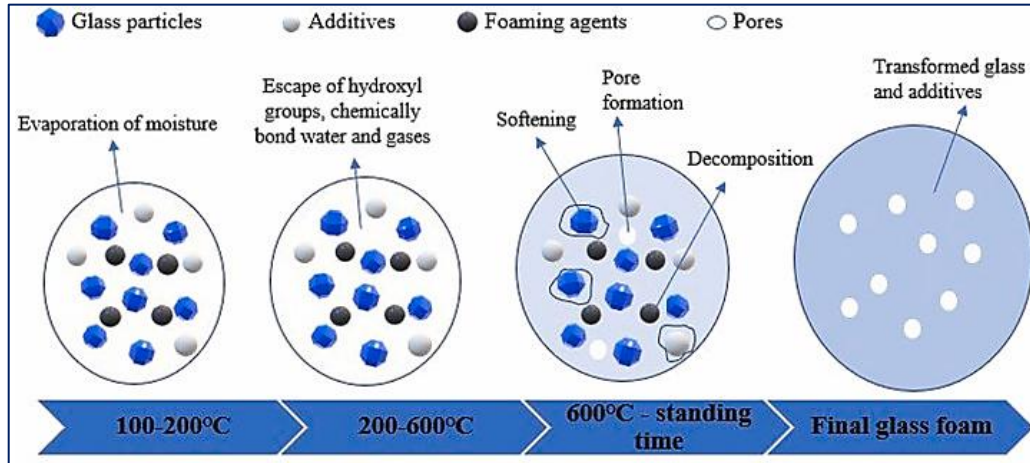
Figure 9. Foaming mechanism during the heating process [36].

Recycling of CRT-GW has received more attention in the recent decade. The CRT has been used to make electronic screens for computers and TVs since the middle of the twentieth century [37]. But recently they have been dispensed with Liquid Crystal Display and plasma display panels [38]. This resulted in the large-scale disposal of CRT monitors, primarily in landfill locations, and this trend is likely to persist in the upcoming decades, giving rise to significant environmental issues [39]. Figure 10. shows that CRT-GW accounts for 42 wt.% of electronic devices such as TVs and computers [40].

Figure 10. CRT-GW from electronic devices [40]

In 2016, the worldwide production of electronic waste was 44.7 million tons, with waste CRTs making up around 6.6 million tons [41, 42]. The CRT monitor is a vacuum tube that generates an image when an electron ray hits a luminous surface. It comprises three main parts: an electron gun, front panel glass, and funnel glass. The front panel, funnel, and neck glass contribute about 65 wt.%, 30 wt.%, and 5 wt.%, respectively. Different chemical compositions are found in the various glass components, each containing different chemical and physical forms of lead [43]. Figure 11. shows the composition of a typical CRT monitor.
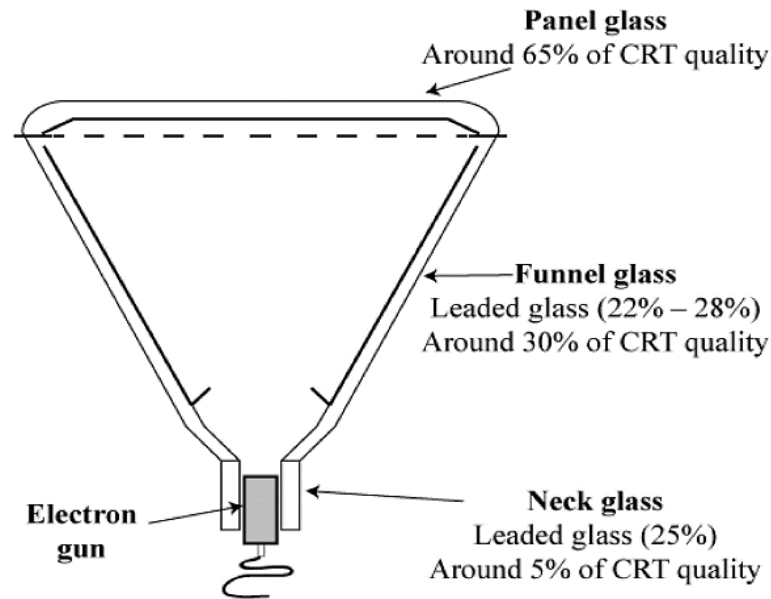
Figure 11. Composition of CRT monitors [43]

CRT glass is a hazardous material because it consists of three heavy metals: lead (Pb), barium (Ba), and strontium (Sr). Previous research has found that CRT-WG contains 21-24 wt.% of lead oxide, 9-13 wt.% of barium oxide, and 1-2 wt.% of strontium oxide [44-46]. As a result of these heavy metals, many research teams have investigated methods for recycling CRT glass to ensure a green environment, such as purifying techniques for eliminating Pb, using it as aggregate in the concrete to encapsulate glass particles, and the production of new materials like foam glass [47-49].

Numerous researchers have investigated foam glasses by the study of the influencing factors on properties such as type and dosages of foaming agent, foaming temperature, and rate of temperature [50]. Petersen et al. [51] used the following: the made-of-foam glass involved the CRT waste glass with varying proportions (2, 6, 10, 14, 18, 22 wt.%) of Na_2CO_3 as a foaming agent, followed by sintering at numerous temperatures 699.85 °C, 749.85 °C, 799.85 °C, 849.85 °C, and 899.85 °C. The lowest bulk density of 0.28 g/cm^3 was obtained by foaming glass powder with 14 wt.% Na_2CO_3 at 749.85 °C.

König et al. [52] investigated the impact of foaming temperatures on foam glass derived from CRT panel glass, using carbon and MnO_2 as foaming agents. The findings indicated that while carbon alone provided a moderate foaming effect, adding MnO_2 significantly enhanced this effect. The foaming process was highly dependent on temperature variations, with the optimal foaming temperature identified as 800 °C. Figure 12. shows the effect of the foaming temperature on foam glass.
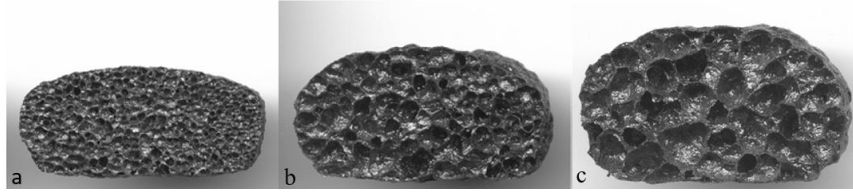
Figure 12. Foam glass samples prepared from CRT glass at different foaming temperatures (a) 780 °C, (b) 800 °C, and 820 °C [52].

Silicon carbide works as a foaming agent at an unspecified temperature range due to its crystalline structure having a high melting point of 2700 °C [53]. Osfouri and Simon [54] found that when 1 wt.% SiC was used as a foaming agent with soda-lime silicate glass, the reaction started at 800 °C and gave the maximum foaming height at a temperature of 986 °C. Guo et al. [55] prepared foam glass using 1 wt.% of SiC with CRT glass containing lead oxide. They noted the reaction commenced at a temperature of 600 °C, during which carbon dioxide (CO_2) is liberated according to the following chemical equation:

$$4PbO(s) + SiC\ (s) ® Pb(s) + SiO_2(s) + CO_2\ (g) \qquad (1)$$
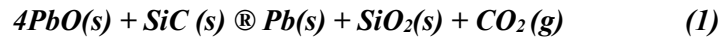
Due to the CRT-WG having high lead oxide content, the leaching test for lead is indispensable to save environmental harm. Several investigations have attempted to investigate the effects of various conditions in the foam glass production on the degree of lead leaching. Specifically, the effects of the types of foaming agents: redox agents and neutralization agents [56]. The neutralization agents generate a foaming effect by thermal decomposition and release gas, such as $CaCO_3$. Usually, the production of foam glass with weak strength and heightened water absorption properties makes it a preferred choice for insulation applications. While the redox agents initiate a foaming phenomenon during intricate chemical reactions, releasing gases directly results from the oxidation reaction triggered by the foaming agents, such as SiC and TiN. The foam glass produced by this agent type has good strength and closed porosity [57]. However, the researchers do not prefer using redox foaming agents of lead silicate glass because they may react with PbO to produce lead heavy metal [57]. Some investigations have been performed to use redox agents with CRT glass for producing foam glass [58, 59]. These two works studied the effects of two types of

foam agents (SiC and TiN) on lead leaching levels when preparing CRT foam glass. The impact of the reducing agent became apparent as the leached concentration of Pb increased; the findings revealed that samples produced with lower concentrations of the reducing agent had lower lead leaching, especially those synthesized using SiC, which remained within regulatory limits for the amounts of Pb released. Conversely, when TiN was utilized, the highest levels of Pb were released over the standard limits.

1.2.4 Geopolymer

The term 'geopolymer' was introduced in the 1970s by French scientist and engineer Professor Davidovits. It refers to a class of solid materials created through the chemical reaction between an aluminosilicate powder and an alkaline solution. Geopolymers are inorganic materials with a polymeric molecular structure, offering exceptional strength and a variety of unique properties [60, 61]. Geopolymer binder is an environmentally superior alternative to OPC for several reasons. It is produced at lower temperatures, significantly reducing greenhouse gas emissions. Additionally, geopolymers provide excellent thermal insulation, further enhancing their environmental friendliness [62, 63]. Figure 13. shows an increased number of scientific papers interested in geopolymers [64].
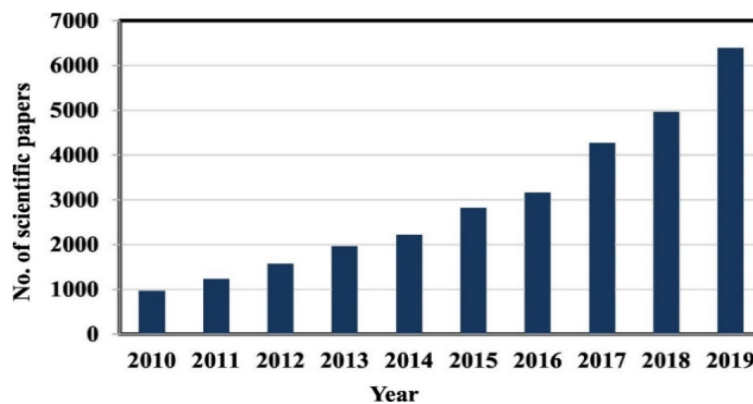
Figure 13. A graphical representation of published data on geopolymers from 2010 to 2019 based on their economic benefits and energy consumption [64].

Figure 14. illustrates the various ingredients and production processes for geopolymers. The synthesis can occur through either an alkaline medium, consisting of hydroxides and silicates, or an acidic medium, such as phosphoric acid. These media react with an aluminosilicate precursor, initiating the polymerization process. The aluminosilicate precursor can be naturally occurring, like kaolinite, or an industrial by-product, such as fly ash [65, 66].
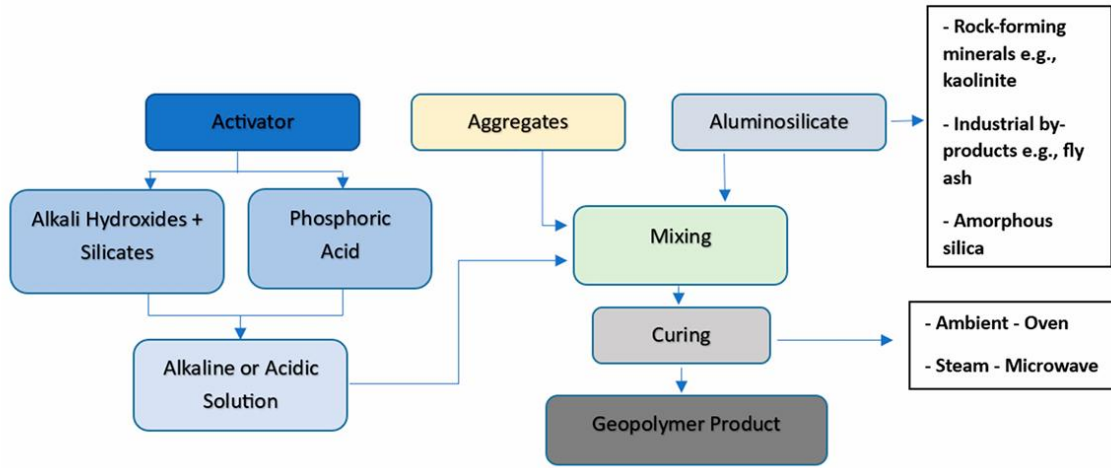
Figure 14. A summary of the geopolymer production process [66].

The structure of geopolymers is composed of a polymeric framework that includes silicon, oxygen, and aluminium. This framework forms a three-dimensional network of SiO_4 and AlO_4 tetrahedra interconnected at their oxygen corners. Within this network, metal cations such as sodium and potassium are found, depending on the following formula [67]:

$$M_n\{-(SiO_2)_z - AlO_2\}_n \cdot aH_2O \qquad (2)$$

Where**: M^+** means alkali cation of K^+, Na^+; **n** means the degree of polymerization; **z** means Si/Al ratio in the range of 1 to 3, and **a** means the molar amount of water [67]. The properties of the geopolymer depend strongly on the value of z. At a high value of z (z>3), geopolymers exhibit sticky and rubbery properties and their structure is a linear 2-D network; at a low value of z (z≤3), the material exhibits stiff and brittle properties and a cross-linked 3-D network. As shown in Table 3., the types of polysialates have different z values [68].

Table 3. Types of polysialates [68].

Poly(sialate) -Si-O-Al-O-	Poly(sialate-siloxo) -Si-O-Al-O-SI-O-	Poly(sialate-disiloxo) -Si-O-Al-O-Si-O-Si-O-	Poly(sialate-disiloxo) -Si-O-Al-O-Si-O-Si-O-	Sialate link
Si:Al = 1	Si:Al = 2	Si:Al = 3	Si:Al = 3	Si:Al > 3

Geopolymers are utilized in various applications due to their versatile properties. They are prominent in the production of fire-resistant materials and innovative ceramics. They are effective alternatives to asbestos, offering safe and durable building materials. Geopolymers also play a critical role in stabilizing hazardous waste, providing a secure method for waste

containment. Additionally, they are used as adsorbent materials in water treatment processes, enhancing the removal of contaminants and improving water quality [69].

Cement and concrete are foundational to infrastructural development and modern civilization. Geopolymers, in turn, represent a cutting-edge approach to constructing infrastructure within various geographical regions, it was applied as shown in Figure 15.

Figure 15. Australia's Global Change Institute Building at the University of Queensland [66].

The University of Queensland's Global Change Institute Building in Australia was constructed using fly ash-based geopolymer concrete. It was built in 2013. The building features 33 precast floor beams, each spanning 11 meters, forming three suspended floors with a total volume of approximately 320 cubic meters of geopolymer concrete [66]. In South Africa, a concrete slab at the City Deep container terminal was constructed using fly ash-slag geopolymer concrete, which reached an impressive compressive strength of 51 MPa within 28 days [66].

Geopolymerization is a multifaceted exothermic process involving multiple stages of dissolution, reorientation, and solidification reactions. During geopolymerization, chemical reactions occur under highly alkaline conditions with aluminosilicate minerals, resulting in a three-dimensional polymer network of Si-O-Al-O bonds. Typically, solutions of sodium hydroxide or potassium hydroxide, along with their corresponding silicates, are used as the alkaline activators. The inclusion of silicates in the alkaline solution accelerates the polymerization process [70]. The process of geopolymer formation may be summarized in Figure 16. as the following steps:
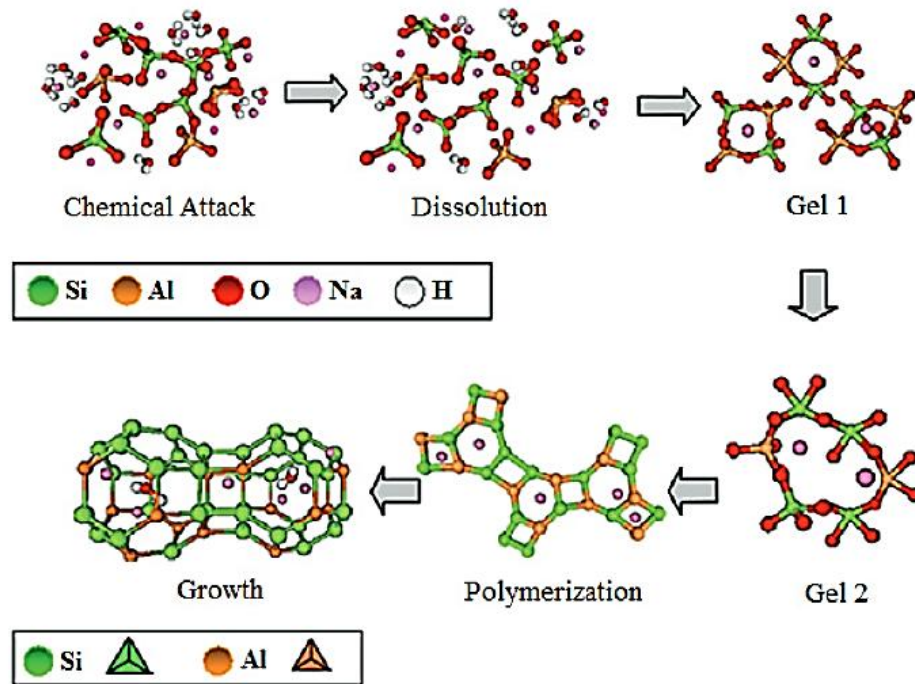
Figure 16. Geopolymerization mechanism [71, 72].

1. An alkaline reaction on the structure of the raw materials leads to the reduction of silicates and aluminates in the solution.

2. The activator solution first supplies silicate; the small, dissolved parts interact with it, and aluminosilicate oligomers (Gel 1) are formed.

3. The silicate solution becomes unstable as the dissolution process continues, and the gel-forming (Gel 2) precipitation of dissolved species begins when the concentration of dissolved aluminate reaches a certain point.

4. The geopolymer gel develops as the slurry becomes solid. The mix composition, temperature, and presence of pollutants determine the curing time, which can range from a few minutes to many days. Persistent strength development evidence that reaction processes persist long after the setting [73].

1.2.5 Metakaolin-based geopolymer

The raw materials used in geopolymers are derived from diverse sources, such as natural aluminosilicate-rich materials like kaolin and industrial by-products like fly ash and slag. Metakaolin (MK), derived from kaolin, will be expected as a major resource for the geopolymer binder due to its main contents of SiO_2 and Al_2O_3. Its excellent chemical stability compared with other waste materials due to technical challenges associated with controlling their supply, which have led to a decline in the use of geopolymers in many countries [74, 75]. For metakaolin-based geopolymers, the final setting time is

approximately 20 hours at room temperature, which is significantly faster compared to fly ash, which requires more than a day to set under ambient conditions [76].

Metakaolin is typically produced by calcining kaolin at temperatures ranging from 650 °C to 750 °C. In kaolin, silica and alumina alternate in tetrahedral or octahedral coordination, forming a phyllosilicate mineral with a layered structure. This layered structure, characteristic of clay minerals, gives rise to small particle size and plate-like morphology. The particles possess properties like softness, a soapy feel, and easy cleavage due to their ability to slide over one another. The primary component of kaolin is $Al_2SiO_5(OH)_4$, known as kaolinite, a hydrated aluminum disilicate. Other minerals are also present in kaolin, including quartz, muscovite-like mica, and rutile. When kaolin is heated between 650 °C and 900 °C, it undergoes dehydroxylation, resulting in a 14% mass loss from the bound hydroxyl ions. This process, called calcination, causes the structure of kaolin to break down, leading to the contraction and loss of long-range order in the alumina and silica layers. The outcome is metakaolinite, an amorphous, highly reactive transition-phase material with pozzolanic and latent hydraulic reactivity, making it suitable for cement applications [77]. At 650 °C, the transformation of kaolinite into metakaolinite is completed, as evidenced by the absence of recognizable reflections except for traces of anatase, a minor impurity originating from the original kaolinite. This indicates the complete conversion of kaolinite into amorphous metakaolin after dehydroxylation. Other studies utilizing thermal activation have reported similar observations.

Figure 17. displays scanning electron microscope (SEM) images of kaolinite and metakaolin following calcination at 650 °C. Both samples exhibit platelet-like structures. However, the transformation of metakaolin is evident from the rounded appearance and the removal of the platelet edges compared to solid kaolinite [78].
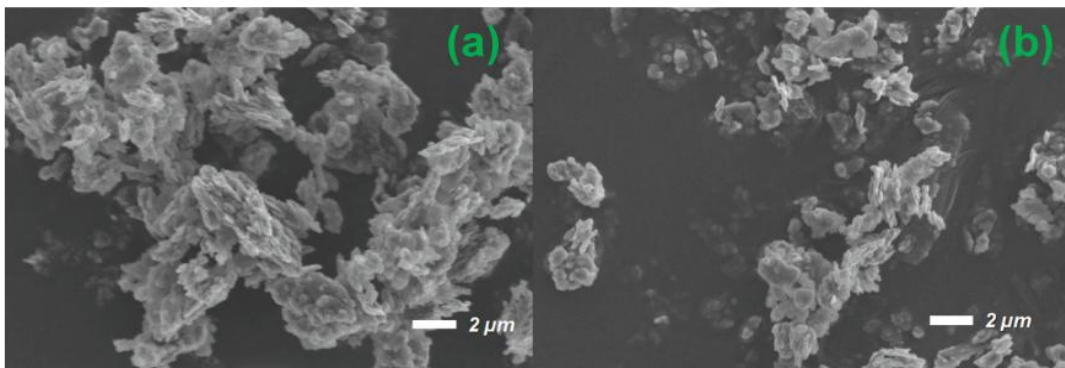
Figure 17. SEM images of (a) kaolinite and (b) metakaolin after calcinations at 650 °C [78].

Many different factors influence the geopolymerization reaction on metakaolin-based geopolymers, such as MK composition, activator type and dosage, and reaction conditions. The composition of MK is used to produce geopolymer made from kaolin, which is mined in deposits. The kaolin formation conditions of these clays vary, resulting in variations in chemical and mineralogical composition [79]. The control of the rheological properties of the fresh mixture and the characterization of the cured geopolymer binder always depend strongly on the type and dosage of the activator [80]. Sodium or potassium hydroxide (NaOH, KOH) in combination with sodium silicate ($n \cdot SiO_2 \cdot Na_2O$) or potassium silicate ($n \cdot SiO_2 \cdot K_2O$) are the most common alkaline liquid activators [80, 81]. Sodium hydroxide solution concentrations range from 8 M to 16 M, and mechanical strength decreases if you use NaOH solutions with concentrations outside this range. An alkaline activator provides better strength than an activator using only NaOH solution or water glass. The water glass promotes polymerization, resulting in a reaction is a higher silicon content and better mechanical properties [82-84].

1.2.6 Factors Affecting Geopolymers Characterization

Geopolymer characterization is influenced by several factors, which can be summarized as follows [85]:

1. **Aluminosilicate source:** The selection and characteristics of the aluminosilicate source used in geopolymers can impact their strength. The presence of amorphous or reactive phases in the source material is desirable as they contribute to the formation of a strong geopolymer network.

2. **Activator concentration:** The concentration of the alkaline activator solution affects the geopolymerization reaction. Higher concentrations can accelerate the reaction, leading to faster strength development. However, excessively high concentrations may also result in excessive heat generation and shrinkage, which can affect the overall strength and durability.

   Chen et al. [86] investigated the impact of varying NaOH concentrations (6 M, 10 M, and 14 M) on the strength and shrinkage of metakaolin-based geopolymer. Their findings reveal that a lower NaOH concentration of 6 M results in reduced shrinkage, while the maximum compressive strength is achieved at a concentration of 10 M.

3. **Curing conditions:** temperature and humidity, significantly influence the strength development of geopolymers. Curing temperatures typically range from room temperature, around 25 °C, to higher temperatures up to 90 °C, depending on the specific

geopolymer formulation and desired properties. The choice of curing temperature is crucial as it affects the rate of chemical reactions and the overall performance of the geopolymer after curing. Adequate curing time is also important to allow sufficient chemical reactions and the development of a well-formed geopolymer structure.

Lopes et al. [87] recommended that to prevent a reduction in the strength of metakaolin-based geopolymers, it is recommended to use curing temperatures below 30 °C. Samples cured at 50 °C show a decrease of over 35% in flexural strength and more than 60% in compressive strength compared to those cured at room temperature.

Some articles suggest that the curing temperature for geopolymers should not exceed 60 °C. This is especially true when testing geopolymer binders using 50 mm cubic specimens because these small binder samples have a higher surface area-to-volume ratio than large concrete specimens, making them more susceptible to curing with heat and leading to higher moisture loss. Moisture must be present for geopolymers to react and become harder [88-90].

4. **Sodium silicate (water glass) to sodium hydroxide ratio:** This ratio is essential for the properties of geopolymer binders to improve performance. By adjusting this ratio, manufacturers can optimize the binder for various construction and industrial applications. Al Bakri et al. [91] studied the effect of water glass/sodium hydroxide ratios of 0.6, 0.8, 1.0, 1.2, and 1.4 on fly ash-based geopolymer. The maximum compressive strength achieved was 8.3 MPa with a water glass/sodium hydroxide ratio of 1. Duxson et al. [92] investigated the influence of the Si/Al ratio on the development of the mechanical strength of MK-GP with different alkali types of sodium hydroxide and potassium hydroxide. They found that the compressive strength of geopolymers increased after 28 days in the Si/Al range between 1.15 and 1.90. They found that when the Si/Al ratio exceeds 1.90, a sharp reduction in the compressive strength of the samples is observed.

5. **Liquid-to-solid ratio (L/S):** This ratio in geopolymer mixtures affects workability, setting time, and strength development. Generally, a lower L/S ratio leads to higher strength due to a more compact and less porous structure. However, excessively low ratios can result in poor workability and difficulty in mixing.

Jaya et al. [93] investigated the impact of various L/S ratios, specifically 1.66, 1.42, 1.25, 1.11, and 1.0, on the properties of metakaolin-based geopolymers. The study used a $NaOH/Na_2SiO_3$ ratio of 1 and a 10 M NaOH solution. After ageing the samples for 28 days, it was found that the optimal compressive strength of 32 MPa was achieved with a

(L/S) ratio of 0.8. Figure 18. shows the microstructure of a metakaolin-based geopolymer with different L/S ratios.
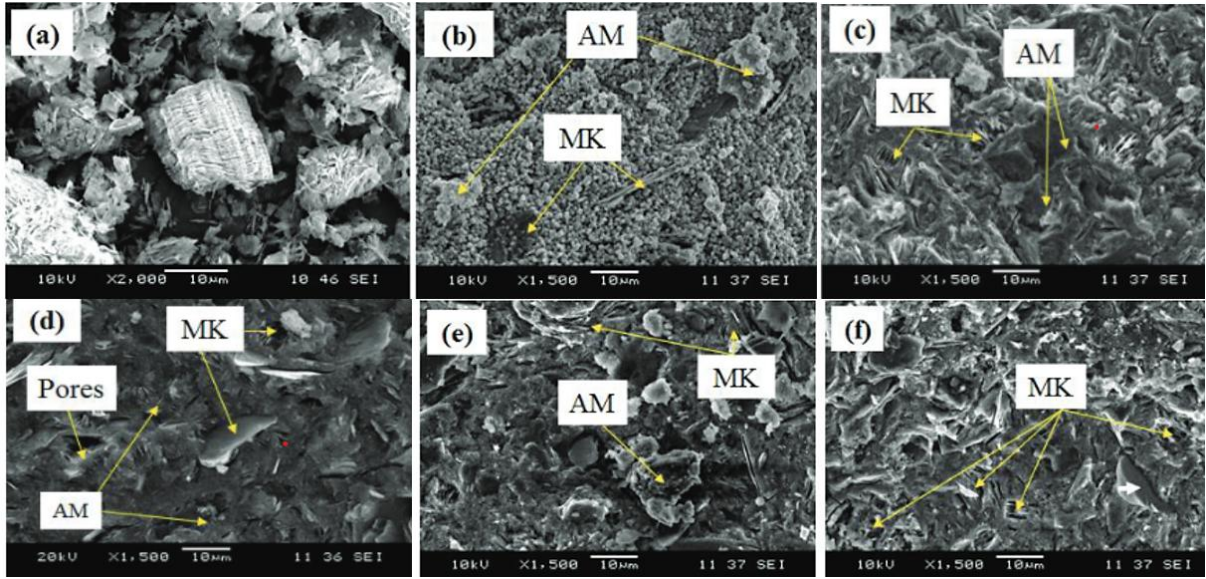
Figure 18. Microstructure of geopolymer-based metakaolin with different L/S ratios (a) 1.66, (b) 1.42, (c) 1.25 (d) 1.11 (e) and (f) 1.0 (MK: unreacted metakaolin, and AM: activated materials) [93]

The activator solution caused alterations on the periphery and surface of the plate-like particles of metakaolin. The appearance of globular units signifies the development of a geopolymer matrix. A higher water concentration helps the alkaline ions to mobilize during mixing, but it also makes the solidified gel microstructure more contractile, crackly, and porous, noticeable in geopolymer binders with L/S ratios of 1.66 and 1.42. In the sample with an L/S ratio of 1.25, the structure became compact and uniform, and the unreacted metakaolin particles became smaller; high strength was achieved. The geopolymer matrix L/S ratio of 1.11 and 1.0 geopolymer matrix appeared rough, the decreased compressive strength was caused by this.

1.2.7 Lightweight geopolymer concrete

Lightweight geopolymer concrete (LWGPC), a special type of concrete, is lighter than conventional concrete. Its reduced density makes it easier to handle and transport during construction, thereby enhancing environmental sustainability. This represents a significant advancement in sustainable building materials, offering a combination of light weight [13, 94]. Numerous studies have explored using lightweight aggregates in geopolymer concrete, including foam glass aggregate, expanded clay aggregate, and natural lightweight aggregates like pumice and volcanic aggregate [95]. Table 4. summarizes various research studies on lightweight geopolymers utilizing lightweight aggregates.

Table 4. Previous studies on the preparation of LWGP using lightweight aggregates.

Author (s)/ year	Year	Based on raw materials	Lightweight aggregate	Curing temperature	Experiments
This work	2024	Metakaolin	Foam glass derived from CRT glass waste	75 °C, 60 °C for 24 hrs and room temperature	Bulk density, compressive strength, thermal conductivity, freezing-thaw cycles test and SEM
A. Niş and Al-Anta [96]	2022	Fly ash, slag, and cement	Volcanic pumice	Room temperature	Visual inspection, weight change, and compressive strength fluctuations caused by sulfuric acid attack.
K. Kalinowska et al. [97]	2022	fly ash and slag	Artificial	65 °C for 24 hrs	Compressive strength, water absorption, dry and saturated density, and thermal conductivity index
B. A. Tayeh et al. [98]	2021	fly ash and furnace slag	Pumice and expanded clay	80 °C for 24 hrs	Flexural and compressive strengths, slump flow, and unit weight.
F. Kristály et al. [99]	2020	Fly ash	Foam glass derived from bottle glass waste	60 °C for 6 hrs	Density, compressive strength, Young's modulus, FTIR, and SEM
M. Saridemir et al. [100]	2020	Blast furnace slag and fly	Basaltic pumice	80 °C for 48 hrs	Bulk density, compressive strength, flexural strength, splitting tensile test, SEM, and exposure tests included sulfuric acid and temperature.
M. Priyanka et al. [101]	2020	Fly ash	Expanded Clay	Room temperature	Bulk density, compressive strength, and workability
F. Aslani et al. [102]	2020	Blast furnace slag and fly ash	Polystyrene and crumb rubber	Room temperature	Slump flow, bulk density, flexural strength, and compressive strength.
S. Top et al. [103]	2018	Fly ash	basaltic pumice	70 °C for 24 hrs	Bulk density, Compressive strength, sonic speed, water absorption, SEM, and Statistical analysis
W. Abbas et al.[104]	2018	Fly ash	Artificial lightweight	60 °C, 80 °C, 90 °C for 48 hrs	Slump test, Ultrasonic Pulse Velocity, dry density, water absorption, thermal conductivity, and strength tests included compressive, flexural, and splitting
S.N. Sarmin et al. [105]	2018	Fly ash and metakaolin	Wood	60 °C for 24 hrs and room temperature	Bulk density, SEM, water absorption, and compressive strength.
B.M.A Huiskes et al. [106]	2015	fly ash and blast furnace slag	Foam glass	Room temperature	Bulk density, water penetration, compressive strength, water absorption, and thermal conductivity.
M.Y.J Liu et al. [107]	2013	fly ash and palm oil fuel ash	Oil palm shell, brick, and block.	65°C for 48 hrs	Thermal conductivity, transport properties, density, ultrasonic pulse velocity test, compressive strength, tensile strength, and modulus of elasticity, porosity.
H. Shu-guan et al. [108]	2009	Metakaolin	Shale haydite	Room temperature	Compressive strength, heat-resistance measurement and SEM.

1.3 Knowledge gap and objectives of the research

1.3.1 Knowledge gap

The knowledge gaps for this research are categorized into three parts based on the experimental plan: the preparation of foam glass aggregates, the development of metakaolin-based geopolymer, and the preparation of lightweight geopolymer. Each part was designed depending on the scientific gap and to enhance it.

- **Knowledge gaps for prepared foam glass aggregate**

  1. Many researchers used CRT-GW to prepare foam glass used in different applications. In contrast, this work is the first investigation to apply foam glass prepared from CRT-GW as a lightweight aggregate in a geopolymer matrix.

  2. Based on the literature, foam glass derived from CRT-GW was synthesized using various foaming agents, yet the temperature range for the foaming process remained unspecified. In this study, silicon carbide (SiC) was employed as the foaming agent, and the temperature range required for the foaming process was determined by inspecting the mixture by heating microscopy.

  3. Some researchers focused on leaching tests to check if the foam glass made from CRT-GW is safer, while others focused on measuring physical and mechanical properties. The knowledge gap in this work is to study the effects of foaming temperatures on all physical, mechanical, and thermal properties and the leaching test for hazardous elements.

- **Knowledge gaps for the development of metakaolin-based geopolymer**

  1. The effect of a wide range of 0 to 100 wt.% water glass in the activator solution for metakaolin-based geopolymer on the occurrence of efflorescence and the change in composition, microstructure, bulk density, volume shrinkage, the average value of compressive strength of and thermal conductivity is studied.

  2. Many researchers aim to prepare geopolymer binders that harden (set) at room temperature and have a suitable setting time by using various additives. In this work, I have focused on controlling the factors that affect the properties of geopolymer binders to achieve this goal, including the water glass/sodium hydroxide ratio and the solid-to-liquid ratio.

- **Knowledge gaps for the preparation of lightweight geopolymer**

  As far as it concerns using foam glass aggregate with geopolymer binder, one scientific paper, by Kristaly et al. [99], used foam glass aggregate made from bottle

waste with fly ash-based geopolymer. In this new work, I used foam glass aggregate driven from CRT-GW with metakaolin-based geopolymer.

1.3.2 Objectives

The main objectives of this work are:

- To produce CRT-GW glass foams ("*lightweight aggregates*") with optimized foaming temperature to decrease energy consumption.

- To encapsulate the CRT lightweight aggregates (*LWAs*) into a metakaolin (MK)-based geopolymer matrix to produce a new, environmentally friendly lightweight building material (*lightweight geopolymer concrete, LWGPC*) by eliminating the hazardous glass waste.

- To optimize the curing conditions of the LWGPC to save energy.

  Investigate the effect of LWA in the geopolymer matrix by physical, mechanical, thermal, and microstructural tests.

Chapter Two/ Materials and Methods

2.1 Main raw materials

The raw materials were used to produce foam glass aggregate:

- Cathode ray tube glass waste was taken from dismantling old televisions and computer monitors. Mishandling CRT waste can lead to the release of toxic substances into the environment, making it essential to manage these materials with care.

- Silicon carbide as a foaming agent, provided by Ibiden Hungary Ltd.

- Methylcellulose – A chemical compound derived from cellulose was used as a binder by dissolving 0.5 g of methylcellulose in 50 ml of distilled water, as shown in Figure 19.

Methylcellulose (0.5 g)   **Distilled water (50 ml)**   **Binder solution**
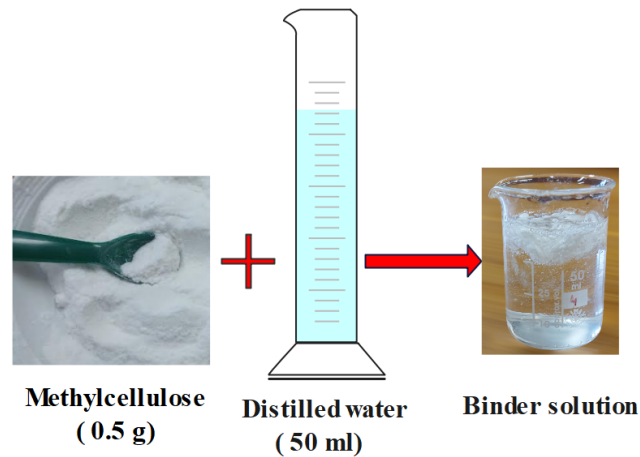
Figure 19. Preparation of binder solution

The raw materials were used to prepare the geopolymer binder:

- Kaolin is a white mineral clay primarily composed of the mineral kaolinite. It is a soft, earthy material, it was supplied by Interkeram Ltd in Hungary.

- Water glass, also known as sodium silicate (Na_2SiO_3), is a chemical compound made from sodium oxide (Na_2O) and silicon dioxide (SiO_2). It is a viscous liquid (solution).

Table 5. contains the physical and chemical properties of water glass.

Table 5. Water glass properties

Name	Sodium silicate
Formula	Na_2SiO_3
State of matter	liquid
Density	1.37 g/cm^3
Silicate modulus (the molar ratio of SiO_2 to Na_2O)	3.80
Chemical composition	H_2O: 61.06 wt.%, SiO_2: 30.95 wt.%, and Na_2O: 8.00 wt.%

- A 10 M sodium hydroxide solution was prepared by dissolving NaOH flakes (purity: 98%) in distilled water, as shown in Figure 20.

23
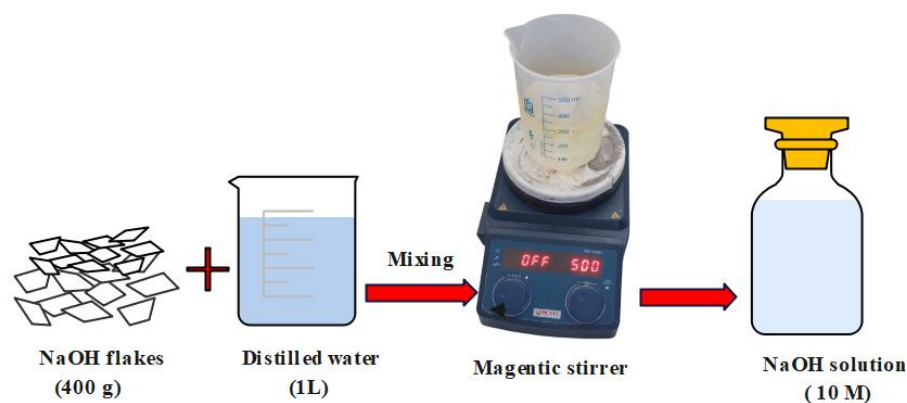
Figure 20. Preparation of NaOH solution

2.2 Characterisation of raw materials

2.2.1 Characterisation of raw materials for preparing FGA: CRT glass and SiC

CRT glass has different chemical compositions depending on the origin of the monitors supplied from various production sources. Table 6. shows the chemical composition measured by a Rigaku SuperMini 200 tabletop X-ray fluorescence spectrometer. The results show that silica is the main oxide (55.9 wt.%), and other oxides are in different percentages. Regarding the oxides contributing to the presence of hazardous elements, the CRT-GW contains 13.36 wt.% of lead oxide and 10.2 wt.% of barium oxide.

Table 6. Chemical composition of CRT glass waste

Oxides	SiO_2	Na_2O	K_2O	CaO	MgO	Al_2O_3	Fe_2O_3	BaO	PbO	SrO	Others	Total
Weight (%)	55.9	5.96	5.49	0.52	0.21	1.7	0.205	10.2	13.36	1.51	5.125	100

The particle size distribution (PSD) of raw materials is an important factor affecting the pore size in foam glass. The particle size was measured by CILAS Granulometre 715 instrument. Distilled water was used as the dispersion medium, and a few grams of powder were added to form a suspension. The laser determined the size distribution of the solid particles using an analysis of the diameters of the particles. The particle size was measured as the suspension flowed between two parallel glass plates. The median particle size (d_{50}) of CRT glass was 11 μm, as highlighted by the red line as shown in Figure 21. The particle size for SiC powder was so fine that it was under the measurement range (d<1 μm). This extreme fineness suggests a high surface area, potentially impacting the foaming behaviour and final pore morphology of the foam glass.
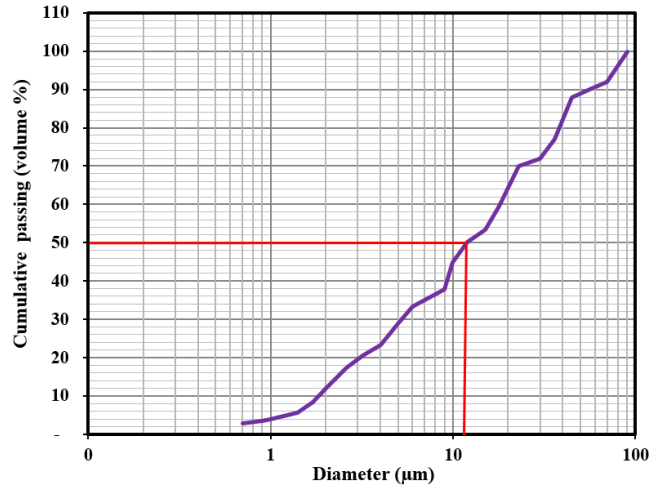
Figure 21. Particle size distribution of CRT glass waste

The phase composition of solid raw materials was investigated using the Rigaku Miniflex II X-ray diffractometer. The samples were examined across a wide range of diffraction angles (2θ) from 5° to 90° using CuKα radiation with a wavelength of 1.54184 Å. The equipment operated at 40 kV and 25 mA. The scan rate was 1°/min with a step size of 0.0101°. X-ray diffraction (XRD) patterns were compared to the Powder Diffraction File database provided by the International Centre for Diffraction Data using X'Pert HighScore Plus software to determine the various phases included in the samples. Figure 22. shows the X-ray spectra of the raw materials, SiC powder, with all peaks indicating the presence of pure silicon carbide in the Moissanite-6h crystal structure. The 6 means the stacking sequence repeats every 6 layers, and H means hexagonal symmetry. The CRT glass waste powder exhibited an amorphous structure, as evidenced by the absence of any peaks in its structure. The absence of peaks indicates a lack of crystalline arrangement, highlighting the glass powder's disordered and non-crystalline composition.
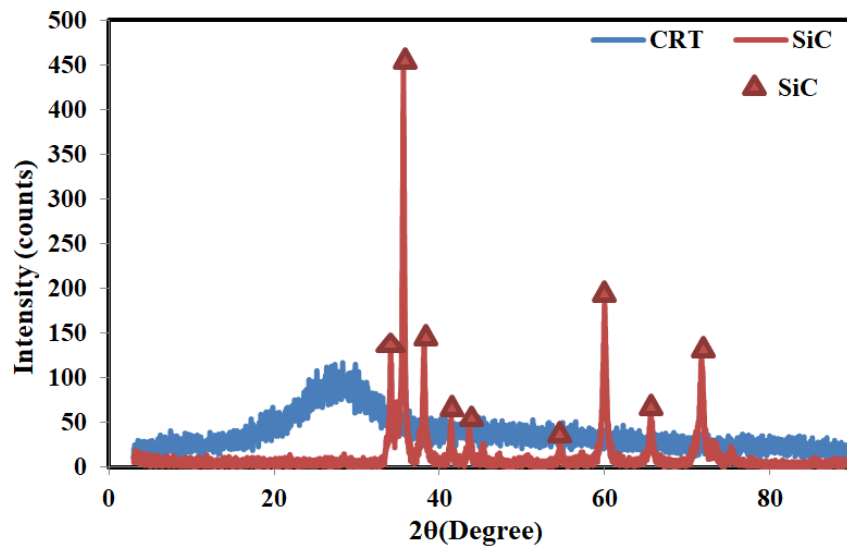
Figure 22. X-ray spectra of raw materials.

25

2.2.2 Characterisation of raw material to prepare metakaolin-based geopolymer

Kaolin was heated up to 750 °C for 3 hours as the first step in this process. Metakaolin leads to the loss of chemically bound water, a downturn of crystalline structure, and phase transformation into amorphous material with high reactivity. The kaolin contained 16 wt.% of amorphous phases. The calcination process's effect on kaolin's phase transformation then increased to 74 wt.%, resulting in the formation of metakaolin, as shown in Figure 23. and Table 7., detected by X-ray diffraction results.
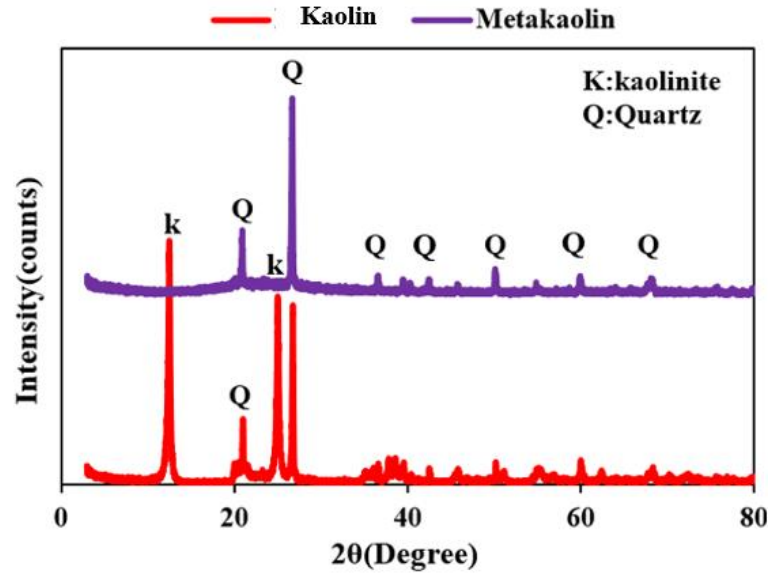
Figure 23. The X-ray spectra for the kaolin and transformation into metakaolin through the calcination process

Table 7. XRD results amount of crystalline and amorphous phases (wt.%) for clay before and after calcination.

Phase composition	Quartz	Kaolinite	Amorphous	SUM
Before calcination (Kaolin)	22.68	61.32	16	100
After calcination (MK)	26	0.00	74	100

Table 8. shows the chemical content of metakaolin. There are two major constituents: silica 58.3 wt.% and alumina 39.4 wt.%, with other minor constituents.

Table 8. The chemical composition of metakaolin obtained from XRF

Chemical composition	SiO_2	Al_2O_3	MgO	CaO	Na_2O	K_2O	Fe_2O_3	MnO	TiO_2	P_2O_3	S
Weight (%)	58.3	39.4	0.33	0.18	0.06	0.26	0.47	<0.005	0.203	0.013	0.02

The particle size distribution of metakaolin exhibits a median diameter (d_{50}) of 5.4 µm, as represented by the red line in Figure 24. This indicates a well-defined and consistent particle size, which can influence its reactivity and performance in geopolymers.

Figure 24. Particle size distribution of metakaolin

Figure 25. shows the flowchart of the experimental work, including three parts:

- Preparation of foam glass aggregate,
- Preparation of metakaolin-based geopolymer binder and statistical analysis, and
- Preparation of lightweight geopolymer.

Foam glass aggregate preparation

Raw materials

CRT-GW Characterizing (PSD, XRF, and XRD)

SiC Characterizing (PSD, and XRD)

Mixed (99 wt % CRT-GW &1 wt% SiC)

The mixture was analysed using a heat microscope to determine the foaming temperatures range 725 - 800 °C

Add methylcellulose dissolved in water as a binder

The dough was shaped into small pellets

The pellets sintered at different temperatures (725 °C ,750 °C ,775 °C and 800 °C)

Characterizing of FGA :
Bulk density, volume expansion, uniaxial compressive stress, apparent porosity, microstructure, leaching test, and thermal conductivity

Compared the results with a standard value of lightweight aggregate
▪ Bulk density < 1.2 g/cm³
▪ Uniaxial compressive strength > 1 MPa

The foam glass aggregate sintered at 750 °C, 775 °C, and 800 °C was selected.

Geopolymer binder preparing

Raw materials

kaolin | Water glass liquid | Sodium hydroxide flakes

Calcination at 750 °C for 3hr and milled

Dissolved 400g in 1 L distilled water

Metakaolin Characterizing (PSD, XRF, and XRD)

10 M sodium hydroxide solution

Study effect: 1- Different dosages of water glass in activator solution (0, 25, 50, 75, and 100) wt%.
2- Cured at two different temperatures: 60 °C, and 75 °C.
Liquid-to-solid ratio:1.1.

Characterizing :
Bulk density, compressive stress, SEM, EDX, efflorescence, XRD, FTIR, and thermal conductivity.

Enhance the properties of the geopolymer study effect :
1-Different liquid-to-solid ratios:1.1, 0.9, and 0.8.
2- Cured at two temperature:60 °C and room temperature

Characterizing :
Bulk density, compressive stress, setting time, and thermal conductivity.

The optimal design was selected, depending on geopolymer properties: Liquid-to-solid ratios: 0.8, water glass content 50 wt% in activator solution, cured at room temperature.

Statistical analysis of geopolymer characterization

Lightweight geopolymer preparing

30 vol % of the foam glass aggregate ➕ 70 vol % of the geopolymer mixture ➡ Characterizing LWGP-FGA:
 Bulk density, compressive stress, thermal conductivity, and freeze-thaw cycles test.

Figure 25. Flowchart of the experimental work

2.3 Preparation and Characterisation of Foam Glass Aggregate (FGA)

2.3.1 Preparation of FGA

CRT glass waste was pulverized and ground using a RETSCH PM 400 planetary ball mill using agate balls and jars for 1 hr at 200 rpm. A mixture of 99 wt.% CRT glass waste powder and 1 wt.% silicon carbide was prepared. A binder made of methylcellulose dissolved in distilled water was used to form a dough that could be hand-shaped into small pellets. The dough was prepared by dissolving 1 g of methylcellulose in 100 ml of distilled water and then thoroughly combining this solution with 200 g of the powder. For measuring thermal conductivity and volume expansion, cylindrical specimens with a diameter of 15 mm were prepared.

These pellets were then subjected to a heating process in a programmable furnace at four different foaming temperatures: 725 °C, 750 °C, 775 °C, and 800 °C, with a holding time of 10 minutes and a heating rate of 360 °C per hour. These temperatures were selected based on a heating microscope analysis. After the heating cycle, the pellets were left to cool to room temperature in the furnace, as shown in Figure 26.
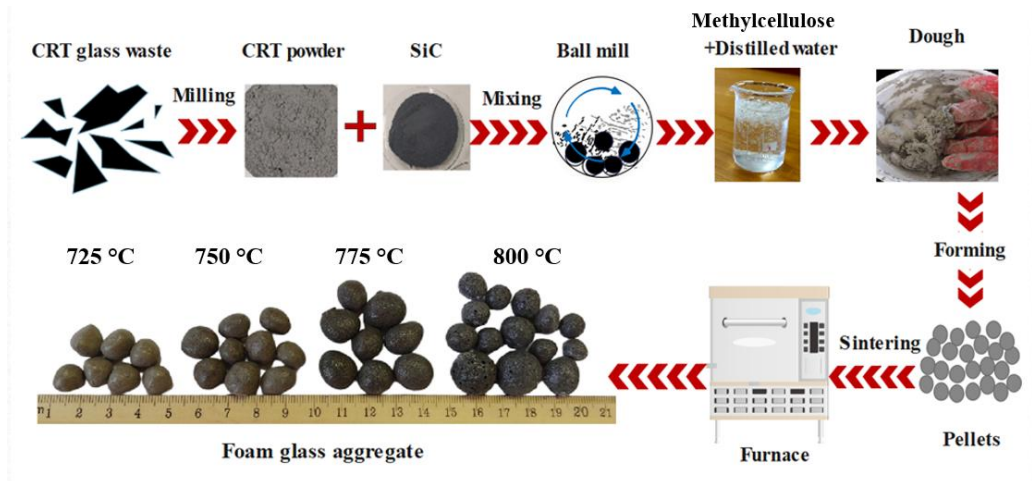
Figure 26. Flowchart for the preparation of foam glass aggregate

2.3.2 Techniques for Characterizing the FGA

A heating microscope (MicrOVis, manufactured by Camar Elettronica s.r.l.) was used to study foaming behaviour with added silicon carbide to waste glass and observe the height change during heating. Figure 27. shows the figure and schematic diagram of the heating microscope.
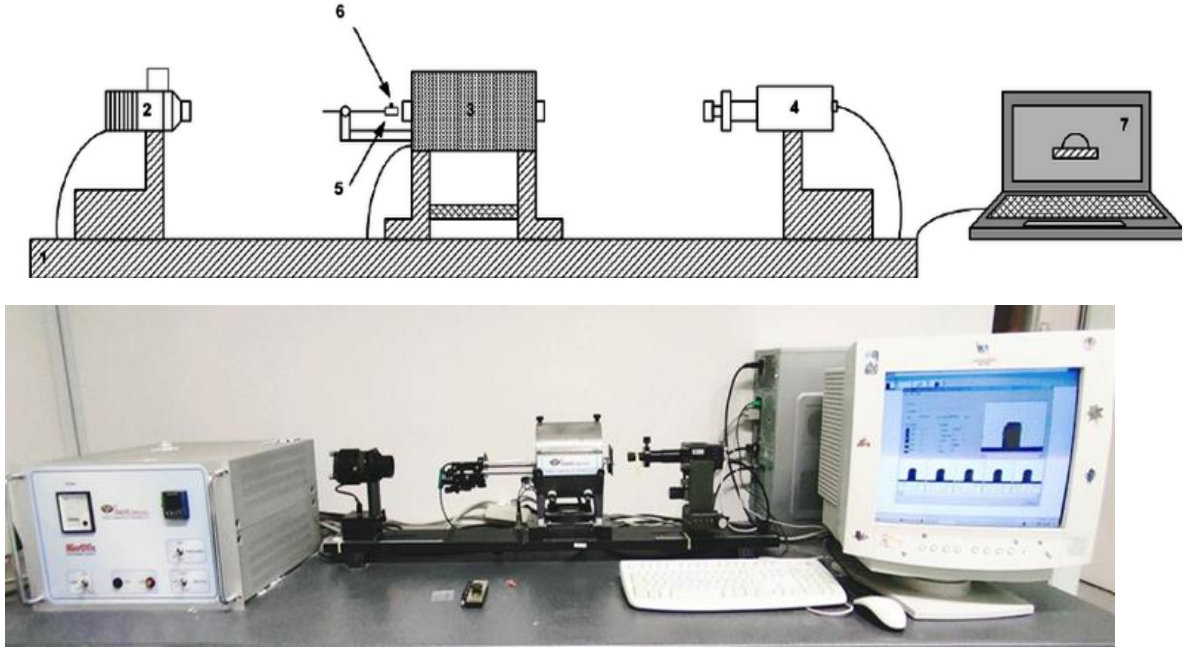
Figure 27.Schematic diagram and figure of the heating microscope: (1) frame, (2) light source, (3) tubular furnace, (4) high-resolution CCD camera, (5) sample holder, (6) sample, (7) control and registering unit (computer with control and image evaluation software).

The tubular furnace has a maximum temperature of 1600 °C and can be adjusted. It utilizes a light source and a camera to generate binary images. The camera takes photos of a sample at every 30 seconds, which tracks variations in the height of the sample as it undergoes heating. The height expansion (HE) of the samples can be determined based on the following equation:

$$HE = \left(\frac{H-H_0}{H_0}\right) \times 100 [\%] \qquad\qquad (3)$$

Where: H is the height during heating, and (H_0) is the original height of the sample. The bulk density (BD) was calculated by dividing the sample mass by volume after sintering. The volume expansion (VE) was calculated based on the equation:

$$VE = \left(\frac{V_0-V_1}{V_0}\right) \times 100; \ [v\%] \qquad\qquad (4)$$

Where (V_0) is the volume sample before the foaming process and (V) is the volume after the foaming process.

The microstructure for FGA samples was inspected using the scanning electron microscope (SEM) type Carl Zeiss with module EVO MA10. Before SEM imaging, the FGA samples were coated with gold to increase conductivity.

The density of the foam glass samples was determined by measuring their weight and dimensions. The apparent porosity (AP) was evaluated according to equation (3), where P_0

is the apparent porosity, DF is the density of foam glass, and DM is the density of the mixture glass waste was 2.5 g/cm^3.

$$P_0 = \left(1 - \frac{DF}{DM}\right) \times 100; \ [\%] \qquad\qquad (5)$$

The uniaxial compressive strength (UCS) of a spherical aggregate was measured. This involved placing the aggregate within a cylindrical mould and subjecting it to force. This procedure is based upon prior studies [109-112] as shown in Figure 28.
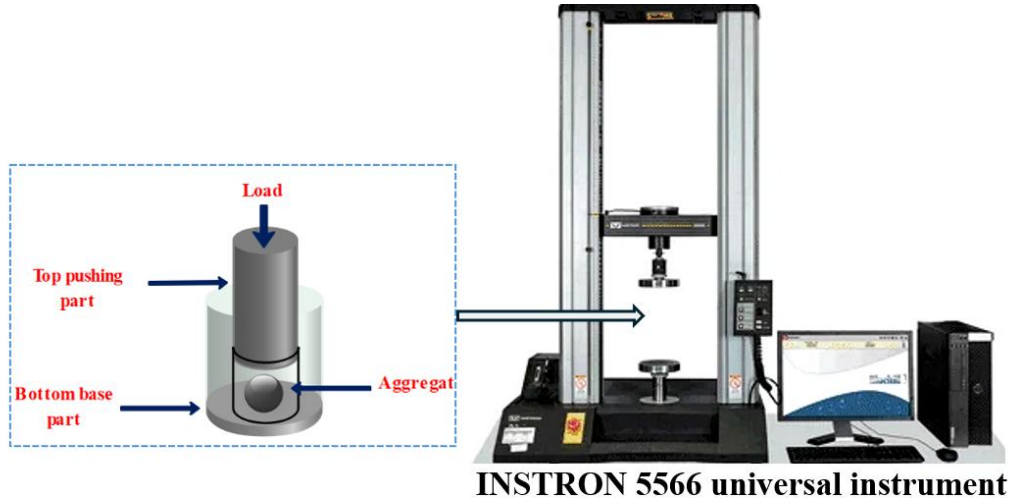
Figure 28. The procedure of the uniaxial compressive strength test of foam glass aggregate.

The INSTRON 5566 universal testing machine was used to measure the individual UCS value of the FGAs. The application of the load was controlled, employing a low loading rate of 0.1 mm/s. The uniaxial compressive strength was calculated using the following equation:

$$UCS = \frac{2.8\,F}{\pi D^2} \qquad\qquad (6)$$

Where F is the maximum load and D is the diameter of the spherical aggregate. The UCS was measured for five samples (pellets) for each mixture.

It is necessary to conduct a leaching test for FGA because CRT glass contains hazardous metals. Leaching tests were conducted according to the EN 12457-3:2004 standard [113]. The FGA underwent a milling process, transforming it into a powder with a particle size of around 4 µm. The test sample was prepared by mixing 500 g of FGA powder with 1L of distilled water and mixing them up for 6 hours using a rotary mixer set at 100 rpm. After this, the solution was filtered using a filter paper with 0.4 µm. An inductively coupled plasma-optical emission spectrometer (ICP-OES) instrument (Varian 720-ES) was used to measure the lead and barium concentrations in the filtered solution. It is an advanced analytical equipment which was used to analyse the components qualitatively and quantitatively in various samples. During the ICP measurement, a high-temperature

31

ionization source creates plasma from flowing inert gases (typically argon). Plasma can atomize and excite sample elements due to its high heat. This method identifies and quantifies sample elements by detecting the excited atom-light. Figure 29. shows the leaching test procedure.
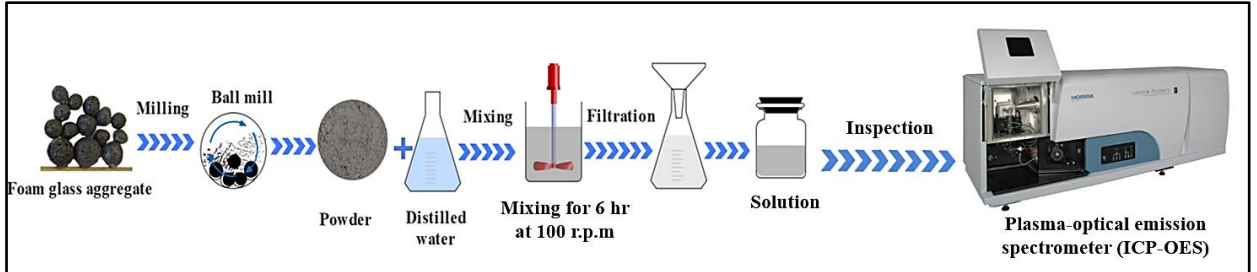
Figure 29. Leaching test procedure of foam glass aggregate.

C-Therm TCi Thermal Conductivity Analyzer was used to measure the thermal conductivity of FGA (Figure 30.) by employing the Modified Transient Plane Source (MTPS) technique.

Figure 30. Thermal conductivity analyser instrument (C-Therm TCi)

The modified transient plane source (MTPS) technique works according to ASTM D7984-16 [114]. A quantity of heat is supplied to the sensor by applying a known current to its heating element, causing a temperature increase at the point where the sensor and sample meet. This rise in interface temperature alters the voltage drop of the sensor element. To determine the thermo-physical properties of the sample material, the rate of increase in the sensor voltage is analysed. As the voltage applied to the sensor increases, the thermal conductivity of the sample material inversely decreases [115]. Consequently, the temperature rise at the sensor interface results in a corresponding change in the voltage drop depicted in Figure 31.
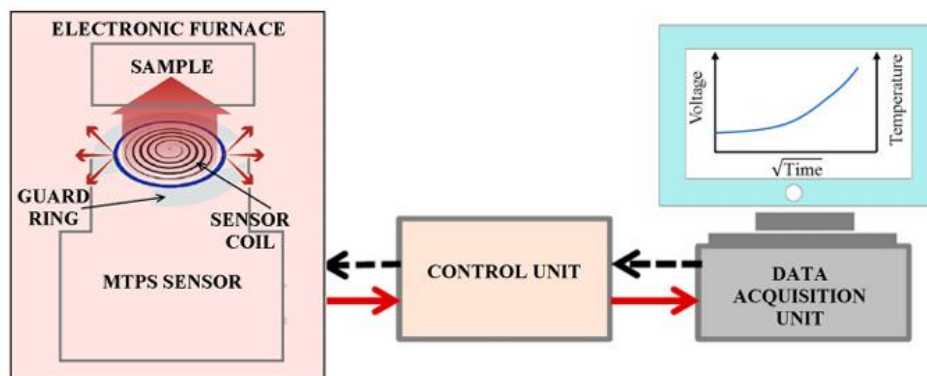
Figure 31. TCi Thermal Conductivity Analyzer mechanism working principle [115].

The cylindrical-shaped sample of FGA was used to measure thermal conductivity. The sample was covered with conductivity materials and placed on the sensor. The sensor of this instrument is sensitive and requires careful handling during operation. The specifications for sample measurement are a minimum thickness of 0.2 cm and a diameter of 1.7 cm with smooth and flat surfaces. The sample surfaces (Figure 32.) were prepared using sandpaper.
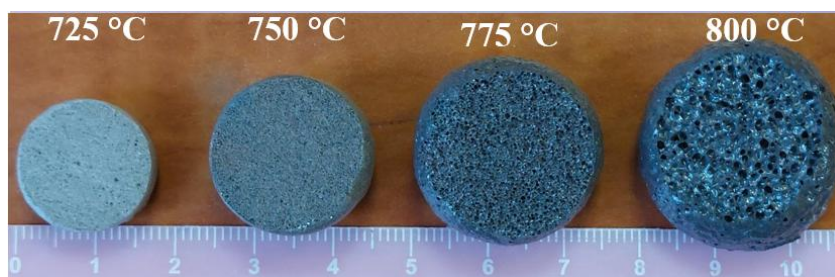
Figure 32. Foam glass samples for thermal conductivity measurement.

2.4 Preparation and characterisation of metakaolin-based geopolymer binder (MK-GP)

2.4.1 Preparation of the MK-GP with different dosages of water in the activator solution and cured at 60 °C and 75 °C

After the calcination of kaolin at 750 °C for 3 hours, metakaolin was formed and ground using a ball mill (Retsch PM 400) with agate balls at 180 rpm for 20 minutes. Five agate balls of different sizes (the diameter of three balls was 1.5 cm and the other two balls were 3 cm) were used. To prepare the NaOH solution, 400 g of sodium hydroxide flakes were dissolved in 1 L of distilled water, resulting in a concentration of 10 M NaOH solution. The influence of the water glass to sodium hydroxide ratio on the properties of the geopolymer binder was investigated. The alkaline activator solutions were prepared by mixing water glass and sodium hydroxide solution with five different dosages (0, 25, 50, 75, and 100 wt.%) of water glass. The solutions were mixed with a blender at 400 rpm for 3 minutes. The MK powder was mixed with the alkaline activators in the blender at 300 rpm for 3 minutes and

at 480 rpm for 2 minutes. The fresh geopolymer paste was poured into cubic silicon moulds of 2.5 cm×2.5 cm ×2.5 cm and 5 cm×5 cm×5 cm geometry and cured at two different curing temperatures (60 ºC and 75 ºC) for 24 hours. The geopolymer sample preparation method is shown in Figure 33., while the mix design is shown in Table 9.
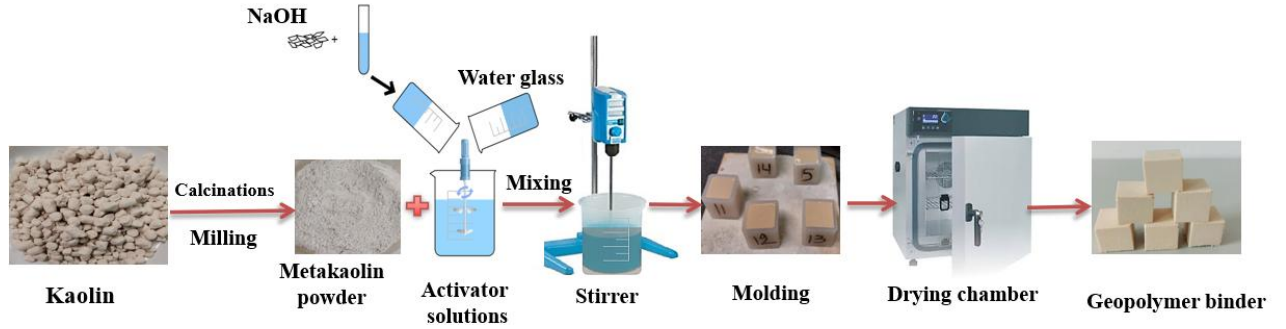
Figure 33. Scheme for the preparation of geopolymer samples.

Table 9. Composition of MK-GP with a L/S ratio of 1.1 and NaOH (10 M)

Sample code	Liquid [wt.%]		Solid [wt.%]
	Waterglass (g)	NaOH (g)	MK powder (g)
MK-GP0	0	100	90.9
MK-GP25	25	75	90.9
MK-GP50	50	50	90.9
MK-GP75	75	25	90.9
MK-GP100	100	0	90.9

2.4.2 Preparation of MK-GP with different liquid-to-solid ratios and curing at 60 °C and room temperature

The goal was to prepare a geopolymer at room temperature to be applied in work life. For this, the properties of geopolymers cured at room temperature were studied after selecting the best water glass percentage in the activator solution (at 50 wt.% water glass).

Figure 34. illustrates that the lighter foam glass aggregate, with a density of 0.58 g/cm³, floated when combined with a geopolymer binder at a liquid-to-solid ratio of 1.1. To prevent this phenomenon, to improve the distribution of aggregates within the binder, and to enhance compressive strength, the impact of varying the liquid-to-solid ratio on the properties of the geopolymer was investigated.

Figure 34. Flotation of foam glass aggregate in the geopolymer binder.

34

MK-GP was prepared by mixing an equal weight percentage of water glass and sodium hydroxide solution to prepare the activator solution [116]. The geopolymer binder samples were prepared using a silicon cubic mold with a length of 5 cm. At this time, the samples were cured at two different temperatures: 60 °C and room temperature and formulated with different liquid-to-solid ratios of 0.8, 0.95, and 1.1. The geopolymer binder mix design is shown in Table 10.

Table 10. The composition of the geopolymer binder with a NaOH/Na$_2$SiO$_3$ ratio of 1 and 10 M NaOH .

Samples codes	L/S	Liquid (g)		Solid (g)
		Na$_2$SiO$_3$	NaOH	Metakaolin
MK-GP 0.8	0.8	50	50	125
MK-GP 0.9	0.9	50	50	111.1
MK- GP 1.1	1.1	50	50	90.9

2.4.3 Characterisation techniques of the geopolymer samples

The bulk density of the MK-GP was measured according to ASTM C642 standard [117]. This involved measuring the dry weight per volume of the sample. Volume shrinkage was determined according to ASTM C1241 standard [118] by measuring the mould volume (V_0) and the volume of MK-GP (V_1). This calculation was performed using equation (7).

$$VS = \left(\frac{V_0 - V_1}{V_0}\right) \times 100; \ [v\%] \qquad (7)$$

The uniaxial compressive strength tests were performed on three cubic samples for each mixture using a Zwick/Roell Z100 universal testing machine at a speed rate of 2 mm/min, following the standard ASTM C-109 [119] test method for measuring the uniaxial compressive strength of hydraulic cement mortars. Cubic specimens with dimensions of 5 cm×5 cm×5 cm were used (Figure 35).
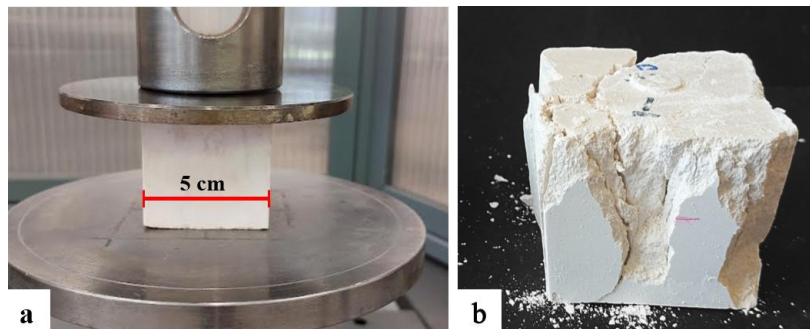
Figure 35.Geopolymer binder sample before (a) and after (b) the compressive strength test.

To determine the degree of efflorescence of the MK-GP, the cubic samples with a length of 2.5 cm were placed in a dish of distilled water with a depth of 5-7 mm. The surface of the sample was allowed to come into contact with distilled water (for 48 hours), and then the sample was dried at room temperature for 7 days [120, 121].

SEM (Scanning electron microscopy) and EDX (energy dispersive X-ray spectroscopy) were used to observe the microstructure and to identify and quantify the main elemental composition of MK-GP. Thermo Helios G4-PFIB CXe Dual scanning electron microscope equipped with a Bruker microprobe at a voltage of 20 kV was used in this work. Before SEM imaging, the fractured samples were coated with a thin layer of gold to increase conductivity. The micrographs were taken under different magnifications.

The geopolymer binders were milled into powder for Fourier transform infrared spectroscopy (FTIR) analysis using a Bruker Tensor 27 FTIR instrument to obtain their infrared (IR) spectra. The equipment has an average resolution of 4 cm^{-1} and covers a 400 – 4000 cm^{-1} wavenumber range.

The Rigaku MiniFlex II desktop X-ray diffractometer was used to measure the mineral composition and crystal structure of MK-GP.

The thermal conductivity of MK-GP was measured using the C-Therm TCi thermal conductivity analyser. The geopolymer sample used was a cube with a side length of 2.5 cm, meeting the minimum requirements of 0.5 cm thickness and 1.7 cm side length, as shown in Figure 36.

Figure 36.Geopolymer binder thermal conductivity sample.

The setting times of the geopolymer binder were measured with the Vicat apparatus according to EN 196-3:2005 standard [122]. The Vicat mould was filled with a geopolymer binder, and the filled mould was put on a glass base. Adjusting the distance between the end of the needle and the sample surface was set to zero. The test was made at room temperature (23 °C). A thin metal needle with a diameter of 1 mm was used to measure the initial setting time. The needle penetration was measured every 15 minutes. The onset of the initial setting time was determined by observing the penetration of the thin metal needle into the mixture until it reached a depth of 1 mm. To measure the final setting time, the mould was inverted to the bottom face, and the hollow circular needle with a diameter of 5 mm was used. The

final setting time was determined by observing the penetration of the hollow needle of 0.5 mm. Figure 37. shows the Vicat apparatus for measuring the geopolymer binder setting time.

Figure 37. Vicat apparatus for the measurement of the setting time of the geopolymer binder.

2.5 Statistical analysis

In the context of regression analysis in the Minitab program, the terms DF, Seq SS, Contribution, Adj SS, Adj MS, F-value, and P-value are key statistical metrics used to evaluate the regression model's quality and the significance of the predictors. Here is what each term means [123]:

1. **DF (Degrees of Freedom):** it refers to the number of independent values or observations in the data that are free to vary while estimating statistical parameters. In regression: it is divided into components like DF for regression (number of predictors), DF for error (remaining unexplained variation), and total DF (number of observations minus one).

2. **Seq SS (Sequential Sum of Squares):** represents the variation explained by each predictor when entering the regression model in sequence. In regression: it helps identify the contribution of each variable based on the order they are added to the model.

3. **Contribution:** it indicates the percentage of total variation in the response variable that a predictor variable explains. In regression: a higher contribution signifies that a variable has a stronger influence on the dependent variable.

4. **Adj SS (Adjusted Sum of Squares)**: it measures the variation explained by a predictor, considering all other variables already in the model. In regression: it quantifies the unique contribution of a variable, independent of the order of entry.

5. **Adj MS (Adjusted Mean Square)**: it is the Adjusted Sum of Squares (Adj SS) divided by its degrees of freedom (DF). In regression: it provides a standardized measure of variability for comparison across predictors.

37

6. **F-value:** it is a ratio of the variance explained by the model to the variance left unexplained. In regression: a higher F-value indicates that the model or predictor has a significant effect.

$$F = \frac{Adj\ MS\ (Regression)}{dj\ MS\ (Error)} \qquad (8)$$

A commonly applied rule of thumb in regression analysis is that if the F-value exceeds 2.5, it provides sufficient evidence to reject the null hypothesis. This suggests that the predictor variable has a statistically significant effect on the response variable and contributes meaningfully to the model.

7. **P-value**: that indicates the probability of observing the data assuming that the null hypothesis is true. In regression: a smaller P-value (typically<0.05) means that the predictor variable is statistically significant and contributes to the model.

In Minitab, this table represents the output of a regression model, showing how different independent variables (predictors) affect the dependent variable (response). Here is how to interpret and use it for model building [123]:

- *Coef (Coefficient)*: the estimated effect of each predictor on the response variable.
- *SE Coef (Standard Error of Coefficient)*: the variability of the coefficient estimate.
- *t-Value*: the statistical test used to determine the significance of a predictor (calculated as Coef / SE Coef).

Figure 38 shows a linear regression model with residuals, as the following equation:

$$y = \beta_0 + \beta_1 x_1 + \beta_2 x_2 + \beta_3 x_3 + \varepsilon \qquad (9)$$

- *y* is the response variable.
- β_0 (constant) is the intercept.
- $\beta_1, \beta_2, \beta_3$ are the regression coefficients, slope β_n how *x* influences *y*.
- x_1, x_2, x_3, are the predictor variables. ε is the error term.
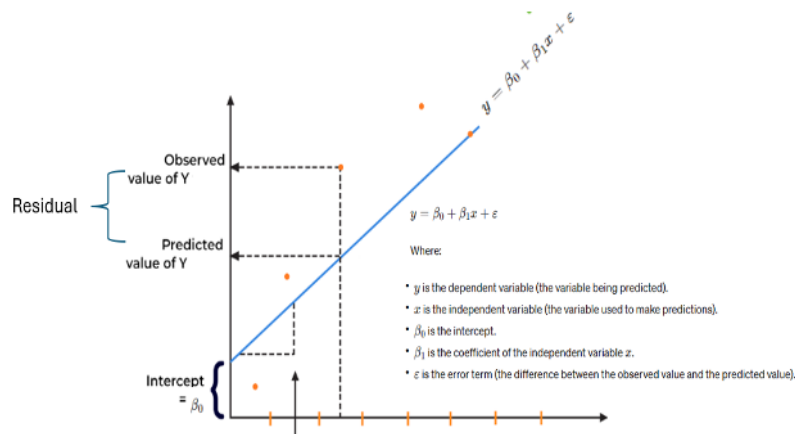
Figure 38. Linear regression model [123]

The critical value in statistical hypothesis testing is a threshold that determines whether the test statistic falls within a region where the null hypothesis can be rejected. It is based on the chosen significance level ($\alpha = 0.05$).

2.6. Preparation and characterisation of lightweight geopolymer with foam glass aggregate (LWGP-FGA)

2.6.1. Preparation of the LWGP-FGA

The lightweight geopolymer with foam glass aggregate (LWGP-FGA) was prepared cubic samples with a length of 5 cm by mixing 70 vol% of geopolymer binder and 30 vol% of FGA [101] (using this design, the bulk density estimates of LWGP-FGA less than 1.44 g/cm^3 according ASTM C 330 get a lightweight structure) for each, and the samples were hardened at room temperature. Figure 39. describes the procedure used to prepare the LWGP-FGA.
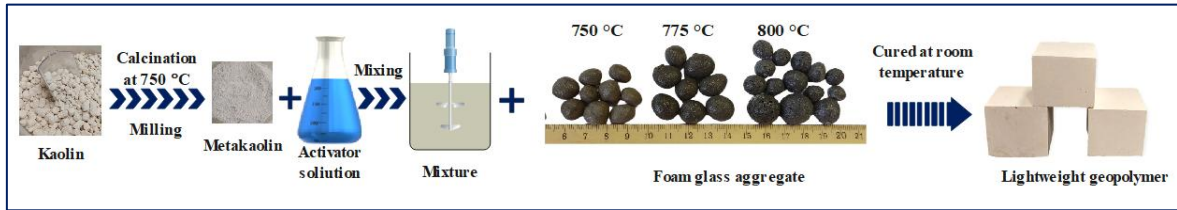
Figure 39. Sketch of the preparation of LWGP-FGA.

The geopolymer binder mix design is shown in Table 11. for a cubic sample with a length of 5 cm with a volume of 125 cm^3. NaOH molarity was 10 M, and the liquid-to-solid ratio was 0.8.

Table 11. Geopolymer binder mix design for a cubic volume of 125 cm^3.

Raw materials	Density (g/cm³)	Weight (g)	Volume (cm³)
Metakaolin	2.156	118.056	54.758
NaOH solution	1.32	47.222	35.774
Waterglass solution	1.37	47.222	34.468
Geopolymer binder before hardening	1.7	212.500	125

Foam glass aggregate was used as a lightweight aggregate. It was made using 99 wt.% of cathode ray tube glass waste and 1 wt.% of silicon carbide foaming at temperatures of 750 °C, 775 °C, and 800 °C. Table 9. shows the properties of the foam glass aggregate.

Depending on the densities of the geopolymer binder and FGA designed for the lightweight geopolymer, Table 12. shows the weight of materials used to prepare LWGP-FGA. The mixture for one cubic sample with a volume of 125 cm^3 (replaced 70 vol% (87.5 cm^3) of geopolymer binder and 30 vol% (37.5 cm^3) of FGA.

Table 12. Sample codes and compositions of LWGP-FGA for cubic samples with a volume of 125 cm^3.

Sample code	FGA sintered at temperature (°C)	Compositions (wt.%)	
		FGA (g)	Geopolymer binder (g)
LWGP	-	-	212.500
LWGP-FGA750	750	34.125	148.750
LWGP-FGA775	775	24.000	148.750
LWGP-FGA800	800	21.750	148.750

2.6.2. Characterization techniques of the LWGP-FGA

The bulk density, water absorption and apparent porosity of LWGP-FGA were measured after 28 days of curing, taking the average of five samples according to ASTM C642 standard [117]. Bulk density was calculated by dividing the weight of the sample by its volume. To determine the water absorption and apparent porosity of LWGP-FGA, first, the samples were dried to record dry weight (W_D). After this, the samples were immersed in distilled water for 48 hours. After the removal of the samples from the water surface moisture was wiped off with a wet cloth and the saturated weight (W_S) was recorded. The water absorption (WA) was measured according to the following equation:

$$WA = \left(\frac{W_S - W_D}{W_D}\right) \times 100; \ [wt\ \%] \qquad (10)$$

The fully saturated specimen was suspended in water using a wire and weighed, while submerged for the recorded subsaturated weight (W_{sub}) for the measurement of apparent porosity (P_0) according to the following equation:

$$P_0 = \left(\frac{W_S - W_D}{W_S - W_{Sub}}\right) \times 100; \ [\%] \qquad (11)$$

The average uniaxial compressive strength of three cubic samples was evaluated using an INSTRON 5566 instrument after 28 days of curing. Samples were subjected to testing at a speed of 2 mm/min, following the ASTM C-109 [119] standard.

The thermal conductivity of LWGP-FGA was assessed using a C-Therm TCi thermal conductivity analyser working in the modified transient plane source (MTPS) technique. It is the same instrument as those used for measuring the thermal conductivity of GP and FGA to ensure the accuracy in comparing results.

The thermal conductivity of the LWGP-FGA sample was determined by taking the average of three samples, each evaluated on six sides. The surface of each sample was prepared before testing, as shown in Figure 40.
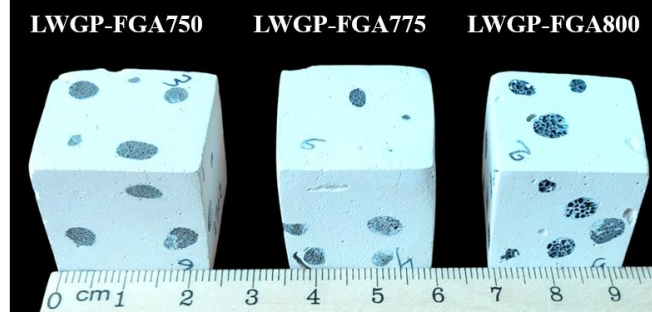
Figure 40. Lightweight geopolymer samples for thermal conductivity measurement.

Freeze-thaw cycles test of LWGP-FGA was measured on cubic samples with a side length of 5 cm and cured for 28 days at room temperature. After this, the samples were immersed in tap water for 4 days to ensure that they were saturated [124, 125]. Each freeze-thaw cycle consists of freezing the samples at -20 °C for 4 hours, followed by thawing the samples through immersion in tap water at room temperature (25 ± 3 °C) for 4 hours, as shown in Figure 41.
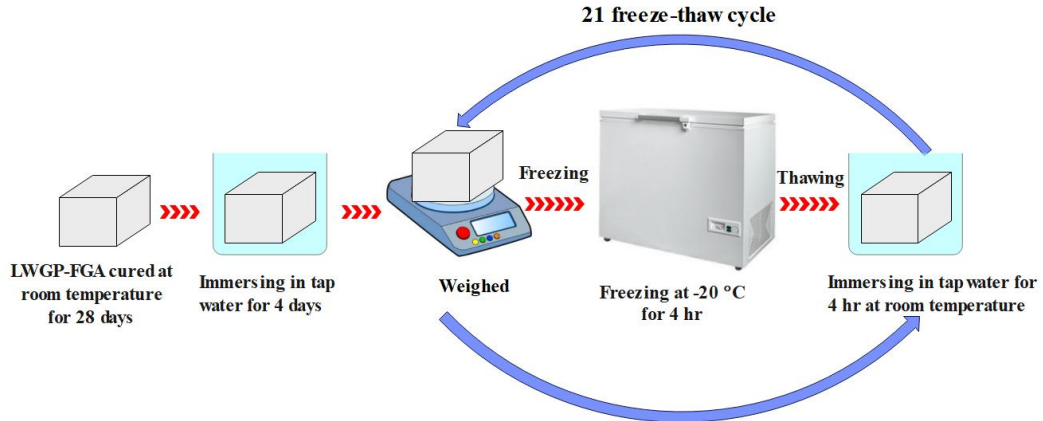
Figure 41. Freeze-thaw cycles test procedure of LWGP-FGA.

After completing 21 cycles, the change in weight and uniaxial compressive strength were recorded [126-129]. The weight change was calculated using the following equation:

$$Weight\ change = \left(\frac{m_0 - m_{cycle}}{m_0}\right) \times 100; \ [wt.\%] \qquad (12)$$

Where m_0 represents the weight of the sample before the freeze-thaw cycles, and m_{cycle} is the weight of the sample after completing the cycles. The compressive strength reduction was calculated using the following equation:

$$Strength\ reduction = \left(\frac{\sigma_0 - \sigma_{cycle}}{\sigma_0}\right) \times 100 \qquad (13)$$

Where σ_0 represents the compressive strength of the sample before the freeze-thaw cycles, and σ_{cycle} is the compressive strength of the sample after completing the cycles.

41

Chapter Three/ Results and Discussion

This chapter includes the results of the PhD research work in six sections: the first discusses the characterization results of FGA samples, the second discusses the results of MK-GP by the effect of water glass dosage and curing temperature, third section discusses the results of MK-GP by the effect of the liquid-to-solid ratio and curing temperature, the fourth section includes the statistical analysis of MK-GP, and the final section presents the results related to LWGP-FGA.

3.1 Results and discussion of foam glass aggregate characterisation[1]

3.1.1 Analysis of the heating microscopy results

Figures 42. and 43. show the silhouettes taken at various temperatures throughout the heating process, at temperatures ranging from 20–1000 °C and the height percentage changes with temperatures during the heating process.
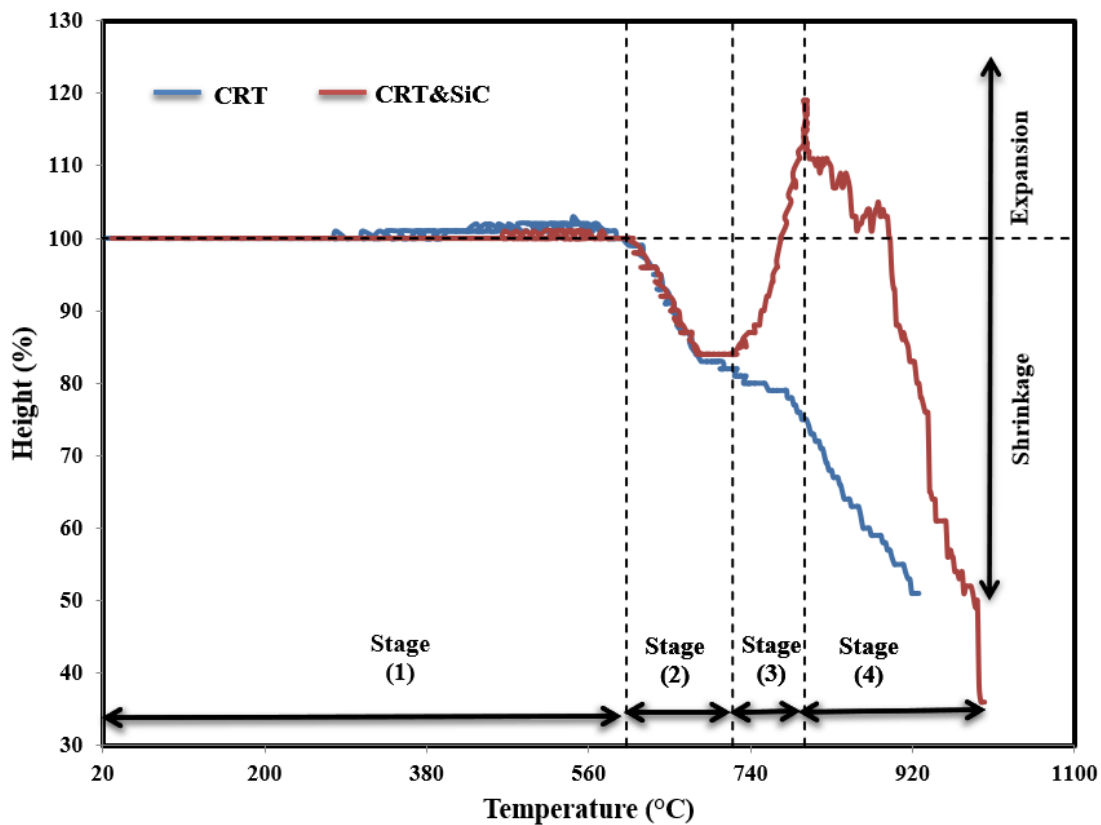
Figure 42. The heating microscopy results for CRT glass and a mixture (99 wt.% CRT-GW with 1 wt.% SiC) samples, heating them at a temperature range of 20-1000 °C at a rate of 5 °C/ min.

Sample code	Temperature (°C)			
	602	720	800	1000
CRT	Height =100%	Height =82%	Height =75%	Height =41%
CRT& SiC	Height =100%	Height =84%	Height =119%	Height =36%

Figure 43. Silhouettes for CRT-GW glass and a mixture (99 wt.% CRT-GW with 1 wt.% SiC) at various heating stages

Four distinguished stages were noticed. First, at the temperature range of 20–602 °C, the specimen was nonreactive without a change in height. Second, at the temperature range of 602-720 °C is the densification or sintering step, in which local melting occurs, leading to the particles' contact. This process results in shrinkage of the sample height, reaching 82% for CRT-GW and 84% for the mixture.

In the third stage, at a temperature range of 720-800 °C, the behaviour became different between glass and the mixture. CRT-GW continued to shrink, reaching 75% of its initial height at a temperature of 800 °C. While in this stage, the mixture started to foam (*expansion*) at a temperature of 720 °C. The reaction happened between the foaming agent and glass particles with the release of CO_2, and the bubbles uniformly spread throughout the liquid mass to form pores and expand in height. The maximum height expansion of 119% was recorded at 800 °C. Fourth, at a temperature range of 800-1000 °C, the mixture becomes softened with low viscosity, resulting in the gas passing through the mixture and escaping to the atmosphere. Then, the foaming process and the reduction in height were stopped. This stage is named *hemisphere*, so the sample height reduces to around ≤ 0.6 to the original height. Temperatures for foaming 725 °C, 750 °C, 775 °C, and 800 °C were selected to study how they influenced the properties of foam glass aggregate, as explained in the previous paragraph.

3.1.2 Characterisation of foam glass aggregate (FGA)

The bulk density and volume expansion results for FGA sintered at different temperatures are shown in Figure 44.
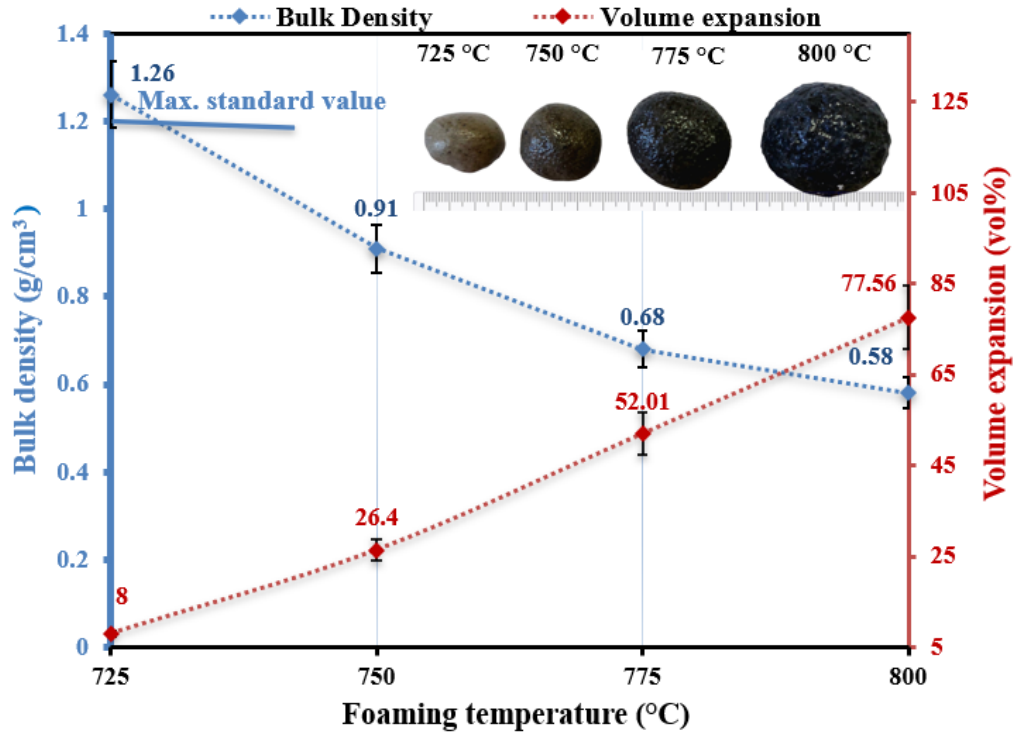
Figure 44. Volume expansion and bulk density for FGA at different foaming temperatures.

The volume expansion increased with the foaming temperature, while the bulk density decreased. The highest volume expansion value was 77.56 vol% for samples sintered at the maximum foaming temperature of 800 °C, while the lowest value was 8 vol% for samples sintered at 725 °C, at which the foaming process started. The foaming temperatures were selected depending on the heating microscopy results and the photographed image in Figure 44., the sample volume change.

The bulk density of the lightweight aggregate used in concrete must be lower than 1.2 g/cm^3, according to EN 13055 standard [22]. The samples sintered at a temperature range of 750-800 °C have a range of bulk density of 0.91-0.58 g/cm^3, which is less than the standard limit, while the bulk density of the sample sintered at 725 °C was 1.26 g/cm^3 over the standard limit, so this sample was neglected for further investigations.

The macrostructures shown in Figure 45. reveal that the pore size and the number of closed pores increased with the foaming temperature, and the distribution of pores was much more uniform due to the rise in foaming temperature, which led to the continuation of the reaction to produce more gas. On the other hand, the increase of foaming temperature led to reduced viscosity of the mixture with higher inner gas pressure.
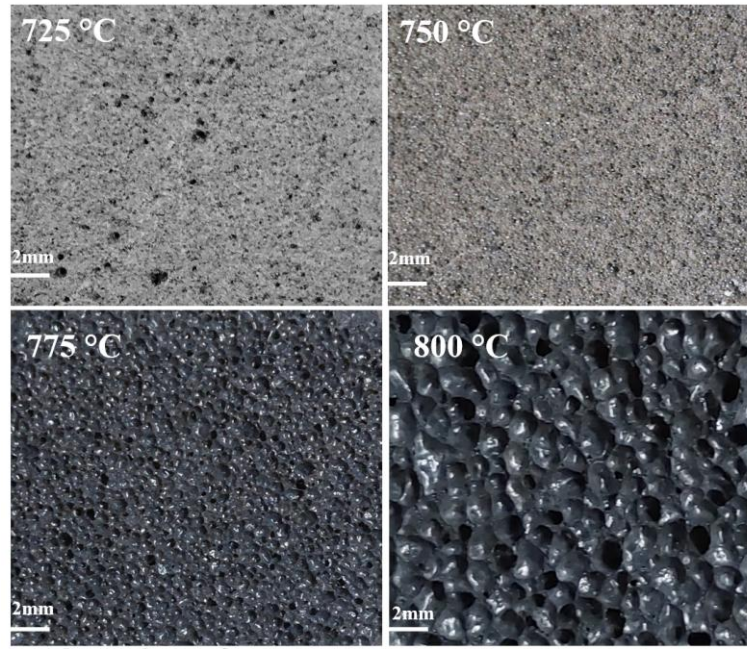
Figure 45. Macrostructure of the FGA (*scale bar = 2 mm*).

As the foaming temperature increased, the sample darkened due to higher lead generation, which is black in colour. Additionally, the melting of K_2O (5 wt.%) at 740 °C formed a glassy phase, creating a shiny surface, especially in samples sintered at 800 °C [130]. Figure 46. shows the microstructure of FGA.
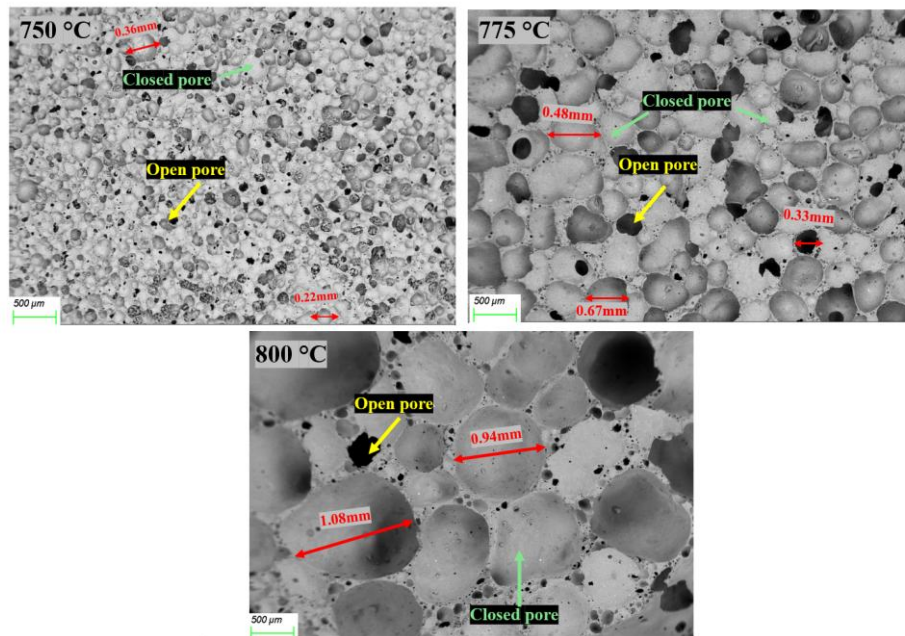
Figure 46. Microstructure of the FGA (scale bar=500 μm).

Many small open pores appeared in the samples sintered at 750 °C, while when the temperature increased to 775 °C and 800 °C, the pores expanded much more, and closed honeycomb-shaped pores were formed. The average pore size of FGA was 0.18 mm, 0.49 mm, and 0.98 mm for samples sintered at 750 °C, 775 °C, and 800 °C, respectively.

Typically, the apparent porosity is inversely proportional to the compressive strength; a high porosity means a low-density material due to the presence of many voids, which reduces the strength and the resistance to forces. The apparent porosity increases, and compressive strength decreases during the foaming process, as shown in Figure 47.
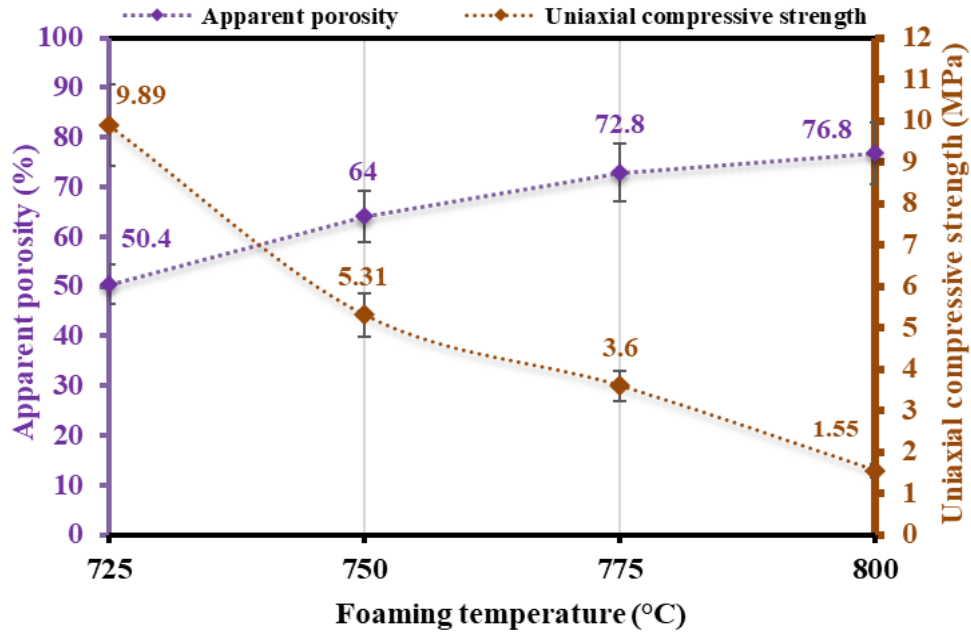
Figure 47. Apparent porosity and uniaxial compressive strength for FGA at different foaming temperatures.

According to the EN 13055 standard [22] the UCS value for FGA must be more than 1 MPa [23, 24, 131]. All samples sintered at temperatures 725-800 °C have UCS values more than the standard limit value. The lowest value, 1.55 MPa, was for the sample sintered at 800 °C. Figure 48. illustrates the thermal conductivity range for FGA as 0.063 to 0.097 W/m·K.
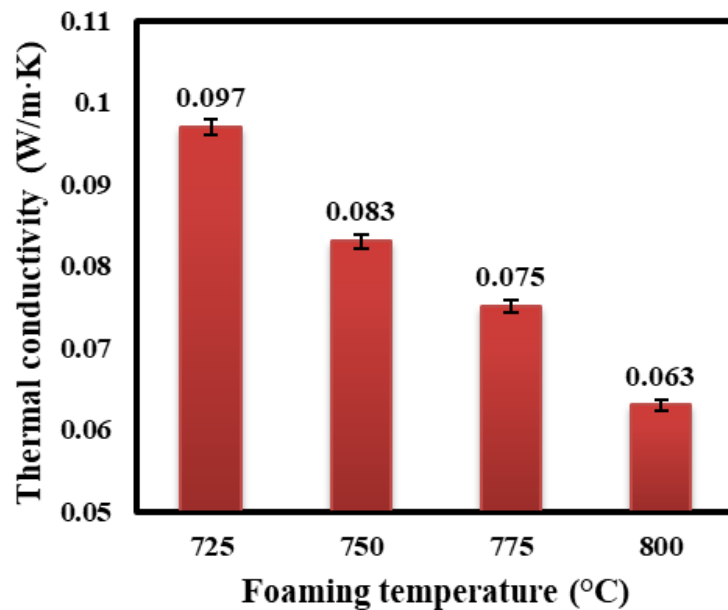
Figure 48. Thermal conductivity of the FGA at different foaming temperatures.

The decline in thermal conductivity with increasing foaming temperature is attributed to reduced density and increased porosity. This phenomenon occurs as air pockets within the foam function as insulators, thus diminishing the ability to conduct heat.

The leaching process for solid waste material is a method used to measure the amount of hazardous elements mass extracted from a waste substance when it comes in contact with a liquid. There are standard limited concentrations for eight contaminants, as shown in Table 13., measured by a leaching test to identify hazardous solid waste when leaching results indicate the same or higher concentration for these toxic elements [132, 133].

Table 13. Maximum acceptable concentration value of toxic contaminants from the leaching test [132, 133].

Contaminant	Max. concentration (mg/L) according to [132, 133]
Arsenic	5.0
Barium	100.0
Cadmium	1.0
Chromium	5.0
Lead	5.0
Mercury	0.2
Selenium	1.0
Silver	5.0

The lead and barium concentrations of the leaching were measured for foam glass aggregates produced at 750 °C, 775 °C, and 800 °C foaming temperatures (Figure 49.).
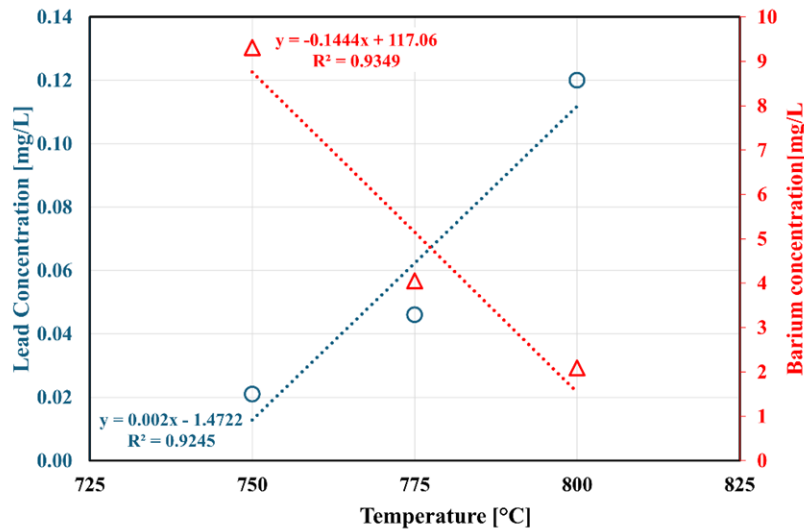
Figure 49. The concentration of Pb and Br contaminants from the leaching test for FGA.

The lead concentrations for FGA recorded a value range of 0.021-0.12 mg/L, lower than the standard maximum limit for lead. The lead concentration increases with the foaming temperature due to the reaction of PbO with SiC, which occurred at a temperature range of

47

720-800 °C and led to the generation of lead according to the following chemical equation (1).

The higher foaming temperature ensures the completed reaction, increasing the amount of lead metal produced. The barium concentration range value of 2.09-9.31 mg/L is also within the standard limit. Note in Figure 49. that when the foaming temperature rises, the barium concentration sharply decreases because the heating process leads to the BaO reaction with SiO_2, resulting in the creation of barium silicate according to the following equation:

$$BaO+SiO_2 \rightarrow BaSiO_3 \qquad (14)$$

This reaction occurs during the heating up of the glass in the range between the transition temperature (T_G) and the melting temperature (T_M). The transition temperature of the CRT glass is approximately 580 °C [51, 134, 135]. The melting temperature of 994 °C was recorded by a heating microscope.

3.1.3 The correlation amongst properties for FGA

The correlation between the bulk density, thermal conductivity, and compressive strength values of the FGA prepared at different temperatures is illustrated in Figure 50. The correlations were presented by using linear equations; both thermal conductivities and compressive strength rise with the increase in density.
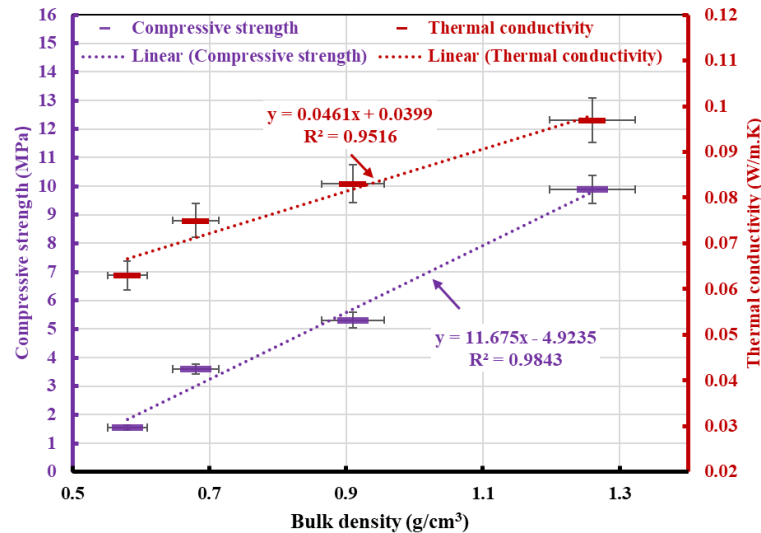
Figure 50. The relationship between bulk density, thermal conductivity, and compressive strength of the FG.

3.1.4 Comparison of characteristics and preparation conditions of the FGA, previous scientific articles

Foam glass is prepared using different types and percentages of foam agents and various sintering conditions (*foaming temperature, heating rate, and holding time*). Table 14. compares the foam glass prepared in this work with other research in the literature review.

A key strength of this work is the relatively low sintering temperature range (725–800 °C), which is more energy-efficient compared to some references that require temperatures as high as 1230 °C. The resulting bulk density (0.58–1.26 g/cm³) and compressive strength (1.55–9.89 MPa) illustrate a good balance between weight and mechanical performance, positioning this material well for structural or semi-structural applications. While the thermal conductivity (0.06–0.09 W/m·K) is adequate for insulation, the use of CRT glass also raises potential environmental concerns due to the presence of lead, a limitation not shared by studies using soda-lime or container glass.

Table 14. Comparison of the results of this work with other previous studies on foam glass preparation.

Main raw materials	Foaming agent		Sintering conditions			Main properties			Ref.
	Type	(wt.%)	Sintering temperature (°C)	Heating rate (°C/min)	Holding time (min)	Bulk density (g/cm³)	Compressive strength (MPa)	Thermal conductivity (W/m·K)	
CRT glass waste	SiC	1	725, 750, 775, 800	5	10	0.58-1.26	1.55- 9.89	0.06-0.09	This work
Container glass+CRT (*glass waste*)	SiC	2	849, 860	5	10	0.17-0.18	-	0.04-0.05	[136]
Soda-lime silicate glass waste	Limestone	2, 4, 6	800	5	10	0.26-0.92	-	0.04-0.13	[137]
Glass +bentonite	Dolomite	-	800, 850, 900	-	7.5	0.3-1.4	-	-	[99]
Container glass+CRT (*glass waste*)	SiC	2	954, 964	5	10	0.23-0.42	0.7-2.5	0.037-0.04	[138]
Soda lime silicate glass waste	SiC	1, 1.5, 2	930, 940, 986	10	5	0.2-0.3	-	0.04-0.05	[139]
Waste glass + mineral wool waste	SiC	2	900, 1000, 1100, 1175, 1200, 1230	20	20	0.55-2.3	-	-	[140]
Glass waste	$CaCO_3$	4	750	-	10	0.535	-	-	[141]
Glass waste + coal fly ash glass	$CaCO_3$	0.5	600, 650,700, 750, 800, 850, 900	20	45	0.46-0.72	4.2–10.5	0.36–1.3	[142]
CRT panel glass	MnO_2	0,1.8, 3.6, 5.4, 7.2, 9	800, 820, 840	10	0-60	0.14-0.32	-	0.038–0.05	[52]

3.2 Results and discussion of MK-GP with different dosages of water glass in the activator solution and cured at 60 °C and 75 °C[2]

3.2.1 Bulk density and volume shrinkage

The analysis of the physical properties of MK-GP was performed after 28 days of curing. Curing conditions were: one day at 60 °C, and 75 °C, 27 days at room temperature. The volume shrinkage of the specimens was found to increase with increasing sodium-silicate (water glass) content and curing temperature because these two reasons lead to chemical shrinkage in forming silica-rich gels and promote the formation of larger gel holes [143]. The results of bulk density and volume shrinkage tests of the geopolymer are shown in Figure 51.
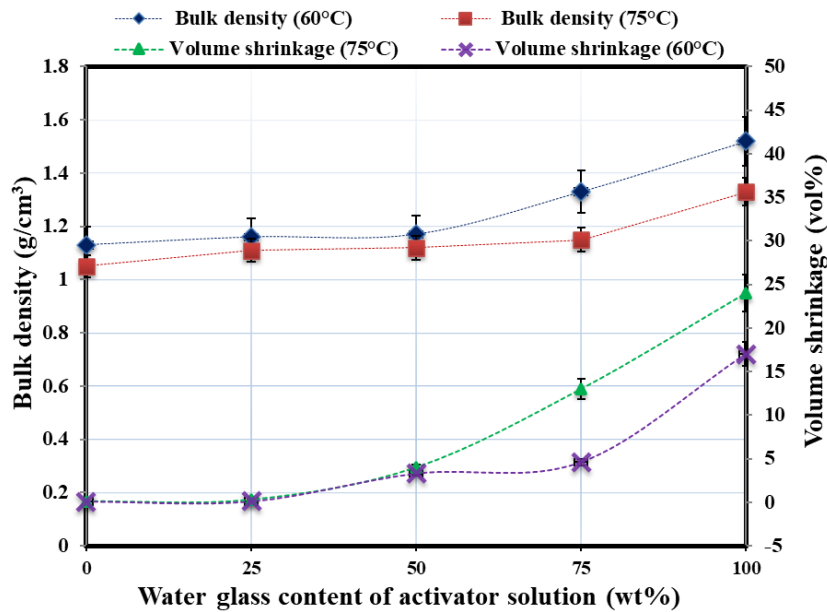
Figure 51. Bulk density and volume shrinkage of MK-GP with different dosages of water glass in activator solution and cured at 60 °C and 75 °C.

The bulk density of the geopolymers prepared at 60 °C and 75 °C curing temperatures ranges from 1.13-1.52 g/cm³ to 1.05-1.33 g/cm³, respectively. The density of the MK-GP samples decreases as the curing temperature increases. The reason for this phenomenon is that the samples lose more moisture during the curing process at higher temperatures. Therefore, preventing water loss before the geopolymer paste is fully cured is critical. If the specimen is cured at higher temperatures and/or in a dry oven, large shrinkage and even small cracks will occur on the surface of the specimen [144]. The relationship between density and

---

apparent porosity depends on factors such as curing conditions (temperature and time), and processing methods. The percentage of pores and pore size distribution effect the GP properties. The samples cured at 75 °C had a lower density and reduced strength [145].

3.2.2 Compressive strength test results

The results of the progression of the compressive strength of MK-GP at different ages (*7, 14, and 28 days*) cured at two different temperatures, 60 °C and 75 °C, are shown in Figure 52.

(a) Curing temperature: 60 °C   (b) Curing temperature: 75 °C
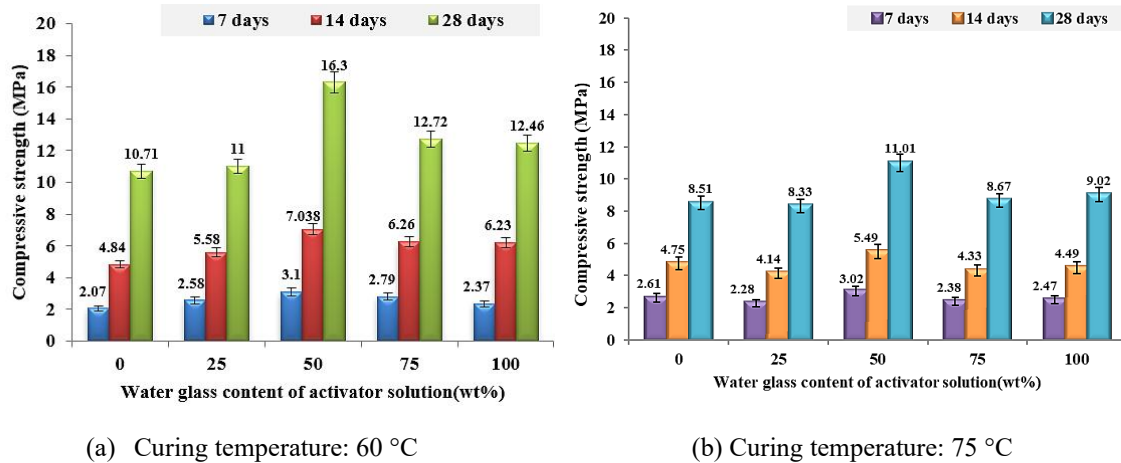
Figure 52. Compressive strength of MK-GP cured at (a) 60 °C and (b) 75°C for one day

The influence of the curing temperature can be seen. Specimens cured at 60 ºC have higher compressive strength values with a range of 10.71-16.3 MPa after 28 days than those cured at 75 ºC with a range of 8.51-11.01 MPa. The compressive strength tends to decrease when the curing temperature is higher than 60 ºC due to the chemical shrinkage of the geopolymer gel increases with the increase of curing temperature and curing time, resulting in more gel holes and micro defects (*explained in later sections of SEM*), and the strength decreases [146]. The strength of the geopolymer was affected by different dosages of water glass in the activator solution, the compressive strength increased with increasing water glass content. The maximum compressive strength of 16.3 MPa was achieved at 50 wt.% water glass. Moreover, the use of water glass helps to improve the geopolymerisation by accelerating the dissolution of the starting material [147]. Increasing the dosage of water glass was found to enhance the rate of geopolymerisation. However, when the water glass content exceeded 50 wt.%, a decline in compressive strength was observed. This reduction in strength can be attributed to the excessively high alkali content, which impedes the geopolymerisation process. Specifically, the precipitation of the Al-Si phase hinders the interaction between the solid precursors and the alkaline activator in its liquid form, ultimately leading to a decrease in the effective concentration of the activator. This finding

aligns with previous research [148,116] indicating that while an optimal alkali content promotes geopolymer formation, an excessive amount can have a detrimental effect on strength development.

3.2.3 Efflorescence

The migration of excess alkali solution within the geopolymer matrix occurs through the material's porous structure, eventually reaching the surface. Once exposed to air, this alkaline solution undergoes evaporation, simultaneously reacting with atmospheric CO_2 to form carbonate deposits, as illustrated in Figure 53.
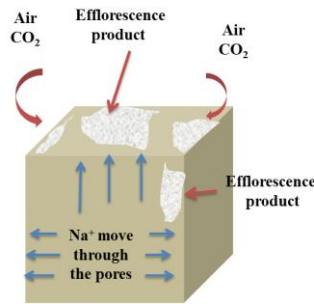
Figure 53. The geopolymer efflorescence mechanism [121].

This process is a result of the natural interaction between alkaline residues and environmental carbon dioxide, leading to the gradual formation of carbonate compounds on the surface of the geopolymer as the following equations [121]:

$$CO_{2\,(g)} + 2OH^-{}_{(aq)} \rightarrow CO_3{}^{2-}{}_{(aq)} + H_2O \qquad\qquad (15)$$

$$2\,Na^+{}_{(aq)} + CO_3{}^{2-}{}_{(aq)} + n\,H_2O \rightarrow Na_2CO_3{\cdot}nH_2O_{\,(s)} \qquad\qquad (16)$$
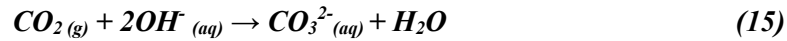
The most common method for detecting efflorescence is visual inspection. Figure 54. shows the geopolymer binders cured at 60 °C for one day and 27 days at room temperature after contact with distilled water for 2 days.

| MK-GP0 | MK-GP25 | MK-GP50 | MK-GP75 | MK-GP100 |
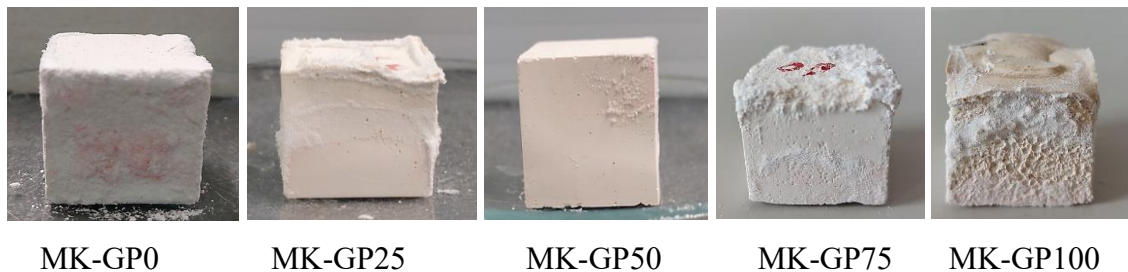
Figure 54. Efflorescence of MK-GP cured at 60 °C for 28 days with different water glass dosages of the activator solution.

For the MK-GP0 (*100 wt.% NaOH*), severe efflorescence (*a heavy salt deposition accompanied by surface pulverization*) occurred due to the excessive amount of Na ions. The

availability of the OH⁻ and Na⁺ ions is critical for this process, leading to the deposition of sodium carbonate hydrates. The N(C)-A-S-H gels of the geopolymers have a significant efflorescence-inhibiting effect due to their compact structure, compressive strength, and water-loss rate. Slight efflorescence (*salt coverage not exceeding 10% by volume*) occurred in MK-GP50 containing [50/50 wt.%] water glass to sodium hydroxide. Si/Al was 1.85 (*measured by EDX analysis, described later*), this can be attributed to a suitable Si/Al ratio of the geopolymer to form gel products formed by reaction with compact structures that effectively solidify [AlO₄] and Na. Moderate efflorescence (*salt deposits of 50% by volume*) occurred in samples containing MK-GP25, MK-GP75, and MK-GP100.

3.2.4 SEM and EDX analysis

The microstructure of MK-GP50 was characterized at two different magnifications (*500x and 1000x*). The sample exhibited a heterogeneous microstructure. Partially reacted and unreacted metakaolin were detected in the matrix sample. Figure 55. (A-B) displays that microcracks and voids are present in the geopolymer matrix of a sample cured at 60 °C, while Figure 55. (C-D) displays a denser, gel-like geopolymer matrix and porosity present in a sample cured at 75 °C.
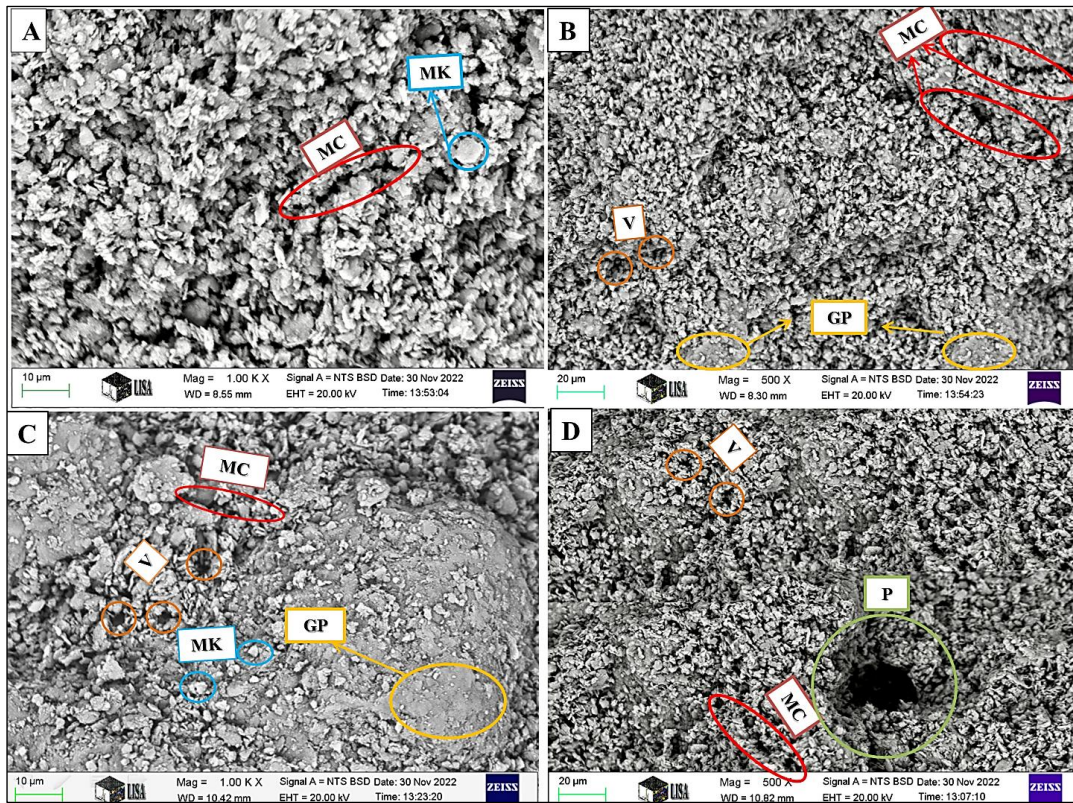
Figure 55. Scanning electron micrographs of specimens containing 50 wt.% water glass at different magnifications (500x and 1000x) at different curing temperatures (A-B) 60 °C and (C-D) 75 °C. (*GP: Geopolymer gel, MK: Unreacted metakaolin, MC: Micro crack, V: Void, P: Porosity*).

This suggests that the pores in the gel phase become coarser upon curing at higher temperatures. Previous studies [149, 150] have shown that MK-GP shrinks chemically as silica-rich gels form. Thus, a higher curing temperature and a longer curing time would increase the chemical shrinkage of the geopolymer and lead to the formation of larger gel pores with a greater number of microdefects. The microstructure of the MK-GP50 at 2000x magnification with EDX (*energy dispersive X-ray*) analysis for two different locations has optimum properties, higher compressive strength compared to other samples' compressive strength, and slight efflorescence. According to EDX examination, the main components were Si, Al, Na, O, and C. Figure 56. shows the microstructure and EDX analysis of a GP50 sample cured at 60 °C.
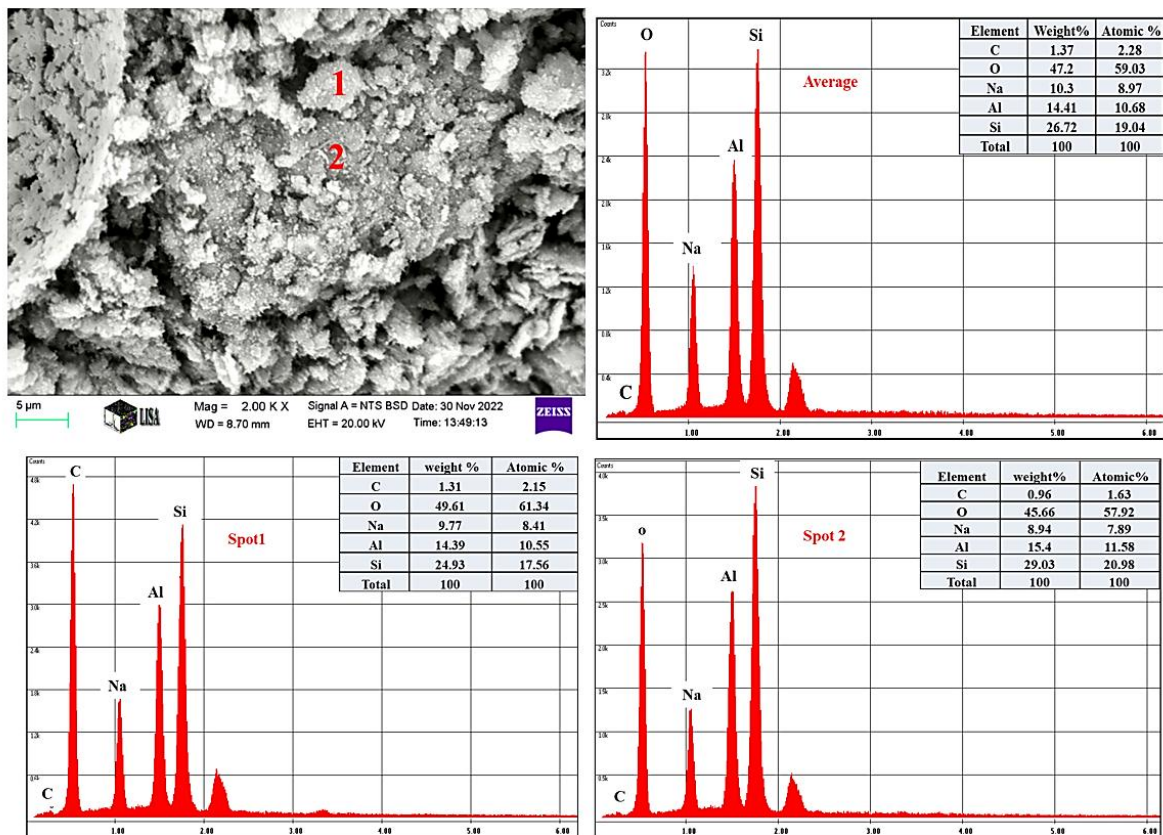
Figure 56. Scanning electron micrographs and EDX analysis for MK-GP50 cured at 60 °C.

The first spot shows characteristics of geopolymer gels with a Si/Al ratio of 1.66 and a Si/Na ratio of 2.55. Conversely, the second spot, which also relates to the geopolymer gel, displays a Si/Al ratio of 1.88 and a Si/Na ratio of 3.24. The average Si/Al ratio and Si/Na ratio for this sample are 1.85 and 2.59, respectively. The EDX and micrograph for the GP50 sample cured at 75 °C can be seen in Figure 57.

54
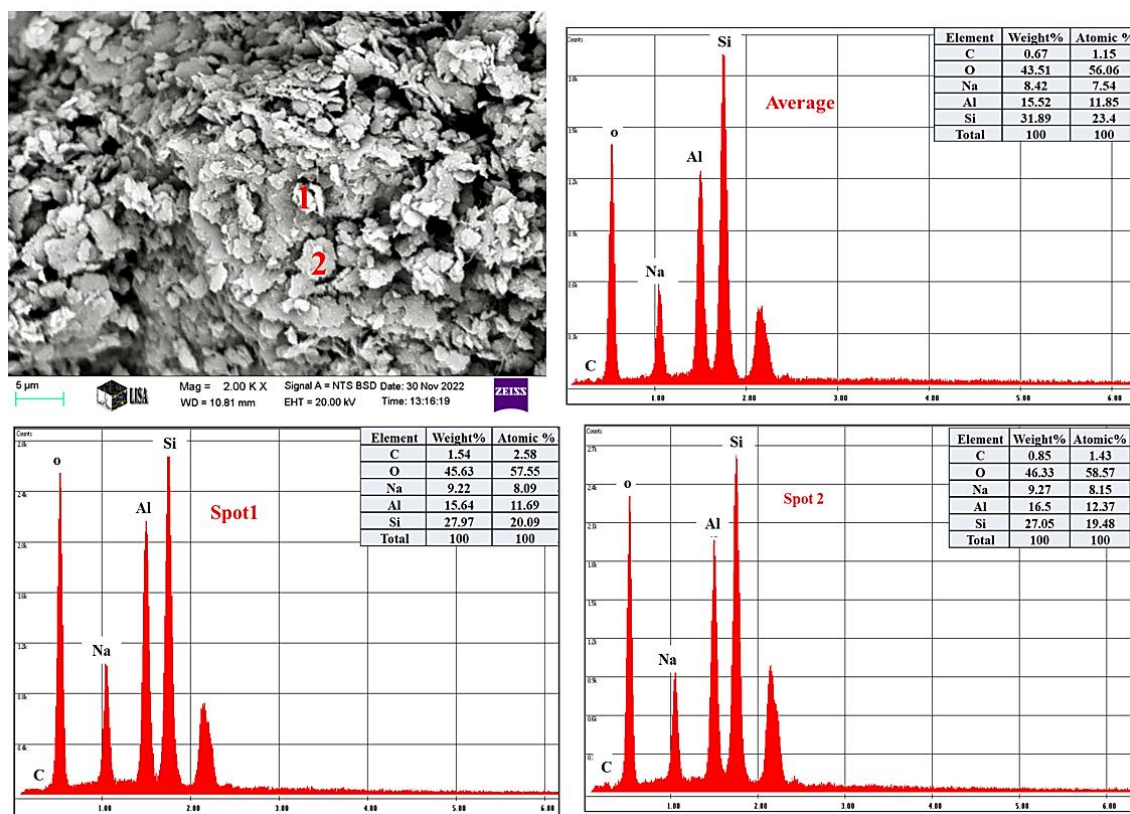
Figure 57. SEM and EDX analysis for MK-GP50 cured at 75 °C.

The micrograph shows two distinct regions: the first has a Si/Al ratio of 1.79 and a Si/Na ratio of 3.03, while the second, containing the unreactive metakaolin, has a Si/Al ratio of 1.63 and a Si/Na ratio of 2.91.

The average Si/Al weight ratio is 2.05, while the Si/N weight ratio is 3.17. Since the reaction is faster and stronger at higher temperatures, the Si/Al and Si/Na ratios were higher for the samples cured at 75 °C than those cured at 60 °C.

3.2.5 Fourier Transform Infrared Spectroscopy (FTIR)

Figure 58. shows the FTIR spectra of the samples (MK-GP0, MK-GP25, MK-GP50, MK-GP75, and MK-GP100) cured at 60 °C for one day and at room temperature for 27 days. The characteristic peaks are summarised in Table 15.
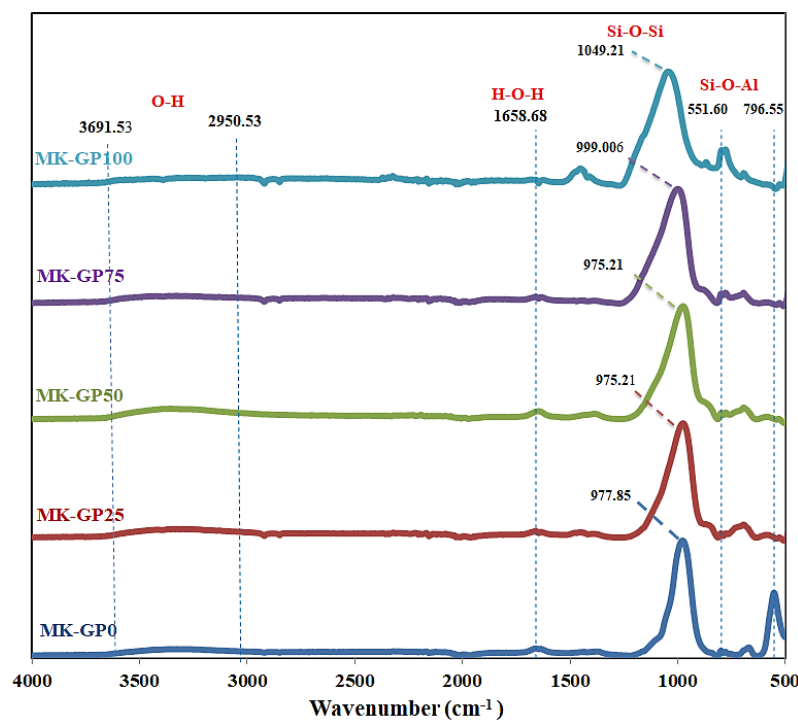
Figure 58. FTIR spectra of MK-GP cured at 60 °C with different water glass dosages of the activator solution.

Table 15. FTIR bands observed on the investigated samples

Peak wavenumber (cm^{-1})	Identification [99][151]
3691.53 - 2950.53	Stretching hydrogen-bonded O-H
1658.68	Chemical vibrations of water H-O-H
1094.21-999.006 - 975.21- 977.85	Deforming vibrations Si-O
796.55	Stretching vibration Al-O
551.60	Bending vibrations Si-O

According to the results of the FTIR tests, the wavenumber range 3691.53 to 2950.53 cm^{-1} and the wavenumber value 1656.68 cm^{-1} originated from O-H valence and H-O-H deformation vibrations of the adsorbed water. The strength of these bonds showed an inverse correlation with the amount of water glass present [152]. The bands at 1100 cm^{-1} and 900 cm^{-1}, which belong to the stretching of the Si-O bonds, are shifted to higher wavenumbers as the water glass content increases. The shape of these bands changes due to structural arrangements in the geopolymer caused by the change in NaOH content in the activator solutions. When using high dosage for water glass, the Si-O stretching of tetrahedra, in which the silicon is surrounded by three bridging oxygen units and one non-bridging oxygen, is more pronounced [153]. The structure is the building block of the Si-O-X (X = Si, H, O) geopolymer. A shift of the Si-O-X stretching band to lower wavenumbers when sodium hydroxide content increases, shows lengthening of the Na or H bonds and shrinkage of the bond angle [154]. The prominent peaks of the Si-O band in the geopolymer binder without

water glass (0 wt.%) appeared at 977.85 cm^{-1}, while those in the samples containing 25 wt.% and 50 wt.% water glass were observed at 975.2 cm^{-1}.

The Si-O bond shifts to the left as the water glass content increases at 75 wt.% and 100 wt.% water glass at 999.006 cm^{-1} and 1049.21 cm^{-1}, respectively. Based on previous scientific works [152, 155] the range of 800- 550 cm^{-1} contains the bands corresponding to the vibrational bonds of the secondary building blocks and represents the fingerprint of the geopolymer structure. The production of these rings is the result of the combination of SiO$_4$ and an AlO$_4$ tetrahedron. The peak at 796.98 cm^{-1} indicates Al-O geopolymer bonding, in which the glassy component of metakaolin reacts with the alkaline activator to produce a new product, the geopolymer gel [155].

3.2.6 XRD phase analysis

Figure 59. illustrates the results of XRD diffraction analysis of MK-GP samples cured at 60 °C with different water glass dosages of the activator solution.
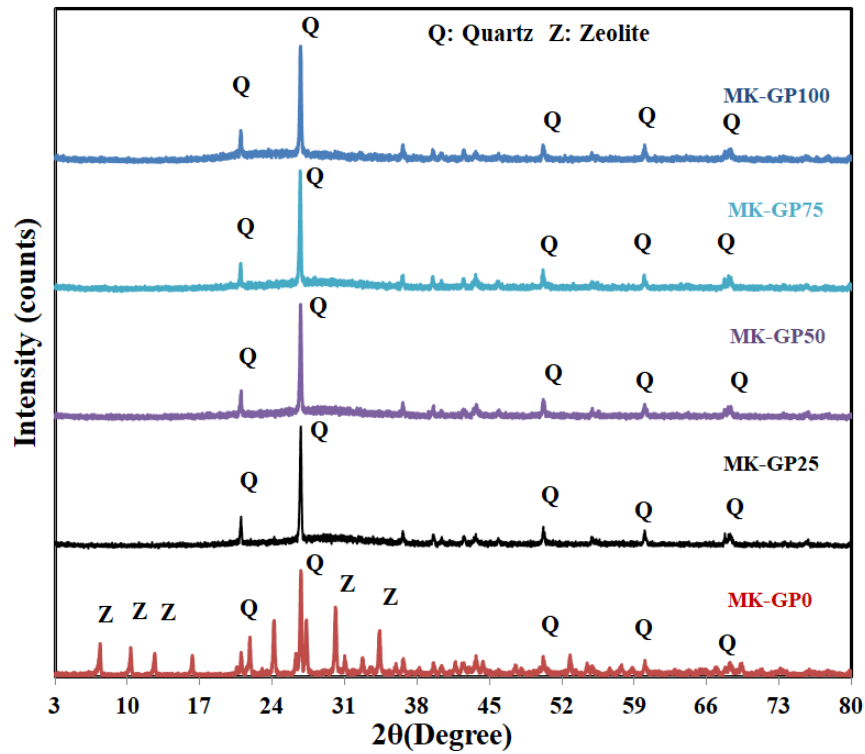
Figure 59. X-ray diffraction of MK-GP cured at 60 °C with different water glass dosages of the activator solution.

The low quartz diffraction peak is visible in the XRD pattern in all samples. The XRD pattern of the samples MK-GP75, MK-GP50, and MK-GP25 shows the typical broad peak at around 28°-36° 2θ, which is the fingerprint of N-A-S-H (*sodium alumino-silicate hydrate*) thought to be the defining characteristic of the diffractogram of all geopolymer [156, 157]. The XRD pattern of the sample MK-GP0 shows several diffraction peaks that can be assigned to the

57

artificial zeolite ($Na_{96}Al_{96}Si_{96}O_{384}.216H_2O$), proving that it is not a geopolymer. The literature has reported that the alkaline activation of metakaolin at elevated temperatures leads to the crystallization of zeolitic phases [149, 158].

3.2.7 Thermal conductivity

The standard value for the thermal conductivity of normal OPC concrete is usually between 1.4-3.6 W/m·K. In comparison, the measured thermal conductivity of MK-GP has lower values in the range of 0.09-0.39 W/m·K. This is one of the main advantages of geopolymer [159]. The thermal conductivity of geopolymer depends on various factors, including chemical composition and density. Typically, materials with higher density also have a higher thermal conductivity value due to the densely packed atoms or molecules, which allows for more efficient heat transfer, but higher density does not necessarily mean higher thermal conductivity in all cases. The thermal conductivity results are shown in Figure 60.
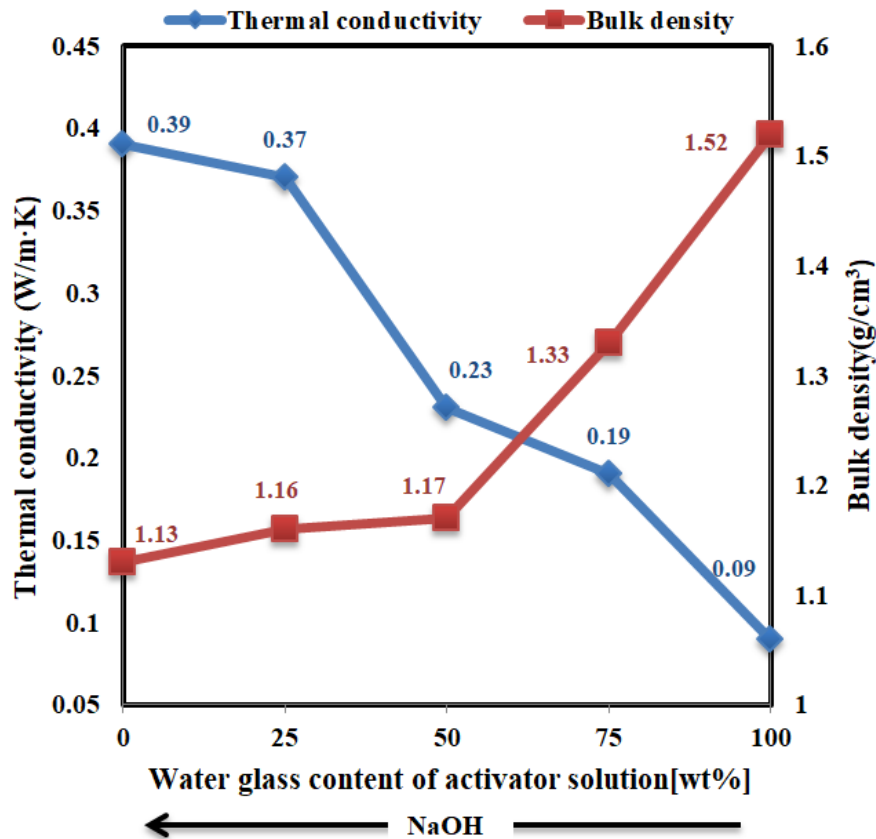
Figure 60. The thermal conductivity values are inversely related to the bulk density of MK–GP.

The value of thermal conductivity is inversely proportional to the bulk density and increases with increasing NaOH content, which is due to the NaOH effect because it contains free ions: Na^+ and OH^- and is, therefore, conductive [160]. When the NaOH content increases, the thermal conductivity also increases, and the bulk density decreases. The sample MK-

GP100 had a higher density of 1.52 g/cm^3 and a lower thermal conductivity of 0.09 W/m·K and the sample MK-GP0 had a lower bulk density and higher thermal conductivity of 0.39 W/m·K. Jaya et al. [161] studied the thermal conductivity at various molarities between 8 M and 14 M. The lowest value, 0.71 W/m·K, was found to be measured at 8 M, and the highest value, 0.97 W/m·K, was discovered to be measured at 14 M. Wongkeo et al. [162] investigated the thermal conductivity for lightweight geopolymer concrete with different NaOH dosages.

3.3 Results and discussion of MK-GP made with different liquid-to-solid ratios and cured at 60 °C and room temperature[3]

Based on the findings from sub-chapter 3.2, this section explores the preparation of the geopolymer binder using a Na_2SiO_3/NaOH ratio of 1, cured at both 60 °C and room temperature, with varying liquid-to-solid ratios of 0.8, 0.95, and 1.1.

3.3.1 Bulk density

The bulk density of the geopolymer binders in samples that were cured at two different temperatures and had different liquid-to-solid ratios was measured. As shown in Figure 61., the bulk density range of the binders cured at 60 °C for 24 hours was 1.172-1.295 g/cm^3, and that of the binders cured at room temperature was 1.213-1.42 g/cm^3.
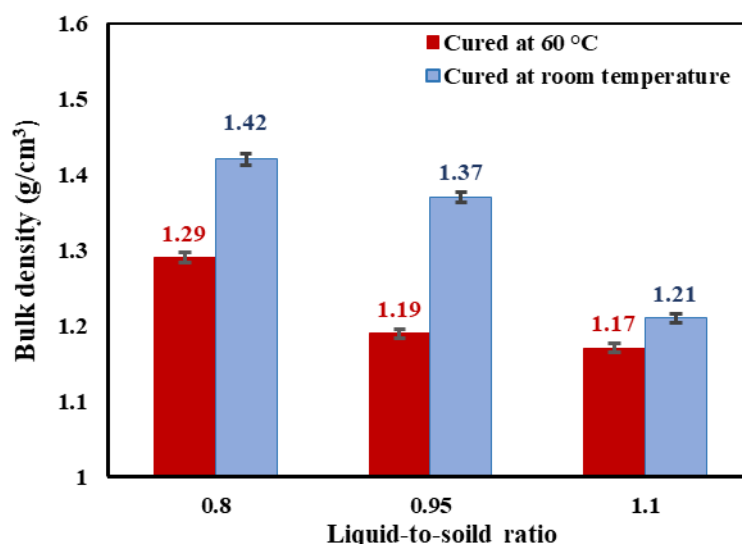
Figure 61. Bulk density of geopolymer binders with different liquid-to-solid ratios cured at two different temperatures.

As the curing temperature increases, the binder density decreases due to increased moisture loss during polymerization. It is necessary to prevent water loss before the binder is

---

completely cured [144]. Note that the bulk density of the binders reduces with the increase of the liquid-to-solid ratio. The highest density was 1.42 g/cm^3 for the sample with a liquid-to-solid 0.8 ratio (cured at room temperature). When the liquid-to-solid ratio in geopolymers is higher, pores are formed, particles are not packed tightly enough, the volume of the sample shrinks more, and the porosity increases. All these factors lead to a notable reduction in the binder's density [165].

3.3.2 Compressive strength

In this work, the metakaolin-based geopolymer achieved its maximum compressive strength for samples cured at room temperature by adjusting the amount of the liquid-to-solid ratio and kaolin calcination temperature depending on previous works [116]. The compressive strength of the geopolymer binders cured for 28 days is presented in Figure 62.
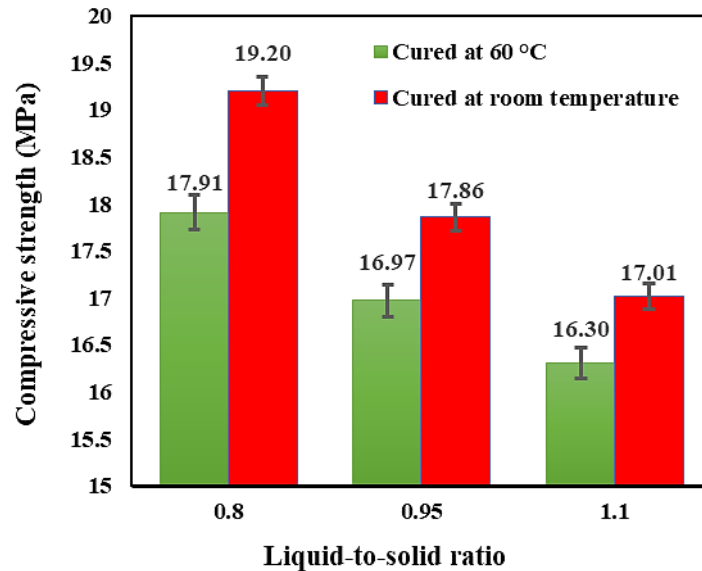
Figure 62. Compressive strength of geopolymer binders with different liquid-to-solid ratios cured at two different temperatures

The compressive strength range of the binders cured at 60 °C for 24 hours and 27 days at room temperature was 16.3-17.91 MPa, and that of the binders cured at room temperature for 28 days was 17.01-19.2 MPa. The compressive strength of the binders was influenced by the ratios of liquid-to-solid components. The highest strength recorded was 19.20 MPa, observed in samples with a liquid-to-solid ratio of 0.8, cured at room temperature. Increasing the solid content in geopolymer binders mainly improves the mixture by good packing, enhanced chemical reaction, and reduced porosity, all which factor in improving compressive strength. According to previous work, poor workability of the fresh paste and the reduction of compressive strength of the hardened binder were observed when the liquid-

to-solid ratio was less than 0.4, This happened because the amount of activator solution was insufficient to complete the polymerization process [163, 164].

3.3.3 Setting time

Both initial and final setting times were measured for geopolymer binders cured at room temperature with different liquid-to-solid ratios, as shown in Figure 63.
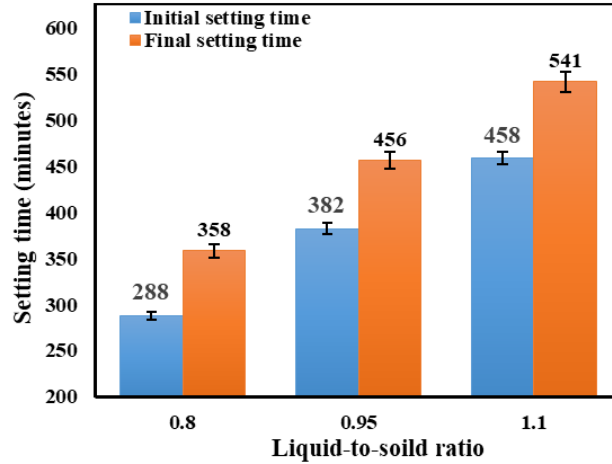
Figure 63. Setting time of geopolymer binders with different liquid-to-solid ratios cured at room temperature.

It was found that the setting times for the geopolymer binder decreased as the liquid-to-solid ratio decreased. The shortest initial setting time was recorded at 288 minutes, and 358 minutes for the final setting for the geopolymer binder with a 0.8 liquid-to-solid ratio. This was due to the increased mixture viscosity leading to the delayed formation of geopolymer gel [165]. The standard setting times of ordinary Portland cement are: the initial setting time should be more than 45 minutes, and the final setting time should be less than 390 minutes. Regarding this matter, the sample with a liquid-to-solid ratio of 0.8 underwent setting within the specified standard setting time limit. This is one of the advantages of metakaolin-based geopolymers advantages their setting at room temperature is more rapid than fly ash-based geopolymers [166]. The ultimate final setting time of fly ash-derived geopolymer solidifying at room temperature is approximately 1800 minutes [167].

3.3.4. Thermal conductivity

Figure 64. presents the thermal conductivity values of geopolymer binders, which were in the range of 0.28-0.49 W/m·K for samples cured at room temperature with different liquid-to-solid ratios. As the liquid-to-solid ratio in a geopolymer binder increases, the thermal conductivity of the material reduces because of the decreased bulk density of the mixture. Denser materials generally have a greater thermal conductivity rating because their atoms and molecules are more closely packed, allowing for active heat transfer.
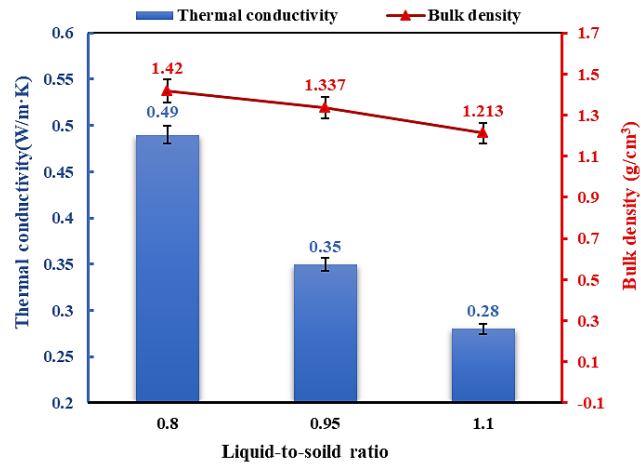
Figure 64. Thermal conductivity of geopolymer binders with different liquid-to-solid ratios cured at room temperature

3.3.5 Microstructure

Figure 65. illustrates the microstructural composition of the geopolymer binders.
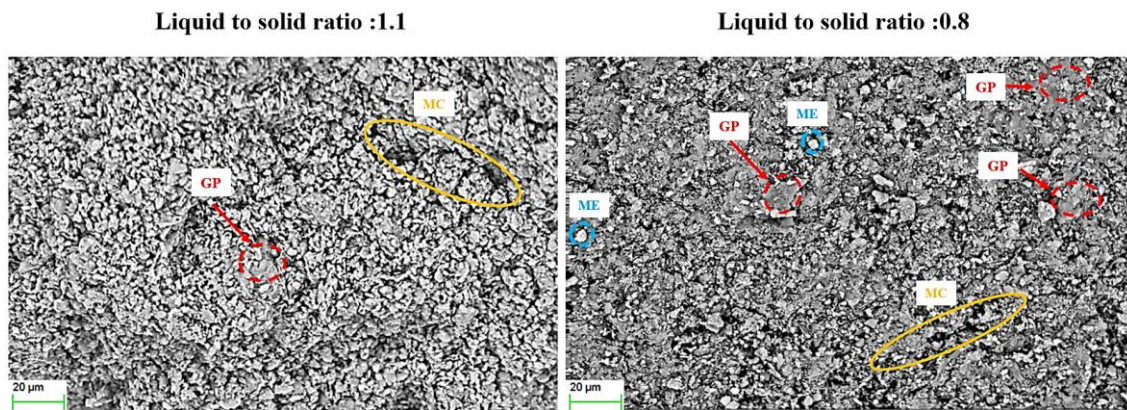
Figure 65. SEM micrographs of geopolymer binders with different liquid-to-solid ratios at magnifications 500x cured at room temperature (*GP: Geopolymer gel, MC: Micro crack, ME: metakaolin*)

The samples were made using two liquid-to-solid ratios: 1.1 and 0.8 cured at room temperature. The microstructure of the two samples displayed unreacted metakaolin and some microcracks in the gel matrix. In a sample with a lower liquid-to-solid ratio of 0.8, the resultant gel exhibited a comparatively denser and more uniformly structured composition characterized by reduced pore size. Conversely, in samples with a ratio of 1.1, geopolymer specimens displayed heightened occurrences of cracks and larger pores. Higher liquid-to-solid ratios in geopolymer binder formulations typically result in increased porosity. This phenomenon occurs because a greater amount of water is present, which facilitates the formation of voids within the binder matrix [163]. As a result, the overall porosity of the geopolymer tends to rise, potentially impacting properties such as strength, durability, and permeability.

3.4 Statistical analysis of metakaolin-based geopolymer characterisation

The statistical analysis aims to identify the key factors following water glass content, curing temperature, and liquid-to-solid ratio. That has the most significant impact on geopolymer performance. Additionally, the analysis is to develop a linear regression model to predict geopolymer properties, including bulk density, compressive strength, and thermal conductivity, according to input variables.

The data collected from previous studies on metakaolin-based geopolymer were systematically analysed and consolidated into a statistical model using the Minitab program. This model predicts the geopolymer binder's bulk density, compressive strength, and thermal conductivity through a multilinear regression approach based on three key variables, as detailed in Table 16. A comprehensive summary of the experimental procedures and results is presented in Table 17.

Table 16. Geopolymer binder variables.

Variables name	Level values
Water glass dosage (wt.%)	0; 25; 50; 75 and 100
Curing temperature (°C)	75; 60; and 25 (*room temperature*)
Liquid-to-solid ratio	0.8; 0.95 and 1.1

Table 17. A summary of the results of the experiments on metakaolin-based geopolymers.

Number of runs	Water glass dosage (wt.%)	Curing temperature (°C)	Liquid-to-solid ratio	Bulk density (g/cm³)	Compressive strength (MPa)	Thermal conductivity (W/m·K)
1	0	75	1.1	1.05	8.51	0.41
2	25	75	1.1	1.11	8.33	0.38
3	50	75	1.1	1.12	11.01	0.26
4	75	75	1.1	1.15	8.67	0.20
5	100	75	1.1	1.33	9.02	0.10
6	0	60	1.1	1.13	10.71	0.39
7	25	60	1.1	1.16	11	0.37
8	50	60	1.1	1.17	16.3	0.23
9	75	60	1.1	1.33	12.72	0.19
10	100	60	1.1	1.52	12.46	0.09
11	50	60	0.95	1.19	16.97	0.33
12	50	60	0.8	1.29	17.91	0.41
13	50	25	1.1	1.21	17.01	0.28
14	50	25	0.95	1.37	17.86	0.35
15	50	25	0.8	1.42	19.2	0.49

3.4.1 Statistical analysis for bulk density

Table 18. summarizes the results of an Analysis of Variance (ANOVA) for a regression model of geopolymer bulk density with the effect of three factors: water glass dosage, curing temperature, and liquid-to-solid ratio.

Table 18. Statistical analysis of geopolymer bulk density (g/cm^3).

Source	DF	Seq SS	Contribution	Adj SS	Adj MS	F-Value	P-Value
Regression	3	0.085258	86.00%	0.085258	0.028419	12.28	0.006
Water glass dosage (wt.%)	1	0.065073	65.64%	0.057455	0.057455	24.83	0.002
Curing temperature (°C)	1	0.012456	12.56%	0.008195	0.008195	3.54	0.109
Liquid-to-solid ratio	1	0.007728	7.80%	0.007728	0.007728	3.34	0.117
Error	6	0.013884	14.00%	0.013884	0.002314	----	----
Total	9	0.099142	100.00%	----	----	----	-----

The regression model is statistically significant (*F-Value=12.28, P-Value=0.006, contribution error=14%)*. This indicates that the predictors, collectively, explain a significant portion (86%) of the variation in the response variable. The remaining 14% is unexplained and attributed to random error or factors not included in the model. The water glass dosage factor has the largest impact on the response, contributing 65.64% of the total variation. Curing temperature explains 12.56% of the variation, the second highest among the predictors. Liquid-to-solid ratio factor contributes the least to the model, accounting for 7.80% of the variation.

The Pareto chart provides a graphical representation of the standardized effects of the predictors on the response variable (*Bulk Density in g/cm^3*) at a significance level as shown in Figure 66.
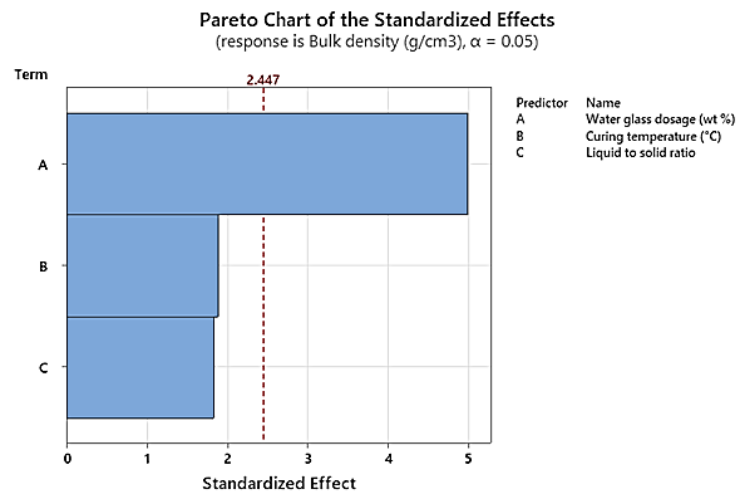
Figure 66. Pareto chart of geopolymer bulk density.

The red dashed line represents the critical value of 2.447, indicating the minimum effect size required for a predictor to be statistically significant at a 95% confidence level (α=0.05). Predictors with effects exceeding this threshold are considered significant, meaning they have a meaningful impact on the response variables. The critical value is derived from the t-distribution based on the chosen significance level (α=0.05) and degrees of freedom (DF=6), ensuring the reliability of the regression model in evaluating geopolymer properties.

The Pareto chart visually confirms that water glass dosage (A) is the most critical factor for bulk density while curing temperature (B) and liquid-to-solid ratio (C) show weaker, non-significant effects in the current model.

The 3D surface plot (Figure 67.) illustrates the relationship between the bulk density of geopolymer materials and two key variables: water glass content and curing temperature.
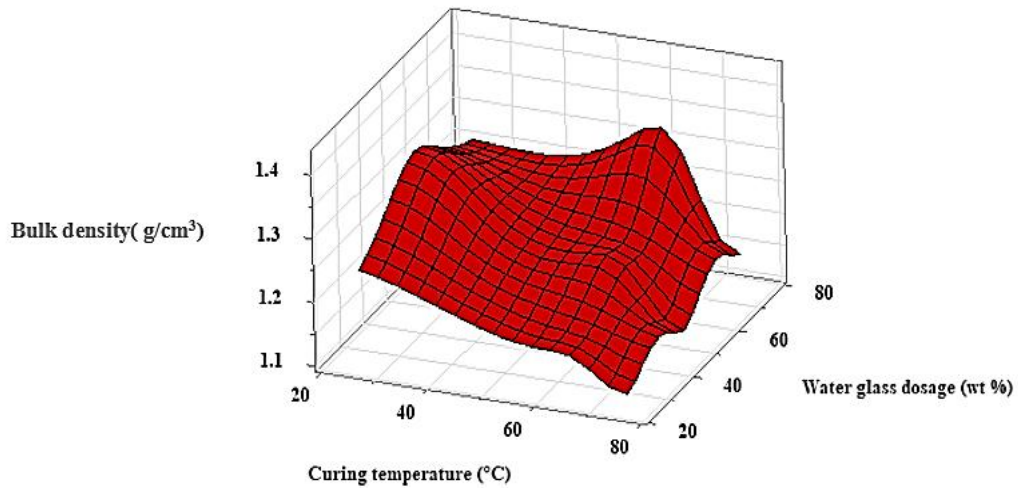
Figure 67. 3D surface plot of geopolymer bulk density with two variables (water glass content and curing temperature)

The plot reveals how variations in these factors influence bulk density, highlighting optimal ranges where the highest density is achieved. A regression equation is a mathematical model that describes the relationship between geopolymer bulk density and the three independent variables, according to regression coefficients (Table 19.), as follows:

$$\textit{Bulk density (g/cm}^3\textit{)} = 1.478 + 0.002920 \cdot \textit{Water glass dosage (wt.\%)} -0.001681 \cdot \textit{Curing temperature (°C)} - 0.286 \cdot \textit{Liquid to solid ratio} \pm \textit{error} \qquad (17)$$

Table 19. Regression coefficients of geopolymer bulk density.

Term	Coef.	SE Coef.	95% CI	T-Value	P-Value
Constant	1.478	0.165	(1.074, 1.882)	8.95	0.001
Water glass dosage (wt.%)	0.002920	0.000586	(0.001486, 0.004353)	4.98	0.002
Curing temperature (°C)	-0.001681	0.000893	(-0.003867, 0.000505)	-1.88	0.109
Liquid-to-solid ratio	-0.286	0.157	(-0.670, 0.097)	-1.83	0.117

The error percentage for the average readings was calculated to be 4.023%, well below the 5% threshold. As shown in Table 20., this indicates a high level of accuracy and reliability in the measurements, as shown in Figure 68., the relationship between the calculated and measured bulk density.

Table 20. Measured and calculated along with the error percentage for the geopolymer bulk density (g/cm^3).

Number of runs	Measured value	Calculated value	Error % (±)
1	1.05	1.0373	1.2071
2	1.11	1.1103	0.0292
3	1.12	1.1833	5.6540
4	1.15	1.2563	9.2456
5	1.33	1.3293	0.0507
6	1.13	1.0625	5.9699
7	1.16	1.1355	2.1086
8	1.17	1.2085	3.2940
9	1.33	1.2815	3.6436
10	1.52	1.3545	10.8855
11	1.199	1.2514	4.3736
12	1.29	1.2943	0.3364
13	1.213	1.2673	4.4826
14	1.37	1.3102	4.3594
15	1.42	1.3531	4.7059
Average error (%)			4.0231
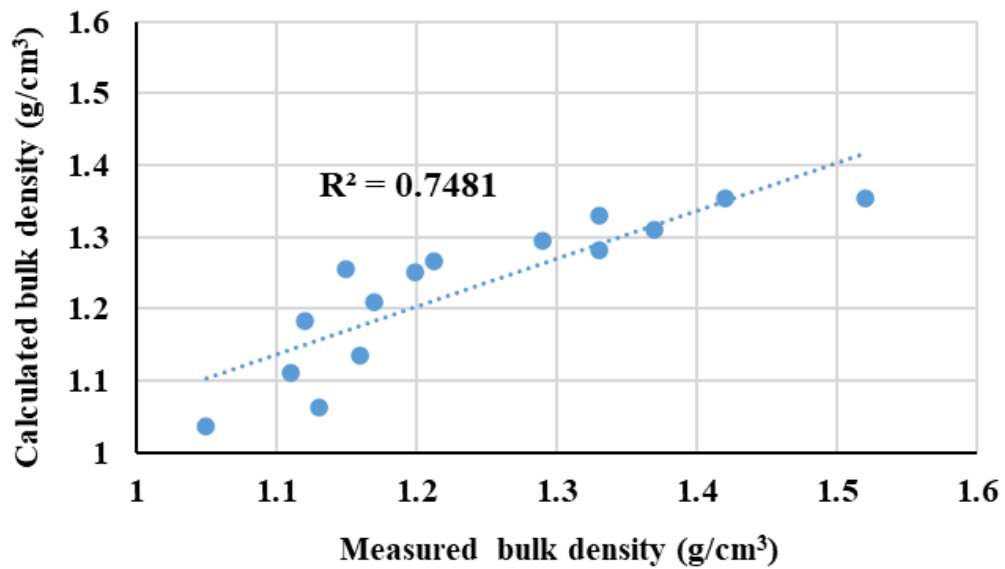
Figure 68. Relationship between the calculated and measured geopolymer bulk density

3.4.2 Statistical analysis for compressive strength

Table 21. presents the results of a regression analysis for geopolymer compressive strength.

Table 21. Statistical analysis of geopolymer compressive strength.

Source	DF	Seq SS	Contribution	Adj SS	Adj MS	F-Value	P-Value
Regression	3	117.773	78.95%	117.773	39.258	7.50	0.019
Water glass dosage (wt.%)	1	5.832	3.91%	1.791	1.791	0.34	0.580
Curing temperature (°C)	1	76.143	51.04%	52.793	52.793	10.09	0.019
Liquid-to-solid ratio	1	35.798	24.00%	35.798	35.798	6.84	0.040
Error	6	31.404	21.05%	31.404	5.234	----	----
Total	9	149.177	100.00%	----	----	----	-----

The overall regression model is statistically significant, with an F-value of 7.50 and a p-value of 0.019. Among the factors, curing temperature has the greatest influence on the response, explaining 51.04% of the total variation. The liquid-to-solid ratio follows, contributing 24% of the variation, while water glass dosage has the smallest impact, accounting for only 3.91% of the variation. A Pareto chart provides graphical proof of this (Figure 69.).
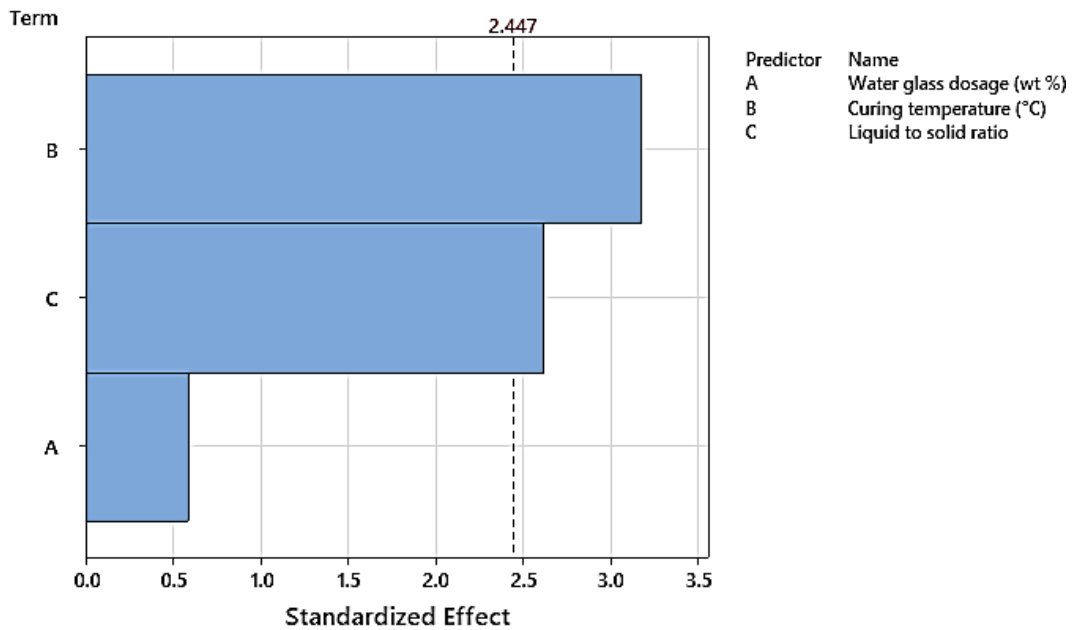
Figure 69. Pareto chart of geopolymer compressive strength.

Based on the statistical analysis for geopolymer compressive strength, curing temperature and liquid-to-solid ratio are identified as the most influential factors. The 3D surface plot (Figure 70.) visually depicts the relationship between these variables and the compressive strength of geopolymer materials.
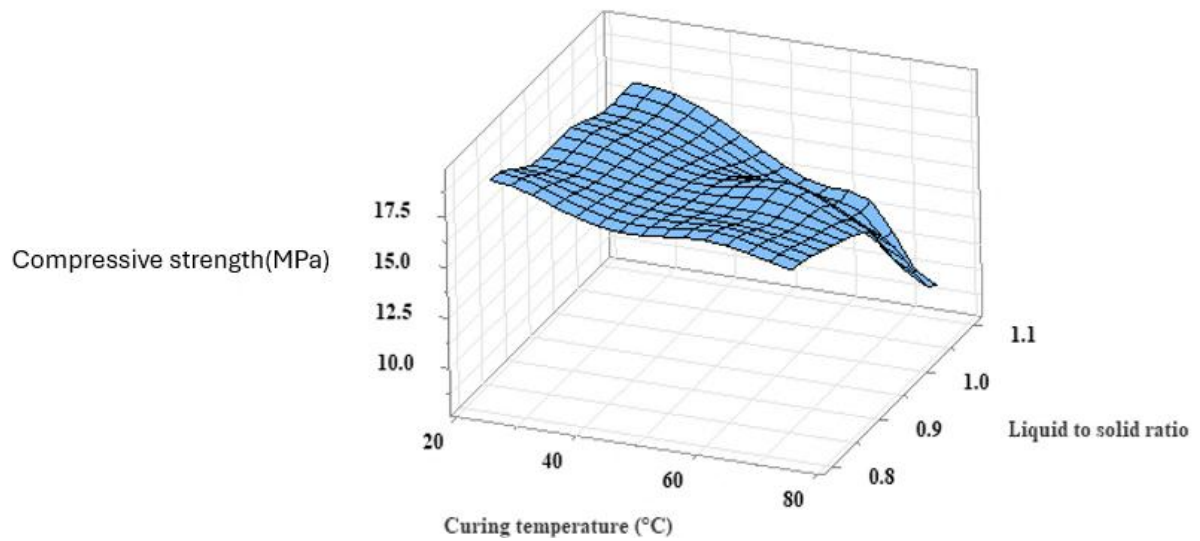
Figure 70. 3D surface plot of geopolymer compressive strength with two variables (*curing temperature and liquid-to-solid ratio*).

A regression equation is a mathematical model that defines the relationship between geopolymer compressive strength and the three independent variables, according to regression coefficients (Table 22.), expressed as follows:

$$\textit{Compressive strength (MPa)} = 40.81 + 0.0163 \cdot \textit{Water glass dosage (wt.\%)} - 0.1349 \cdot \textit{Curing temperature (°C)} - 19.49 \cdot \textit{Liquid-to-solid ratio} \pm \textit{error} \qquad (18)$$

Table 22. Regression coefficients of geopolymer compressive strength.

Term	Coef	SE Coef	95% CI	T-Value	P-Value
Constant	40.81	7.85	(21.60, 60.02)	5.20	0.002
Water glass dosage (wt.%)	0.0163	0.0279	(-0.0519, 0.0845)	0.59	0.580
Curing temperature (°C)	-0.1349	0.0425	(-0.2389, -0.0310)	-3.18	0.019
Liquid-to-solid ratio	-19.49	7.45	(-37.72, -1.25)	-2.62	0.040

Table 23. shows the error percentage for compressive strength readings. The error percentage for the average readings was 10.58%, depending on the references [168, 169] an error percentage of up to 20% in engineering applications is often considered acceptable due to the inherent complexity and natural variations in materials and processes, as shown in Figure 71., the relationship between the calculated and measured compressive strength.

Table 23. Measured and calculated data, along with the error percentage, for the geopolymer compressive strength (MPa).

Number of runs	Measured value	Calculated value	Error (%) (±)
1	8.51	9.253	8.7367
2	8.33	9.661	15.9783
3	11.01	10.068	8.5513
4	8.67	10.476	20.8304
5	9.02	10.883	20.6596
6	10.71	11.277	5.2941
7	11	11.684	6.2227
8	16.3	12.092	25.8159
9	12.72	12.499	1.7334
10	12.46	12.907	3.5874
11	16.97	15.015	11.5173
12	17.91	17.939	0.1619
13	17.01	16.813	1.1552
14	17.86	19.737	10.5095
15	19.2	22.660	18.0234
	Average Error (%)		**10.5851**
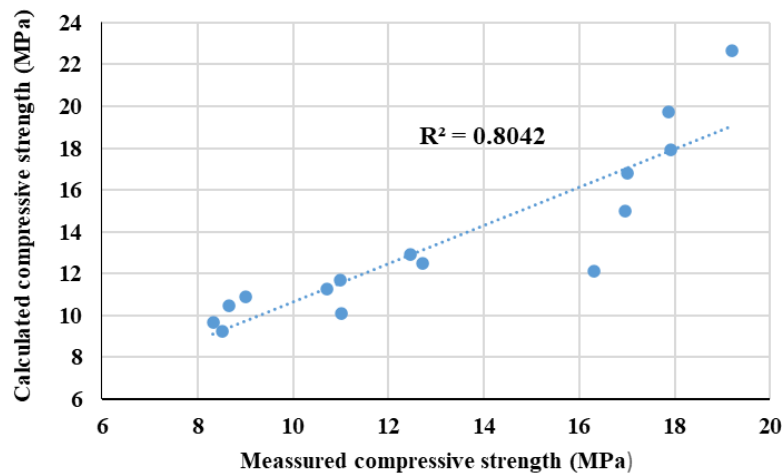
Figure 71. Relationship between the calculated and measured geopolymer compressive strength.

3.4.3 Statistical analysis for thermal conductivity

Table 24. shows the regression analysis of the geopolymer thermal conductivity.

Table 24. Statistical analysis of geopolymer thermal conductivity.

Source	DF	Seq SS	Contribution	Adj SS	Adj MS	F-Value	P-Value
Regression	3	0.096652	80.75%	0.096652	0.032217	8.39	0.014
Water glass dosage (wt.%)	1	0.067696	56.56%	0.070295	0.070295	18.31	0.005
Curing temperature (°C)	1	0.000003	0.00%	0.001416	0.001416	0.37	0.566
Liquid-to-solid ratio	1	0.028953	24.19%	0.028953	0.028953	7.54	0.033
Error	6	0.023038	19.25%	0.023038	0.003840		
Total	9	0.119690	100.00%				

The overall statistical model has an F-value of 8.39 and a p-value of 0.014. The water glass dosage and liquid-to-solid ratio had the most substantial, accounting for water glass dosage for 56.56% of the total variation, and the liquid-to-solid ratio contributed 24.19%, while curing temperature had no impact, with a contribution of 0%. This is further supported by the Pareto chart shown in Figure 72.
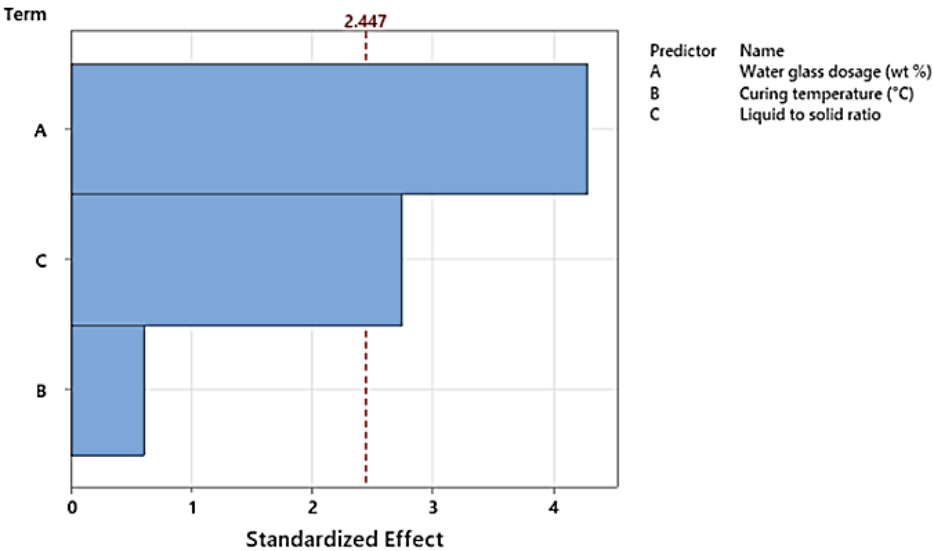
Figure 72. Pareto chart of geopolymer thermal conductivity.

Figure 73. represents the 3D surface plots for geopolymer thermal conductivity with influencing factors: water glass dosage and the liquid-to-solid ratio.
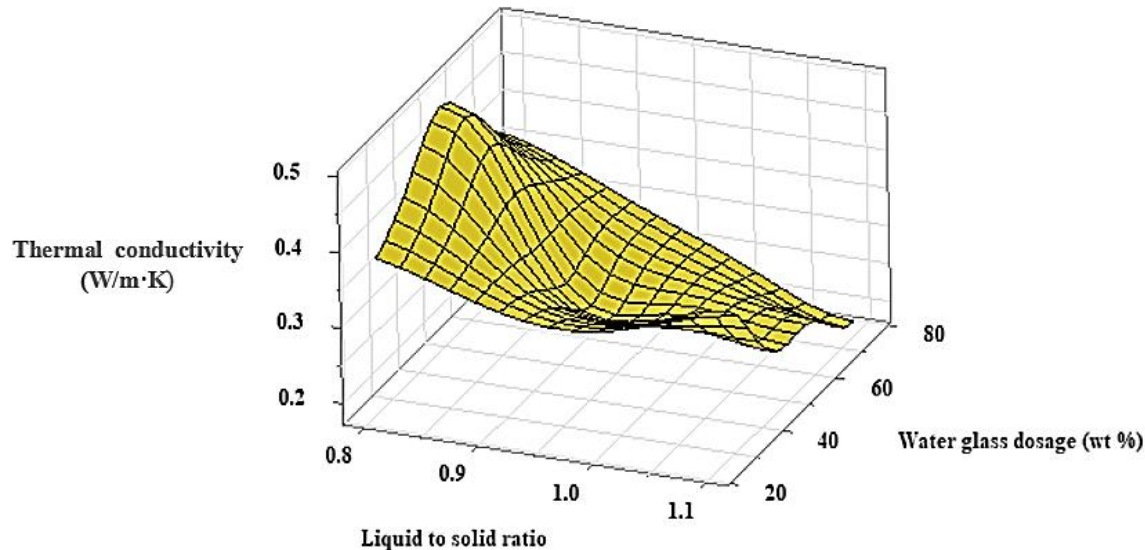
Figure 73. 3D surface plot of geopolymer thermal conductivity with two variables (*liquid-to-solid ratio and water glass dosage*)

A regression equation is a mathematical model that defines the relationship between geopolymer thermal conductivity and the three independent variables, according to regression coefficients (Table 25.), expressed as follows:

70

Thermal conductivity (W/m·K) = *0.981 - 0.003229 · Water glass dosage (wt.%) + 0.00070 · Curing temperature (°C) - 0.554 · Liquid-to-solid ratio ± error*   (19)

Table 25. Regression coefficients of geopolymer thermal conductivity

Term	Coef	SE Coef	95% CI	T-Value	P-Value
Constant	0.981	0.213	(0.460, 1.501)	4.61	0.004
Water glass dosage (wt.%)	-0.003229	0.000755	(-0.005076, -0.001383)	-4.28	0.005
Curing temperature (°C)	0.00070	0.00115	(-0.00212, 0.00351)	0.61	0.566
Liquid-to-solid ratio	-0.554	0.202	(-1.048, -0.060)	-2.75	0.033

The average error percentage of the geopolymer thermal conductivity readings was 7.47 % (Table 26.). Figure 74. shows the relationship between the calculated and measured thermal conductivity.

Table 26. Measured and calculated data, along with the error percentage, for the geopolymer thermal conductivity (W/m·K).

Number of runs	Measured value	Calculated value	Error (%) (±)
1	0.412	0.4241	2.9368
2	0.38	0.3433	9.6381
3	0.261	0.2626	0.6321
4	0.2	0.1819	9.0375
5	0.1	0.1012	1.2
6	0.39	0.4136	6.0512
7	0.37	0.3328	10.0337
8	0.23	0.2521	9.6304
9	0.19	0.1714	9.7763
10	0.09	0.0907	0.7777
11	0.331	0.3352	1.2839
12	0.412	0.4183	1.5412
13	0.28	0.2276	18.6964
14	0.35	0.3107	11.2142
15	0.49	0.3938	19.6224
Average Error			**7.4715**
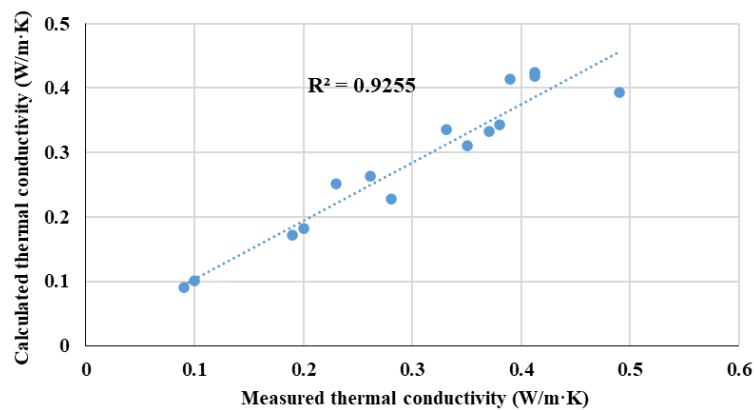
Figure 74. Relationship between the calculated and measured geopolymer thermal conductivity.

3.5 Characterisation of lightweight geopolymer with foam glass aggregate (LWGP-FGA)

Based on the results of the previous sub-chapters, the geopolymer binder was used to produce LWGP_FGA (water glass/NaOH ratio was 1, L/S ratio was 0.8, sodium hydroxide molarity 10 M, and cured at room temperature). Foam glass aggregate, sintered at temperatures of 750°C, 775°C, and 800°C, was used in the production of LWGP-FGA.

3.5.1 Bulk density and compressive strength[4]

Figure 75. shows the results of the bulk density and compressive strength for LWGP-FGA. The samples were measured after 28 days and cured at room temperature. LWGP-FGA had a bulk density range of 1.17-1.29 g/cm^3 and a compressive strength range of 8.02-19.2 MPa. These values comply with the requirements of LWC to classify the second group as *"Structural/Insulating"*. A big reduction was observed for compressive strength values reaching 53.18%, 52.56%, and 57.86% using FGA sintered at 750 °C, 775 °C, and 800 °C, respectively.
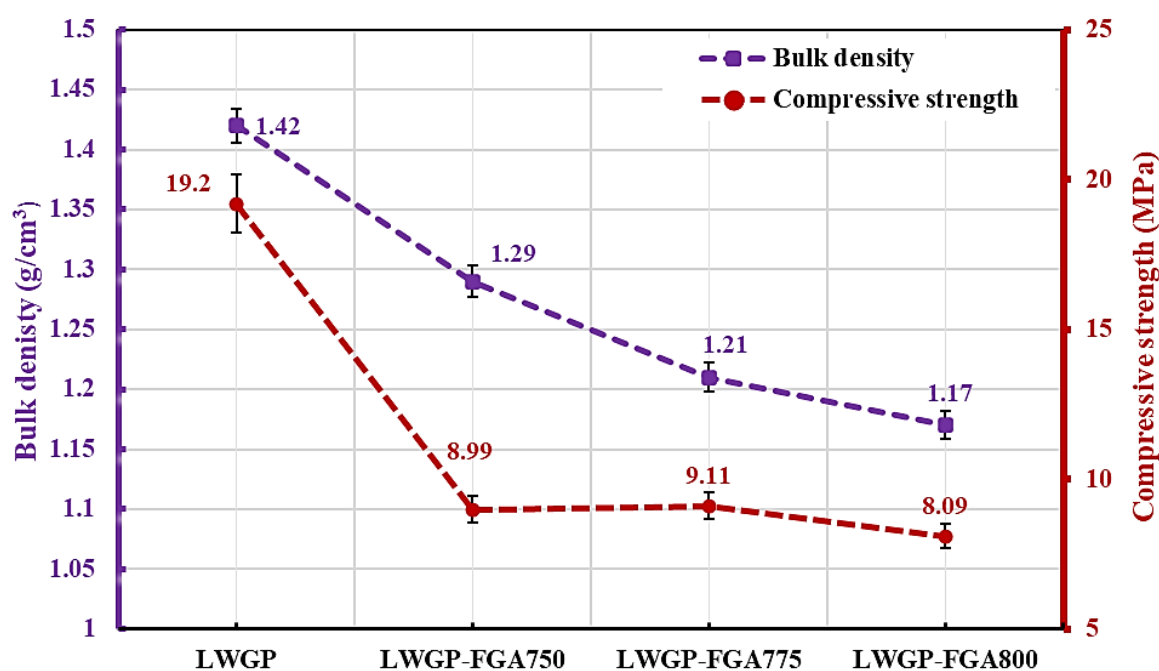
Figure 75. Bulk density and compressive strength results for LWGP-FGA.

The compressive strength of LWGP-FGA depended mainly on different factors, such as the compressive strength of the FGA, the interfacial adhesion of the aggregate grain to the geopolymer binder and the strength of the geopolymer binder. The cut cross-section area for LWGP-FGA, the sample LWGP-FGA750, shows the adhesion failure between the FGA and

---

geopolymer binder, which led to a weak contact surface around the FGA inside the geopolymer binder, therefore, the compressive strength was reduced (Figure 76.). The samples LWGP-FGA775 and LWGP-FGA800 show good binding between the geopolymer binder entered the FGA pores on the surface.

(A) LWGP-FGA750   **(B)** LWGP-FGA775   **(C)** LWGP-FGA800
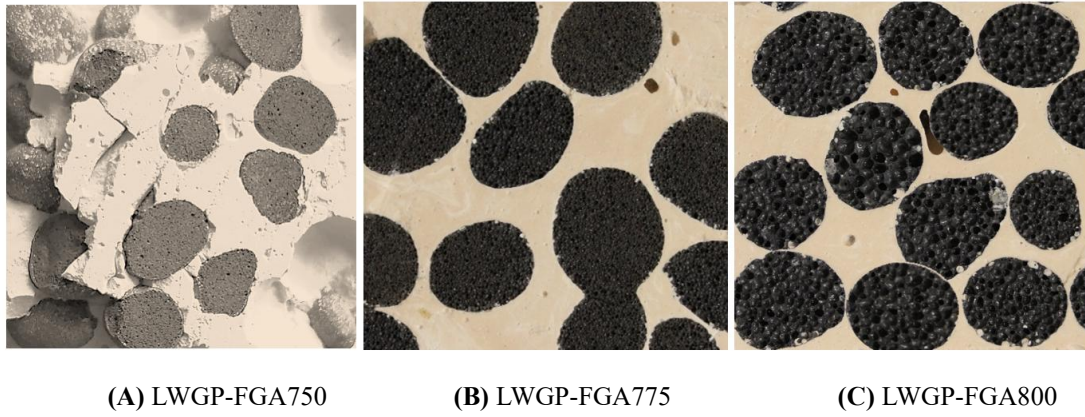
Figure 76. The failure surface of concrete, which can be used to determine the quality of adhesion/bond between the aggregate and the binder.

Figure 77. shows that fracture FGA surfaces differed significantly from each other. When lightweight geopolymer concrete incorporating FGA undergoes compressive loads, the force is transmitted from the geopolymer matrix to the FGA granules through the bonding at their interface. Note that in the LWGP-FAG750 samples, no crushing was observed because the stress transfer in the weak interface bond prevented the aggregate from being subjected to stress. As shown in the sample LWGP-FGA775, FGA was split and separated. The FGA in sample LWGP-FGA800 was crushed in the matrix due to adequate surface roughness, promoting mechanical interlocking and adhesion with the geopolymer paste, enhancing the bond strength.

Figure 77. The FGA fracture shape after the compressive test for LWGP.

3.5.2 The thermal conductivity

The thermal conductivity in the normal concrete structure is usually between 1.4 to 2.9 W/m·K. In contrast, according to ASTM standard [170], lightweight concrete typically has much lower values, generally ranging from 0.065 to 1.05 W/m·K. This lower thermal

conductivity is advantageous in such applications where thermal insulation is important: building envelopes used in walls, roofs and floors. They improve the energy efficiency of buildings by reducing the need for heating and cooling, and the lower thermal conductivity, as it slows down heat transmission [171]. Figure 78. shows the thermal conductivity results for LWGP-FGA.
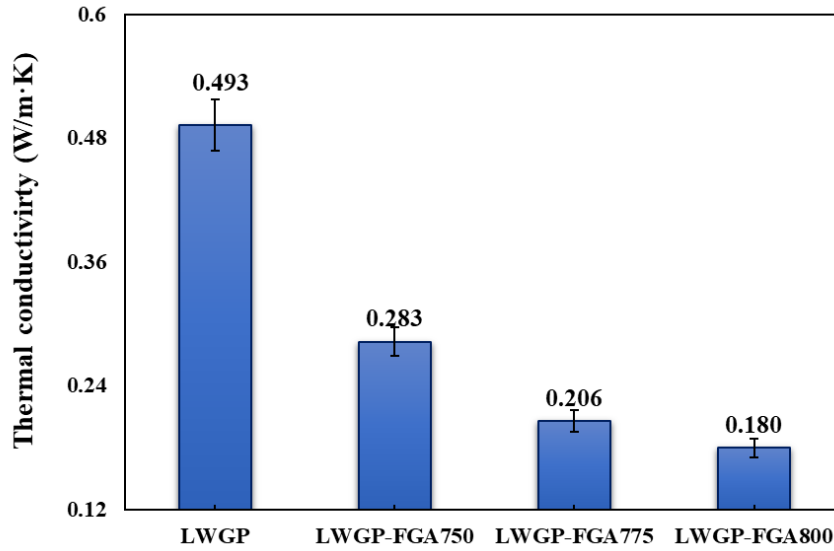
Figure 78. Thermal conductivity for LWGP-FGA and FGA.

The thermal conductivity of LWGP-FGA ranged between 0.18-0.283 W/m·K, by the standards required for lightweight concrete as insulation. The thermal conductivity of lightweight geopolymer concrete depends on the properties of the lightweight aggregate, like density, porosity, air voids, etc. [172].

LWGP-FGA800 exhibited a lower thermal conductivity value of 0.18 W/m·K, which can be attributed to the characteristics of the used FGA. The FGA itself had a thermal conductivity of 0.063 W/m·K and a bulk density of 0.58 g/cm³, both of which contributed to the reduced thermal conductivity of the lightweight geopolymer concrete.

3.5.3 Apparent porosity and water absorption

The apparent porosity and water absorption of hardened concrete are fundamental qualitative characteristics that are considered during the design phase of the concrete mix composition [173]. Apparent porosity significantly affects water absorption in lightweight geopolymers. The weak interface between the geopolymer matrix and foam glass aggregates creates additional voids and channels, facilitating greater water infiltration and absorption. Water absorption is crucial to concrete durability, particularly in environments subjected to freezing and thawing cycles. According to former scientific research, water absorption should be 4-6 wt.% to ensure high-quality concrete [174].

Figure 79. illustrates the apparent porosity and water absorption characteristics of LWGP-FGA.
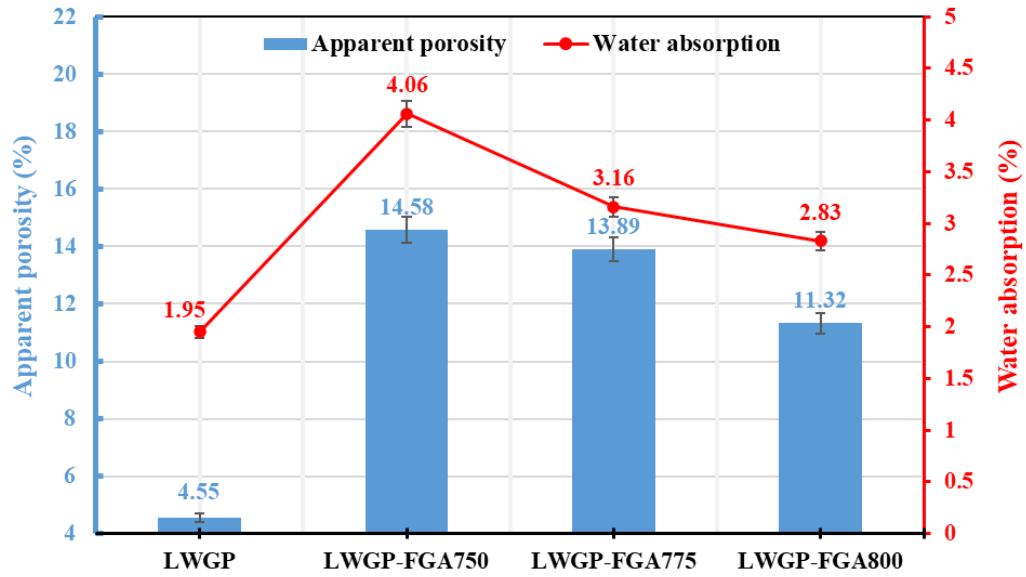
Figure 79. The apparent porosity and water absorption results for LWGP-FGA.

The apparent porosity range was 11.32-14.58 %, while water absorption varied from 2.83-4.06%. In comparison, the water absorption of the metakaolin-based geopolymer without FGA was significantly lower (1.95 %). A notable increase in water absorption was observed with the incorporation of FGA sintered at different temperatures, reaching values of 4.06 %, 3.16 %, and 2.83 % for FGAs sintered at 750 °C, 775 °C, and 800 °C, respectively. This indicates that the sintering temperature of FGA plays a critical role in influencing the characterisation behaviour of the geopolymer composite.

3.5.4 Freeze-thaw cycles test

The mechanism of freeze-thaw damage of lightweight geopolymers describes a series of processes [125]:

1) Water penetrates the pores, including the interfacial cavities between the geopolymer matrix and foam glass aggregates. After this, the temperature drops until the water freezes.

2) When water freezes, the volumetric expansion reaches 10 vol%, which leads to internal pressure within the confined pores of the geopolymer matrix.

3) The stress caused by ice formation may surpass the tensile strength, resulting in the initiation and propagation of microcracks. This microstructural damage weakens the material over time.

4) Due to repeated freeze-thaw cycles, the thawing water penetrates deeper into the material, aggravating the damage. This cyclic infiltration and freezing progressively erode the structural integrity of the geopolymer.

Figure 80. illustrates the weight loss of lightweight geopolymer samples subjected to multiple freeze-thaw cycles.
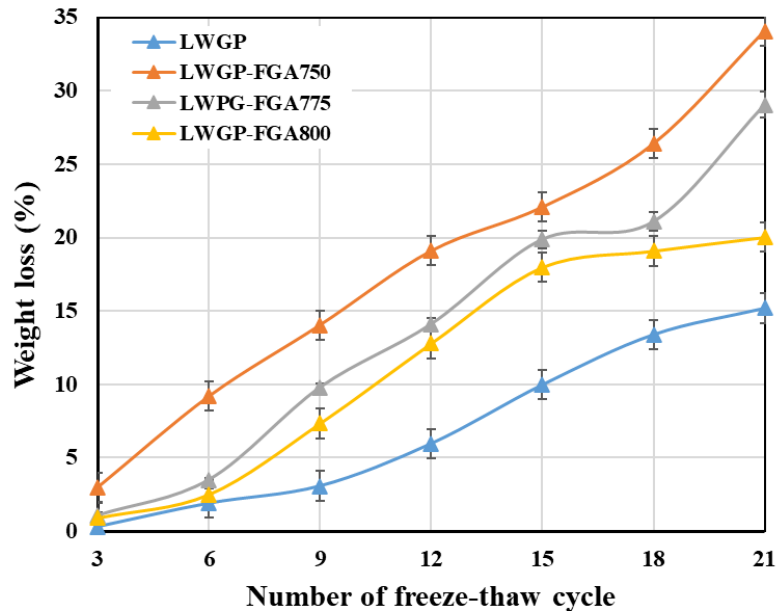
Figure 80. Weight loss of LWGP-FGA in freeze-thaw cycles

The results indicate that as the number of cycles increases, the weight loss becomes progressively more significant. Notably, sample LWGP-FGA750 exhibited the highest weight loss, reaching 34.09 wt.% after 21 cycles. This significant loss is likely attributed to the weak bonding between the geopolymer matrix and the foam glass aggregates. Additionally, the weight loss is observed to increase with apparent porosity.

Figure 81. presents images of lightweight geopolymer samples after numerous freeze-thaw cycles. The LWGP sample without foam glass aggregates exhibited the lowest weight loss, while visible surface peeling was observed on the LWGP-FGA775 and LWGP-FGA800 samples. In contrast, the LWGP-FGA750 sample experienced severe damage, with portions breaking off entirely.
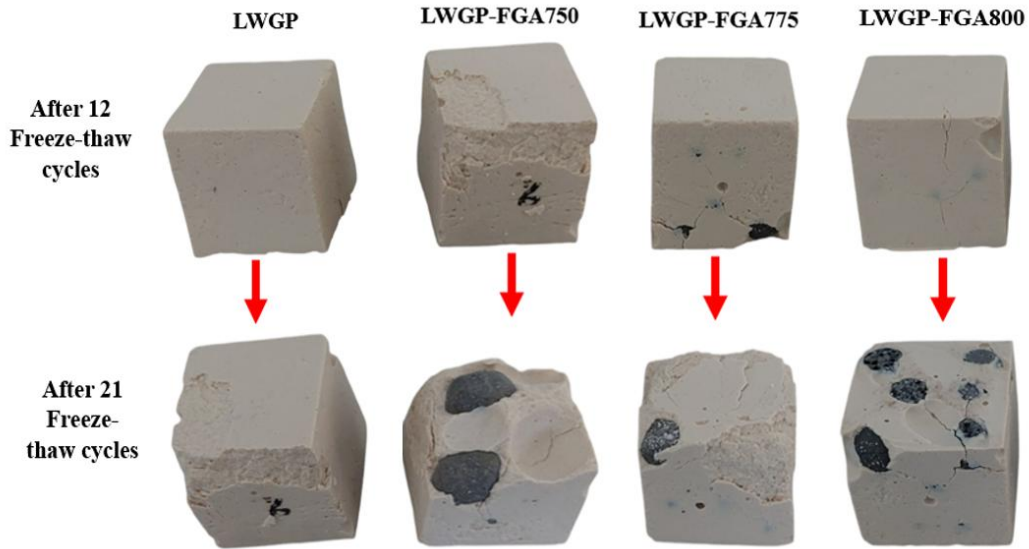
Figure 81. Illustration of LWGP-FGA after a numbers of freeze and thaw cycles.

Figure 82. shows the compressive strength of lightweight geopolymer samples before and after 21 freeze-thaw cycles. During the freeze-thaw cycles, the freezing temperature of -20 °C was set. It is important to note that outdoor conditions are generally less extreme than the controlled freeze-thaw cycles at -20 °C. As a result, the degradation in the compressive strength of lightweight geopolymer materials under natural outdoor conditions is expected to be less severe. The reduction in compressive strength of lightweight geopolymer specimens after 21 freeze-thaw cycles. The LWGP-FGA750 sample exhibited a substantial decline in compressive strength, with a decrease of 77.9%. The LWGP-FGA775 sample showed a reduction of 36.3%, while the LWGP-FGA800 sample experienced a decline of 32.5%. The geopolymer sample LWGP demonstrated a decrease of 29.84%.
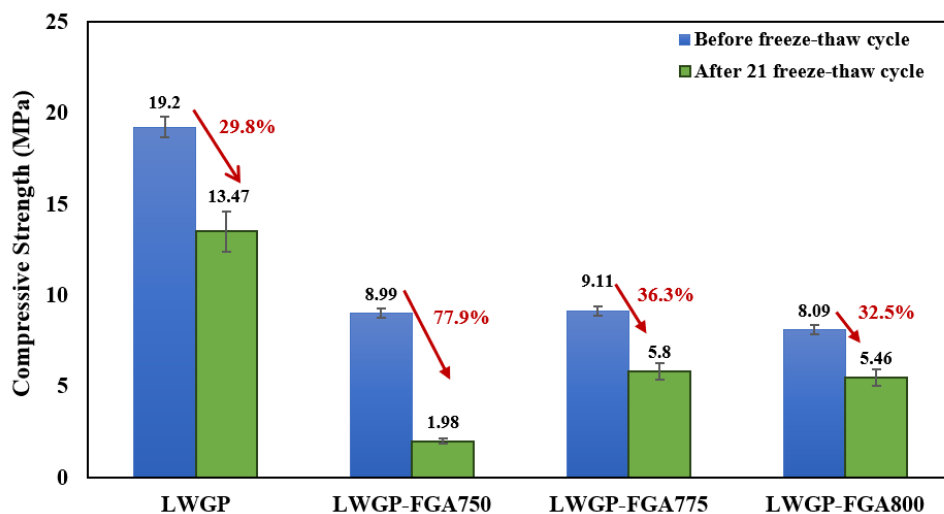
Figure 82. Compressive strength before and after 21 freeze-thaw cycles.

3.5.5 The correlation between the properties of LWGP-FGA and the properties of FGA

The correlations between LWGP-FGA and FGA properties were presented by using linear equations, where the y-axis is the LWGP-FGA properties, and the x-axis is FGA. Figure 83. shows the correlation between the bulk density of LWGP-FGA and FGA.
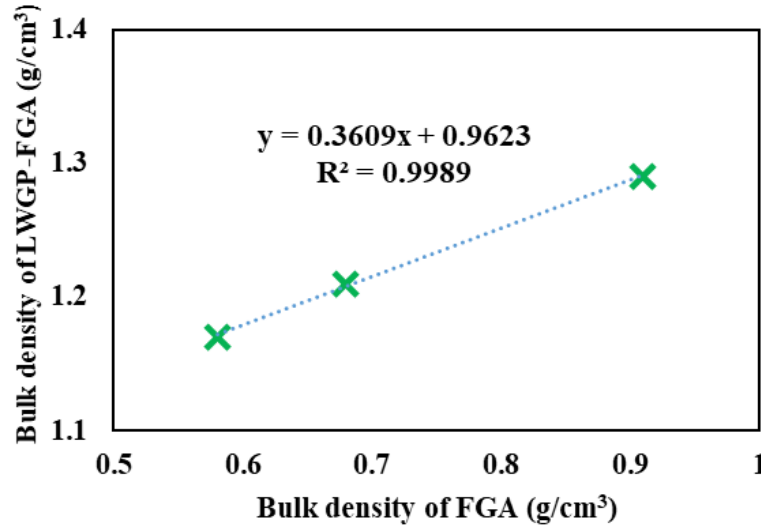
Figure 83. The relationship between the bulk density of LWGP-FGA and of FGA.

Here, a linear equation was used. The R^2 value of 0.9989 indicates an excellent fit between the variables. The positive slope (0.3609) suggests that as the bulk density of FGA increases, the bulk density of LWGP-FGA also increases.

Figure 84. shows the correlation between the compressive strength of LWGP-FGA and FGA. FGAs were made at the following temperatures: 750 °C, 775 °C and 800 °C.
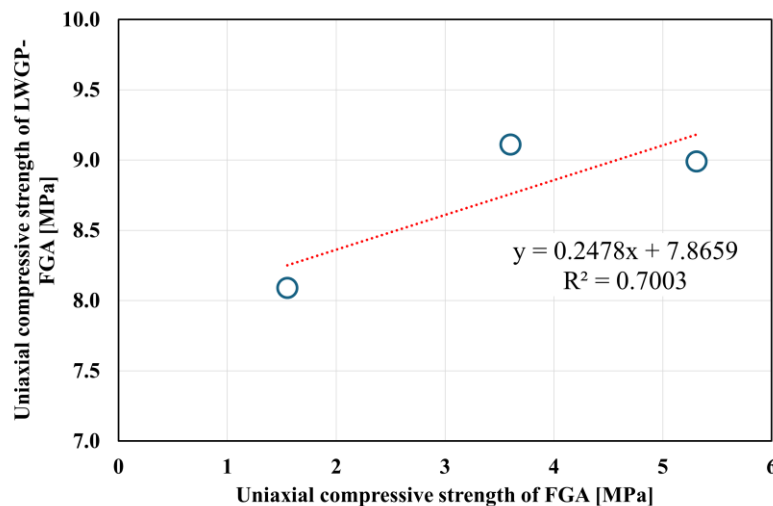
Figure 84. The relationship between the uniaxial compressive strength of LWGP-FGA and FGA.

Here, a linear equation was used. The R^2 value of 0.7003 indicates a moderate correlation between the two variables. The positive slope (0.2478) suggests that an increase in the

compressive strength of FGA results in an increase in the compressive strength of LWGP-FGA. However, the relatively low R^2 value means that factors other than the FGA compressive strength influence the LWGP-FGA compressive strength. It is a bond between the LWA and the geopolymer binder. Figure 85. shows the correlation between the thermal conductivity of LWGP-FGA and FGA.
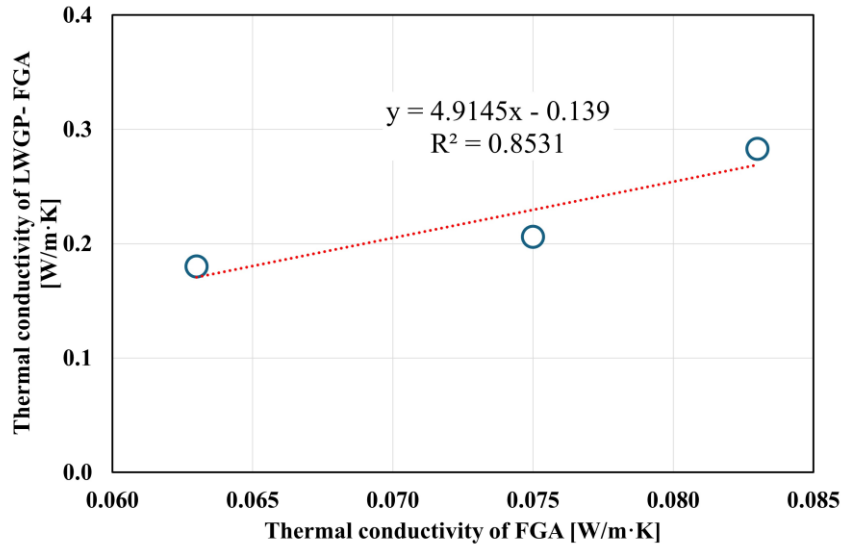
Figure 85. The relationship between the thermal conductivity of LWGP-FGA and FGA.

Here, a linear equation was used. The R^2 value of 0.8531 indicates a strong correlation between the two variables, which means that the thermal conductivity of FGA strongly affects the thermal conductivity of LWGP samples.

3.5.6 Comparison of LWGP characteristics and preparation conditions, previous scientific articles

According to studies published in the literature, different types of lightweight aggregates were used to prepare lightweight geopolymers or concrete. Table 27. compares the results of the prepared LWGP in this work with other researchers' studies. This work offers a low-energy, sustainable geopolymer composite using metakaolin and 30% foam glass aggregate, cured at room temperature. Its main advantages include energy-efficient curing, moderate strength (8.09–8.99 MPa), and low thermal conductivity (0.18–0.28 W/m·K), making it suitable for lightweight and insulating applications. The use of recycled FGA also supports sustainability.

Table 27. Presents the results of this study from previous research on the preparation of LWGP.

Geopolymer-based raw materials	Lightweight aggregate		Natural aggregate	Geopolymer conditions					Main properties			Ref.
	Type	(vol%)		Activator type	Molarity of NH (M)	NS/NH ratio	L/S ratio	Curing temperature (°C)	Bulk density (g/cm³)	Compressive strength (MPa)	Thermal conductivity (W/m·K)	
Metakaolin	FGA	30	-	NS+NH	10	1	0.8	RT	1.17-1.29	8.09-8.99	0.18-0.28	This work
Fly ash+ slag	Artificial	28	-	NH	8, 10, 12	-	1	65 °C for 24 hr.	1.21-1.41	2.54-15.47	0.22-0.46	[97]
Fly ash + furnace slag	Pumice, expanded clay	-	Fine	NS+NH	14	-	0.5	80 °C for 24 hr.	1.66-2.26	51.4-61.9	-	[98]
Fly ash	FGA	20-80	-	NS+NH	12	3	0.82	60 °C for 6 hr.	-	0.6-7.5	-	[99]
Blast furnace slag and fly	Basaltic pumice	-	-	NS+NH	-	-	-	80 °C for 48 hr.	1.58-1.76	12-32	-	[100]
Fly ash	Expanded clay	20-40	Fine + coarse	NS+NH	8	2	0.5, 0.6	RT	1.55-2.03	26.6-43.4	-	[101]
Blast furnace slag and fly ash	Expanded poly styrene beads	25-100	Fine + coarse	NS+NH	14	2.5	-	RT	1.76-2.21	7.70-25.4	-	[102]
Blast furnace slag and fly ash	Crumb rubber	10, 20	Fine + coarse	NS+NH	14	2.5	0.4-0.6	RT	2.28-2.30	26.3-29.1	-	[102]
Fly ash	Artificial	-	Fine	NS+NH	16	2.5	0.6	90 °C for 48 hr.	0.6	35.8	0.95	[104]
Fly ash and blast furnace slag	FGA		-	NH	2-3	-	0.27-0.37	RT	0.8-0.86	8-10	0.07-0.10	[106]

FGA: Foam glass aggregate, **NS**: Sodium silicate (Na$_2$SiO$_3$), **NH**: Sodium hydroxide, **RT**: Room temperature

Chapter Four/Conclusions

4.1 Conclusion of foam glass aggregate results

In this work, FGA was prepared using cathode-ray tube glass waste and silicon carbide (foaming agent) foaming at various temperatures. These FGA were subsequently employed to create lightweight geopolymers under ambient conditions. The following conclusions are established for preparing the FGA:

- In the heating microscope investigation, the foaming process happened at a temperature range of 720-800 °C for the mixture containing (99 wt.% CRT glass + 1 wt.% SiC), and the maximum height expansion of 119% occurred at 800 °C.

- Both the bulk density and compressive strength increase with the foaming temperature, while thermal conductivity reduces.

- The bulk density and uniaxial compressive strength standard values for lightweight aggregate, bulk density must be less than 1.2 g/cm^3 and uniaxial compressive strength more than 1 MPa. The sample sintered at 725 °C had a density of 1.26 g/cm³, more than the limited value; therefore, this sample was excluded from further investigations. The samples sintered at 750-800 °C had a density range of 0.58-0.91 g/cm³ and a compressive strength range of 1.55-5.31 MPa; therefore, these foam glass can be used as lightweight aggregate.

- The leaching of lead from FGA increases with the rise in foaming temperature, while the barium leaching reduces; however, all leaching results values were below the standard limit.

4.2 Conclusion of metakaolin-based geopolymer results by effect of the water glass dosages and curing temperatures at 60 °C and 75 °C.

In this study, the effects of two factors were investigated: curing temperature and different water glass and sodium hydroxide contents in the activator solutions. MK was synthesised using calcined kaolin at 750 °C for 3 hours as raw material.

- As a result of the curing temperature, the MK-GP cured at 60 °C had fewer voids than the sample cured at 75 °C, resulting in higher mechanical strength.

- Regarding the effect of water glass and sodium hydroxide content, it was found that the geopolymer binder with 50 wt.% water glass and appropriate sodium hydroxide content in the activator solution exhibited the highest compressive strength of 16.4 MPa and slight efflorescence. This is due to a suitable Si/Al ratio of 1.85, which allows efficient reaction with compact structures and successful consolidation of the product.

- In addition, FTIR analysis revealed that as the water glass content increased, the strong peak at 796.98 cm^{-1} increased, indicating an increase in Al-O. Thus, increasing the water glass content by more than 50 wt.% led to precipitation of the Al-Si phase, which prevented the interaction between the MK powder and the alkaline activator solution, thus reducing the compressive strength.

4.3 Conclusion of metakaolin-based geopolymer results by effect of liquid-to-solid ratio and curing temperatures at 60 °C and room temperature

A study was made on the effects of curing temperature and liquid-to-solid ratio on metakaolin-based geopolymer binders.

- The curing temperature affects the compressive strength and bulk density of the geopolymer binder; the samples cured at room temperature have higher values.

- As the liquid-to-solid ratio rises, the hardening times increase because of the high fluid content, requiring a longer duration for complete hardening.

- The sample made with a liquid-to-solid ratio of 0.8 cured at room temperature achieved a maximum compressive strength of 19.12 MPa with shorter setting times, an initial setting time of 288 minutes, and a final setting time of 358 minutes, respectively.

4.4 Conclusion of metakaolin-based geopolymer statistical analysis

The following conclusions can be made on the regression analysis of metakaolin-based geopolymer for three variables (*water glass dosage, curing temperature, and liquid-to-solid ratio*):

- The water glass dosage factor is a more effective variable for bulk density and thermal conductivity of metakaolin-based geopolymer. Due to the water glass dosage effect for silicate content and viscosity in the geopolymer mixture, water glass density is higher than sodium hydroxide solution density with 10 M.

- The curing temperature and liquid-to-solid ratio are controlling variables for the compressive strength of metakaolin-based geopolymer. The curing temperature affected the reaction kinetics and structural development of the geopolymer. Higher curing temperatures lead to rapid evaporation of water, causing shrinkage and microcracking, leading to a reduction in compressive strength. The selected optimal liquid-to-solid ratio assists in ensuring suitable workability while preventing excessive porosity or unreacted materials.

4.5 Conclusion of lightweight geopolymer results

The following conclusions were drawn regarding the preparation of the LWGP-FGA characterisation:

- Replacing lightweight geopolymer with 30 vol% of three different types of FGA resulted in a reduction of compressive strength by 53.18% to 57.86% and a reduction in bulk density by 9% to 17.6%.

- The apparent porosity and uniaxial compressive strength of the FGA greatly influence the bond between the geopolymer matrix and the lightweight aggregate. The bonding between the geopolymer matrix and foam glass was weak when the apparent porosity was 64% for foam glass with a smooth surface.

- The maximum compressive strength of LWGP-FGA was recorded at 9.11 MPa with the use of FGA sintered at 775 °C, which has properties of bulk density 0.68 g/cm^3, uniaxial compressive strength of 3.6 MPa, and apparent porosity 72.8%.

- The thermal conductivity of lightweight geopolymer incorporating foam glass aggregate ranged from 0.18 to 0.283 W/m·K. This variation is significantly influenced by the thermal conductivity and the bulk density of the foam glass aggregate used.

- The LWGP-FGA apparent porosity ranged from 11.32 % to 14.58 %, while water absorption fluctuated between 2.83 % and 4.06 %. These properties were significantly influenced by the bond between the geopolymer matrix and the foam glass aggregate.

- An increase in freeze-thaw cycles resulted in a noticeable reduction in compressive strength and a significant increase in weight loss, according to the statistical analysis. The number of freeze-thaw cycles and water absorption of LWGP-FGA are more effective variables on weight loss.

- The porosity and voids between geopolymer and glass aggregate are responsible for failure caused by the freeze-thaw cycles. Noted that the LWGP-FGA750 sample experienced failure, identified by a weight loss reach of 34.09 % and a compressive strength reduction reached 77.97 % after 21 freeze-thaw cycles at -20 °C. This degradation was attributed to the weak bonding between the geopolymer matrix and the foam glass aggregate.

New scientific results

Thesis 1: Preparation of foam glass aggregate from CRT glass waste

I have successfully produced foam glass aggregate from 99 wt.% of CRT glass waste (*chemical composition:* SiO_2:55.90 wt.%, **PbO**:13.36 wt.%, **BaO**:10.20 wt.%, Na_2O:5.96 wt.%, K_2O:5.49 wt.%, **SrO**:1.51 wt.%, Al_2O_3:1.70 *others*: 5.88 wt.%; median particle size d_{50}=11 μm), and 1 wt.% of SiC (*Mineral composition: Moissanite 6H: 83,2 wt.%, Moissanite 4H, syn: 16,8 wt.%; particle size d>1μm*) as foaming agent on different sintering (*foaming*) temperatures (*750 °C; 775 °C; 800 °C*) using 360 °C/h heating rate and 10 min holding time. Using the above parameters, glass foams with the physical properties given in **Table A** can be produced.

Table A. Properties of the foam glass aggregate derived from CRT glass waste.

Physical property	Foam glass aggregate sintered at			Standard value / Limit	Reference
	750 °C	775 °C	800 °C		
Bulk density (g/cm³)	0.91	0.68	0.58	> 1.2	EN 13055-1
Compressive strength (MPa)	5.31	3.6	1.55	<1	https://doi.org/10.1016/j.jobe.2022.105426
Volume expansion (vol%)	26.4	52.1	77.56	-	-
Apparent porosity (%)	64	72.8	76.8	-	-
Thermal conductivity (W/m·K)	0.083	0.075	0.063	0.065 -0.220	ASTM C 332– 07
Lead concentration (mg/L)	0.021	0.046	0.12	5	EN 12457-3:2004; WHO guideline
Barium concentration (mg/L)	9.31	4.05	2.09	100	EN 12457-3:2004; WHO guideline

Related publications: *Sarah Kareem Mohammed Al-Saudi, Robert Géber: Production of lightweight geopolymer concrete with foam glass aggregate derived from cathode-ray glass waste, Case Studies in Construction Materials, 2024. (Q1)* https://doi.org/10.1016/j.cscm.2024.e03888

Thesis 2: Effect of foaming temperature on the leaching of lead and barium in CRT foam glass

It was experimentally demonstrated that the leaching of lead from foam glass derived from CRT glass waste (*99 wt.% of CRT glass waste /chemical composition:* SiO_2:55.9 wt.%, **PbO**:13.36 wt.%, **BaO**:10.2 wt.%, Na_2O:5.96 wt.%, K_2O: 5.49 wt.%, **SrO**:1.51 wt.%, Al_2O_3:1.70 wt.%, **others**: 5.88 wt.%; median particle size d_{50}=11 μm), and 1 wt.% of SiC /Mineral composition: Moissanite 6H: 83,2 wt.%, Moissanite 4H, syn: 16,8 wt.%; particle

84

size d>1µm/) increasing with foaming temperature. The lead concentration (*standard limit: 5 mg/L*) more than doubled when the foaming temperature increased from 750 °C to 775 °C, and increased more than five times when the foaming temperature increased to 800 °C (*maximum lead concentration at T=800°C: 0.12 mg/L*). The changes in lead concentration over temperature can be described by the following linear equation:

$$\textbf{y = 0.002x – 1.4722}\ (\textit{Coefficient of Determination, } R^2=0.9245)$$

The leaching of barium decreases with the foaming temperature. The barium concentration (*standard limit: 100 mg/L*) decreased to 56.49 % when the foaming temperature was increased from 750 °C to 775 °C and to 77.55 % when the foaming temperature was increased to 800 °C (*maximum barium concentration at T=750°C: 9.31 mg/L*) (**Fig. A**). The changes in barium concentration over temperature can be described by the following linear equation:

$$\textbf{y = - 0.1444x + 117.06}\ (\textit{Coefficient of Determination, } R^2=0.9349)$$
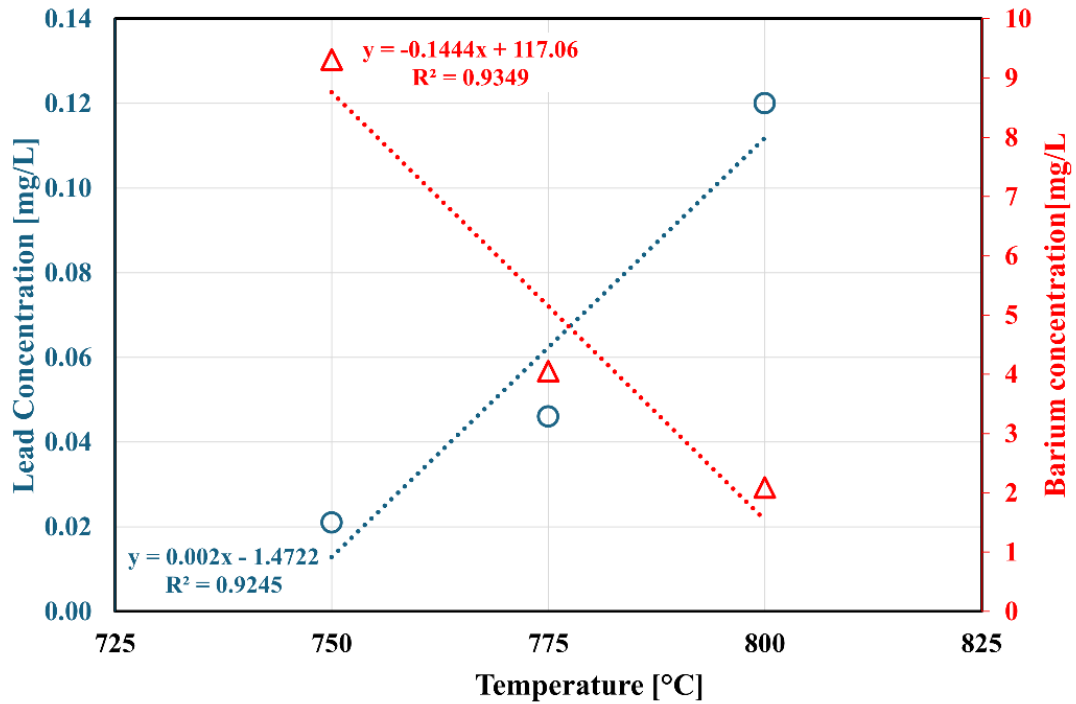
Figure A. The concentration of lead and barium contaminants from the leaching test for foam glass over the foaming temperature.

Thesis 3. Prediction of physical, mechanical and thermal properties of metakaolin-based geopolymer binder

Using multilinear regression, statistical models were built to predict the bulk density, compressive strength and thermal conductivity of metakaolin-based geopolymer binders by investigating the effects of three variables, namely water glass dosage, curing temperature and liquid-to-solid ratio (**Table B**).

The metakaolin-based geopolymer binder was prepared from metakaolin (*calcinated kaolin at 750 °C for 3 hours; median particle size* (d_{50}=5.4μm)). Chemical composition (**SiO_2**: 58.3 wt.%; **Al_2O_3**:39.4 wt.%; **MgO**: 0.33 wt.%; **CaO**: 0.28 wt.%; **Na_2O**:0.06 wt.%; **K_2O**:0.26 wt.%; **Fe_2O_3**:0.47 wt.%; **MnO**:0.005 wt.%; **TiO_2**: 0.203 wt.%; **P_2O_3**: 0.013 wt.%; **S**: 0.02 wt.%). Alkali activator solution: M_{NaOH}=10 M; water glass silicate modulus: 3.8.

Table B. Geopolymer binder variables

Variables name	Level values
Water glass dosage (wt.%)	0; 25; 50; 75 and 100
Curing temperature (°C)	25, 60 and 75
Liquid-to-solid ratio	0.8; 0.95 and 1.1

Predictive models:

Bulk density (g/cm³) = *1.478 + 0.002920 · Water glass dosage (wt.%) -0.001681 · Curing temperature (°C) - 0.286 · Liquid to solid ratio ± error (Error (%) = 4.02)*

Compressive strength (MPa) = *40.81 + 0.0163 · Water glass dosage (wt.%) - 0.1349 · Curing temperature (°C) - 19.49 · Liquid-to-solid ratio ± error (Error (%) =10.58)*

Thermal conductivity (W/m·K) = *0.981 - 0.003229 · Water glass dosage (wt.%) + 0.00070 · Curing temperature (°C) - 0.554 · Liquid-to-solid ratio ± error (Error (%) =7.47)*

Related publications:
1. A Al-Saudi Sarah Kareem Mohammed et al.: Comparative study of metakaolin-based geopolymer characteristics utilizing different dosages of water glass in the activator solution, Results in Engineering, 2023. (Q1) https://doi.org/10.1016/j.rineng.2023.101469
2. Al-Saudi Sarah Kareem Mohammed and Róbert Géber, Effect of liquid- solid ratio on metakaolin-based geopolymer binder properties, Pollack Periodica, 2024. (Q3) https://doi.org/10.1556/606.2024.01141

Thesis 4. Determination of Setting Times for Geopolymer Binder and Innovation of Lightweight Metakaolin-Based Geopolymer Concrete

A. It was experimentally proved that metakaolin-based geopolymer binder with the following composition and conditions (*kaolin was calcinated at 750 °C for 3 hours; Metakaolin median particle size (d_{50}=5.4μm)). Metakaolin chemical composition (SiO_2: 58.3 wt.%; Al_2O_3:39.4 wt.%; MgO:0.33 wt.%; CaO: 0.28 wt.%; Na_2O:0.06 wt.%; K_2O:0.26 wt.%; Fe_2O_3:0.47 wt.%; MnO:0.005 wt.%; TiO_2: 0.203 wt.%; P_2O_3: 0.013 wt.%; S: 0.02 wt.%). Alkali activator solution: M_{NaOH}=10 M; water glass silicate modulus: 3.8. NaOH/Na_2SiO_3 ratio=1. Liquid-to-solid ratio: 1.1.*) can be set at room temperature, with an initial setting time of 288 minutes and a final setting time of 358 minutes. Both setting times meet the standard requirements for the setting time of cement (*EN 196-3:2017 standard; initial setting time should exceed 45 minutes; final setting time should not exceed 390 minutes*). The prepared geopolymer binder has the following properties: uniaxial compressive strength: 19.12 MPa; bulk density: 1.42 g/cm³; thermal conductivity: 0.49 W/m·K.

Related publications:
1. A Al-Saudi Sarah Kareem Mohammed et al.: Comparative study of metakaolin-based geopolymer characteristics utilizing different dosages of water glass in the activator solution, Results in Engineering, 2023. (Q1) https://doi.org/10.1016/j.rineng.2023.101469
2. Al-Saudi Sarah Kareem Mohammed and Róbert Géber, Effect of liquid- solid ratio on metakaolin-based geopolymer binder properties, Pollack Periodica, 2024. (Q3) https://doi.org/10.1556/606.2024.01141

B. I have experimentally proved that it is possible to produce metakaolin-based lightweight geopolymer with foam glass aggregates derived from waste CRT glass cured at room temperature. Based on its properties (**Table C**), the newly developed lightweight geopolymer concrete meets the requirements of ASTM C 330 Standard and can therefore be classified as a structural/insulating material.

Table C. The properties of the lightweight geopolymer, along with a comparison to the lightweight concrete defined by ASTM and EN standards

Properties	ASTM C 330		BS EN: 206-1	MK-based lightweight geopolymer concrete with foam glass aggregate derived from CRT waste glass
	Structural/ insulating group	Insulating group		
Density (g/cm³)	0.72 – 1.44	0.24 – 0.80	0.88 – 2.00	1.17 – 1.29
Compressive strength (MPa)	3.4 – 17	0.70 – 3.40	8.00 – 80.00	8.09 – 9.11
Thermal conductivity (W/m·K)	0.45 – 1.05	0.065 – 0.22	–	0.18 – 0.283

The lightweight geopolymer was prepared from 70 vol% of metakaolin-based geopolymer and 30 vol% of foam glass aggregate. Samples were cured at room temperature for 28 days. The metakaolin-based geopolymer was prepared with the following composition and conditions: *Metakaolin (kaolin calcinated at 750 °C for 3 hours; median particle size (d_{50}=5.4µm)). Chemical composition (SiO_2: 58.3 wt.%; Al_2O_3:39.4 wt.%; MgO:0.33 wt.%; CaO: 0.28 wt.%; Na_2O:0.06 wt.%; K_2O:0.26 wt.%; Fe_2O_3:0.47 wt.%; MnO:0.005 wt.%; TiO_2: 0.203 wt.%; P_2O_3: 0.013 wt.%; S: 0.02 wt.%). Alkali activator solution: M_{NaOH}=10 M; water glass silicate modulus: 3.8. $NaOH/Na_2SiO_3$ ratio=1. Liquid-to-solid ratio:1.1.*

Foam glass aggregate was made from 99 weight% of waste CRT glass waste (*median particle size d_{50}: 11 µm*) and 1 weight% of SiC (*d ≥ 1µm*) as foaming agent. The chemical compositions of waste CRT glass: SiO_2: 55.9 wt.%, PbO: 13.36 wt.%, BaO: 10.2 wt.%, Na_2O: 5.96 wt.%, K_2O: 5.49 wt.%, SrO: 1.51 wt.%, Others: 7.85 wt.%). Foaming temperatures: 750 °C, 775 °C and 800 °C.

List of Publications

International Journal articles

1. **Al-Saudi Sarah Kareem Mohammed**, Róbert Géber, Production of lightweight geopolymer concrete with foam glass aggregate derived from cathode-ray glass waste, Case Studies in Construction Materials, (2024). https://doi.org/10.1016/j.cscm.2024.e03888. **(Q1, IF= 6.5)**
   Number of Independent Citations: 4

2. **Al-Saudi Sarah Kareem Mohammed**, Róbert Géber, Andrea Simon, Emese Kurovics, Alexandra Hamza, Comparative study of metakaolin-based geopolymer characteristics utilizing different dosages of water glass in the activator solution, Results in Engineering (2023). https://doi.org/10.1016/j.rineng.2023.101469 **(Q1, IF= 6)**
   Number of Independent Citations:24

3. **Al-Saudi Sarah Kareem MOHAMMED, Róbert GÉBER**, Effect of liquid-solid ratio on metakaolin-based geopolymer binder properties, Pollack Periodical, (2024) **(Q3, IF=0.83)**
   Number of Independent Citations: 4

4. **Al-Saudi Sarah Kareem Mohammed**, Emese Kurovics, Jamal-Eldin F.M. Ibrahim, Mohammed Tihtih, Andrea Simon, Róbert Géber, Preparation of an Aluminum Titania /Mullite Composite from the Raw Materials Alumina, Titania, and Silica Fume, Revue des Composites et des Materiaux Advances, (2022). https://doi.org/10.18280/rcma.320502 **(Q3, IF=1.26).** *Number of Independent Citations: 3*

Papers published in conference proceedings:

1. **Al-Saudi Sarah Kareem Mohammed,** Andrea Simon, and Róbert Géber, Preparation and characterization of foam glass from soda lime silicate glass waste by using different dosages of limestone, Multidisciplinary Sciences, (2022). https://doi.org/10.35925/j.multi.2022.4.20
   Number of Independent Citations: 4

2. **Sarah Kareem**, Luay S.Al-Ansari, László A. Gömze, Modeling of Modulus of Elasticity of Nano-Composite Materials: Review and Evaluation, Journal of Physics: Conference Series, (2022). https://doi.org/10.1088/1742-6596/2315/1/012038 **(Q4, IF=0.56)**
   Number of Independent Citations: 7

Papers published in Almanach (ISSN 2939-7294):

1. **Al-Saudi Sarah Karem Mohammed,** Phase transformation of silica fume during sintering with alumina (2022) https://www.kerpely.uni-miskolc.hu/phd_students_almanach

2. **Al-Saudi Sarah Kareem Mohammed,** Geopolymer: An overview of polymerization on metakaolin-based geopolymer, (2023) https://www.kerpely.uni-miskolc.hu/phd_students_almanach

3. **Al-Saudi Sarah Kareem Mohammed,** Foam glass derived from waste glass: A review, (2024). *https://www.kerpely.uni-miskolc.hu/phd_students_almanach*.

Conference presentations

1. **Sarah Kareem**, Luay S.Al-Ansari, László A. Gömze, **Oral presentation**, Simulations of the Tensile Modulus of Elasticity of Various Nano-silica Particles Modified Epoxy Polymer, The 6th International Conference on Competitive Materials and Technology, Miskolc -Lillafüred, Hungary, October 6th, 2021.

2. **Sarah Kareem**, László A. Gömze, **Oral presentation,** Aluminum Titanate (Al_2TiO_5) formation with small additives of oxides: Review, The Day of Hungarian Science, Miskolc, Hungary, December 11th, 2021.

3. **Sarah Kareem Mohammed**, Emese Kurovics, Jamal-Eldin F. M. Ibrahim, Mohammed Tihtih, Andrea Simon, Róbert Géber, **Poster presentation,** Development of Properties of Aluminum Titanate by Addition of Silica Fume, 25th Spring Wind Conference, Pécs, Hungary, July 5th, 2022.

4. **Sarah Karem Mohammed Al-Saudi**, Andrea Simon, Róbert Géber, **Oral presentation**, Preparation and Characterization of Foam Glass From Soda Lime Silicate Glass Waste, MultiScience - XXXV. microCAD International Multidisciplinary Scientific Conference, Miskolc University, Hungary, October 10th, 2022.

5. **Al-Saudi Sarah Kareem Mohammed**, Andrea Simon, Róbert Géber, **Oral presentation,** Investigation of the properties of foam glass produced from window glass waste and various foaming agents**,** 26th Spring Wind Conference, Miskolc, Hungary, June 5th, 2023.

6. **Al-Saudi Sarah Kareem Mohammed**, Andrea Simon, Róbert Géber, **Oral presentation**, Some properties of foam glass produced from window glass waste and various foaming agents, Glass industry professional conference, Budapest, Hungary, June 23 [th],2023.

7. **Al-Saudi Sarah Kareem Mohammed**, **Oral presentation**, Study characterisation of metakaolin-based geopolymer by using different dosages of sodium silicate in the activator solution, MultiScience - XXXVI. microCAD International Multidisciplinary Scientific Conference**,** Miskolc, Hungary, December 10th, 2023.

8. **Al-Saudi Sarah Kareem Mohammed**, Robert Geber, Andrea Simon, **Oral presentation**, Produce foam glass aggregate utilising waste glass from cathode-ray tubes, 9th International Scientific Conference on Advances in Mechanical Engineering, Debrecen, Hungary, September 11th, 2023.

9. **Al-Saudi Sarah Kareem Mohammed, Oral presentation,** Investigation of the Influence of Temperature on the Properties of Geopolymer Binders, The Day of Hungarian Science, Miskolc, Hungary, August 11th, 2023.

10. **Al-Saudi Sarah Kareem Mohammed**, Robert Geber, Andrea Simon, **Oral presentation,** Investigation of the effect of sintering temperature on the properties of the foam glass composition, XXVII. Spring Wind Conference, Budapest, Hungary, May 4th, 2024.

References

[1] M. Caniato, G. Kyaw, J. Kaspar, and A. Gasparella, "Sound absorption performance of sustainable foam materials: Application of analytical and numerical tools for the optimization of forecasting models," *Applied Acoustics*, vol. 161, Apr. 2020, doi:10.1016/j.apacoust.2019.107166.

[2] R. Lebullenger, S. Chenu, J. Rocherullé, O. M. Conanec, F. Cheviré, F. Tessier, A. Bouzaza, S. Brosillon, "Glass foams for environmental applications," *Journal of Non-Crystalline Solids*, vol. 356, pp. 2562–2568, 2010, doi: 10.1016/j.jnoncrysol.2010.04.050.

[3] M. Smol, J. Duda, A. Czaplicka-Kotas, and D. Szołdrowska, "Transformation towards circular economy (CE) in municipal waste management system: Model solutions for Poland," *Sustainability (Switzerland)*, vol. 12, no. 11, Jun. 2020, doi: 10.3390/su12114561.

[4] N. Li, C. Shi, Z. Zhang, H. Wang, and Y. Liu, "A review on mixture design methods for geopolymer concrete," *Composites Part B: Engineering*, vol. 178, 2019, doi:10.1016/j.compositesb.2019.107490.

[5] C. Chen, R. Xu, D. Tong, X. Qin, J. Cheng, J. Liu, B. Zheng, L. Yan and Q. Zhang., "A striking growth of CO_2 emissions from the global cement industry driven by new facilities in emerging countries," *Environmental Research Letters*, vol. 17, no. 4, Apr. 2022, doi: 10.1088/1748-9326/ac48b5.

[6] M. Schneider, M. Romer, M. Tschudin, and H. Bolio, "Sustainable cement production- present and future," *Cem Concr Res*, vol. 41, no. 7, pp. 642–650, 2011, doi:10.1016/j.cemconres.2011.03.019.

[7] D. K. Parmar, A. D. Patil, and A. Deshmukh, "Investigation on geopolymer concrete for different proportions of alkaline activator," *International Advanced Research Journal in Science, Engineering and Technology*, vol. 8, 2021, doi: 10.17148/IARJSET.2021.8869.

[8] C. Alessandra, L. Leoni, Fi. De Carlo, M. Salvio, C. Martini, and F. Martini, "Technological Energy Efficiency Improvements in Cement Industries, " *Sustainability*, vol. 13, 2021, doi.org/10.3390/su13073810

[9] M. Nawaz, A. Heitor, and M. Sivakumar, "Geopolymers in construction - recent developments," *Construction and Building Materials*, vol. 260, 2020, doi:10.1016/j.conbuildmat.2020.120472.

[10] N. A. Lloyd and B. V. Rangan, "Geopolymer Concrete with Fly Ash." *Second International Conference on Sustainable Construction Materials and Technologies,* Italy, 2010.

[11] J. E. F. M. Ibrahim, M. Tihtih, E. İ. Şahin, M. A. Basyooni, and I. Kocserha, "Sustainable zeolitic tuff incorporating tea waste fired ceramic bricks: Development and investigation," *Case Studies in Construction Materials*, vol. 19, 2023, doi:10.1016/j.cscm.2023.e02238

[12] M. De Simone and G. Fajilla, "Occupant behavior: a factor in energy performance of buildings. Methods for its detection in houses and offices," *Journal of World Architecture*, vol. 2, no. 2, 2019, doi:10.26689/jwa.v2i2.544.

[13] S. S. Chanda and S. Guchhait, "A comprehensive review on the factors influencing engineering characteristics of lightweight geopolymer concrete," *Journal of Building Engineering*, vol. 86, 2024, doi: 10.1016/j.jobe.2024.108887.

[14] M. M. Jomaa'h, B. T. Kamil, and O. S. Baghabra, "Mechanical and Structural Properties of a Lightweight Concrete with Different Types of Recycling Coarse Aggregate," *Tikrit Journal of Engineering Sciences*, vol. 26, no. 1, pp. 33–40, 2019, doi: 10.25130/tjes.26.1.05.

[15]   K. S. Elango, J. Sanfeer, R. Gopi, A. Shalini, R. Saravanakumar, and L. Prabhu, "Properties of light weight concrete - A state of the art review," *Mater Today Proc*, vol. 46, pp 4059–4062, 2020, doi: 10.1016/j.matpr.2021.02.571.

[16]   J. Newman and P. Owens, "Advanced Concrete Technology Processes: Chapter Two, Properties of lightweight concrete", *Elsevier*, 2003.

[17]   C. R. Hays, "ACI 121R-98 Quality Management System for Concrete Construction," *Management*, pp. 1–9, 1998.

[18]   V. R. Dalvi, D. L. Pawar, and A. M. Walekar, "A Review Paper on No-Fines Concrete," vol. 9, no. 6, pp. 518-520, 2021.

[19]   G. Zhou and R. K. L. Su, "A Review on Durability of Foam Concrete," *Buildings*, vol. 13, no. 7, 2023, doi: 10.3390/buildings13071880.

[20]   R. R.Villarreal, S. Krayer, "Ancient Structural Concrete in Mesoamerica", *Concrete International,* vol.18 ,pp.67-70 ,1996.

[21]   ASTM C330-04, "Standard Specification for Lightweight Aggregates for Structural Concrete," *ASTM International*, vol. 552, no. 18, p. 4, 2009.

[22]   EN 13055–1, "Standard lightweight aggregates part 1, lightweight aggregate for concert mortar and grout,"1 (2020).

[23]   M. Mostafa, "Production of Lightweight Concrete : Modelling and Assessment of Changes in Textures and Mineral Phases," PhD thesis, *Faculty of Materials and Chemical Engineering, University of Miskolc*, 2022.

[24]   C. H. Huang and S. Y. Wang, "Application of water treatment sludge in the manufacturing of lightweight aggregate," *Constr Build Mater*, vol. 43, pp. 174–183, 2013, doi: 10.1016/j.conbuildmat.2013.02.016.

[25]   H. Zhang, "Section 5: Concrete and structure," *Building Materials in Civil Engineering*, pp. 81–150, 2011, doi: 10.1533/9781845699567.81.

[26]   B. Vakhshouri and S. Nejadi, "Review on the mixture design and mechanical properties of the lightweight concrete containing expanded polystyrene beads," *Australian Journal of Structural Engineerin* , vol. 19, pp 1-23,2018, doi: 10.1080/13287982.2017.1353330.

[27]   H. M. Hamada, B. Skariah Thomas, B. Tayeh, F. M. Yahaya, K. Muthusamy, and J. Yang, "Use of oil palm shell as an aggregate in cement concrete: A review," *Construction and Building Materials,* vol. 265,2020. doi: 10.1016/j.conbuildmat.2020.120357.

[28]   S. Y. Chung, P. Sikora, D. J. Kim, M. E. El Madawy, and M. Abd Elrahman, "Effect of different expanded aggregates on durability-related characteristics of lightweight aggregate concrete," *Mater Charact*, vol. 173, 2021, doi: 10.1016/j.matchar.2021.110907.

[29]   N. Ghafari, "Assessment of mechanical and thermal properties of foam glass aggregates for use in pavements," *The Transportation Association of Canada,*2019.

[30]   W. S. Mustafa, J. Szendefy, and B. Nagy, "Thermal Performance of Foam Glass Aggregate at Different Compaction Ratios," *Buildings*, vol. 13, no. 7, 2023, doi:10.3390/buildings13071844.

[31]   M. Osfouri, J. Ibrahim, M. Sambucci, M. Valente, J. Tirillò, and S. Andrea, "Sustainable structural lightweight concrete containing foam glass aggregates", *Journal of Building Engineering*, vol. 104, 2025, doi:10.1016/j.jobe.2025.112270.

[32]   Q. Tushar, S. Salehib, J. Santosc, G. Zhanga, M.A. Bhuiyana, M. Arashpourb, and F. Giustozzi "Application of recycled crushed glass in road pavements and pipeline bedding: An integrated environmental evaluation using LCA," *Science of the Total Environment*, vol. 881, 2023, doi: 10.1016/j.scitotenv.2023.163488.

[33]   G. Scarinci, G. Brusatin, and E. Bernardo, "Glass Foams," in Cellular Ceramics (Structure, Manufacturing, Properties and Applications), ed. by M. Scheffler, *P. Colombo (Wiley-VCH Verlag   GmbH   &   Co.   KGaA,   Weinheim,   FRG*,   pp.   158–176, 2006, doi:10.1002/3527606696.ch2g.

[34]   R. Heidari, R. Yazdanparast, and A. Jabbarzadeh, "Sustainable design of a municipal solid waste management system considering waste separators: A real-world application", *Sustainable Cities and Society*, Vol. 47, 2019, doi.org/10.1016/j.scs.2019.101457.

[35]   T.-Y. Lim, H.-W. Ku, J.-H. Hwang, J.-H. Kim, and J.-K. Kim, "A study on the fabrication of foamed glass by using refused coal ore and its physical properties," *Journal of the Korean Crystal Growth and Crystal Technology*, vol. 21, no. 6, pp. 266–273, 2011, doi: 10.6111/jkcgct.2011.21.6.266.

[36]   A. Siddika, A. Hajimohammadi, and V. Sahajwalla, "Powder sintering and gel casting methods in making glass foam using waste glass: A review on parameters, performance, and challenges",   *Ceramics   International*,   vol.   48,   pp.   1494-1511,2021, doi.org/10.1016/j.ceramint.2021.10.066.

[37]   L. Rocchetti and F. Beolchini, "Environmental burdens in the management of end-of-life cathode ray tubes," *Waste Management*, vol. 34, no. 2, pp. 468–474, 2014, doi: 10.1016/j.wasman.2013.10.031.

[38]   N. Singh, J. Wang, and J. Li, "Waste Cathode Rays Tube: An Assessment of Global Demand for   Processing,"   *Procedia   Environ   Sci*,   vol.   31,   pp.   465–474,   2016, doi:10.1016/j.proenv.2016.02.050.

[39]   C. S. Poon, "Management of CRT glass from discarded computer monitors and TV sets," *Waste Management*, vol. 28, no. 9, p. 1499, 2008, doi: 10.1016/j.wasman.2008.06.001.

[40]   Z. Yao, T.C. Ling, P.K. Sarker, W. Su, J. Liu, and J. Tang*, "Recycling difficult-to-treat e-waste cathode-ray-tube glass as construction and building materials: A critical review," *Renewable and Sustainable Energy Reviews*, vol. 81, pp.595-604, 2018, doi: 10.1016/j.rser.2017.08.027.

[41]   J. S. Lee, H. M. Yoo, S. W. Park, S. J. Cho, and Y. C. Seo, "Recycling of cathode ray tube panel glasses as aggregates of concrete blocks and clay bricks," *J Mater Cycles Waste Manag*, vol. 18, no. 3, pp. 552–562, 2016, doi: 10.1007/s10163-015-0350-6.

[42]   N. Singh, Y. Tang, and J. Li, "Uncovering material flow analysis of waste cathode ray tubes television in China," *Waste Management and Research*, vol. 37, no. 11, pp. 1170–1177, Nov. 2019, doi: 10.1177/0734242X19871600.

[43]   J. Bawab, J. Khatib, H. El-Hassan, L. Assi, and M. S. Kırgız, "Properties of cement-based materials containing cathode-ray tube (Crt) glass waste as fine aggregates—a review," *Sustainability (Switzerland)*, vol. 13, no. 20, pp. 1–23, 2021, doi: 10.3390/su132011529.

[44]   F. Méar, P. Yot, M. Cambon, and M. Ribes, "The characterization of waste cathode-ray tube glass,"   *Waste   Management*,   vol.   26,   no.   12,   pp.   1468–1476,   2006,   doi: 10.1016/j.wasman.2005.11.017.

[45]   S. Herat, "Recycling of cathode ray tubes (CRTs) in electronic waste," *Clean (Weinh)*, vol. 36, no. 1, pp. 19–24, 2008, doi: 10.1002/clen.200700082.

[46] F. Andreola, L. Barbieri, A. Corradi, I. Lancellotti, R. Falcone, and S. Hreglich, "Glass-ceramics obtained by the recycling of end of life cathode ray tubes glasses," *Waste Management*, vol. 25, no. 2 SPEC. ISS., pp. 183–189, 2005, doi:10.1016/j.wasman.2004.12.007.

[47] L. E. Et and L. E. Déchet, "Integrated Recycling of End-Of-Life Cathode Ray Tube Glass," pp. 1–3, 1999.

[48] M. Chen, F. S. Zhang, and J. Zhu, "Lead recovery and the feasibility of foam glass production from funnel glass of dismantled cathode ray tube through pyrovacuum process," *J Hazard Mater*, vol. 161, no. 2–3, pp. 1109–1113, 2009, doi: 10.1016/j.jhazmat.2008.04.084.

[49] F. Méar, P. Yot, R. Viennois, and M. Ribes, "Mechanical behaviour and thermal and electrical properties of foam glass," *Ceram Int*, vol. 33, no. 4, pp. 543–550, 2007, doi: 10.1016/j.ceramint.2005.11.002.

[50] E. Bernardo and F. Albertini, "Glass foams from dismantled cathode ray tubes," *Ceram Int*, vol. 32, no. 6, pp. 603–608, 2006, doi: 10.1016/j.ceramint.2005.04.019.

[51] R. R. Petersen, J. König, M. M. Smedskiaer, and Y. Yue, "Foaming of CRT panel glass powder using Na_2CO_3," *Glass Technology: European Journal of Glass Science and Technology Part A*, vol. 55, no. 1, pp. 1–6, 2014.

[52] J. König, R. R. Petersen, and Y. Yue, "Fabrication of highly insulating foam glass made from CRT panel glass," *Ceram Int*, vol. 41, no. 8, pp. 9793–9800, Sep. 2015, doi: 10.1016/j.ceramint.2015.04.051.

[53] P. S. Sokolov, V. A. Mukhanov, T. Chauveau, and V. L. Solozhenko, "On melting of silicon carbide under pressure," *Journal of Superhard Materials*, vol. 34, no. 5, pp. 339–341, 2012, doi: 10.3103/S1063457612050097.

[54] M. Osfouri, M.Valente, J. F.M. Ibrahim, J. Tirillucci, and S. Andrea, "Sustainable structural lightweight concrete containing foam glass aggregates*", Journal of Building Engineering*, Vol. 104, pp. 1-22, 2025, doi:10.1016/j.jobe.2025.112270.

[55] H. W. Guo, Y. X. Gong, and S. Y. Gao, "Preparation of high-strength foam glass-ceramics from waste cathode ray tube," *Mater Lett*, vol. 64, no. 8, pp. 997–999, 2010, doi: 10.1016/j.matlet.2010.02.006.

[56] Y. A. Spiridonov and L. A. Orlova, "Problems of foam glass production," *Glass and Ceramics (English translation of Steklo i Keramika)*, vol. 60, no. 9–10, pp. 313–314, 2003, doi:10.1023/B:GLAC.0000008234.79970.2c.

[57] H. Elkersh, "Innovative Cleaner Production Technique : Foam Glass Production from Lead Crystal Glass Sludge," *Thesis. The American University in Cairo*, no. April, 2014, doi:10.13140/RG.2.1.4850.9849.

[58] F. Méar, P. Yot, M. Cambon, and M. Ribes, "The changes in lead silicate glasses induced by the addition of a reducing agent (TiN or SiC)," *J Non Cryst Solids*, vol. 351, no. 40–42, pp. 3314–3319, 2005, doi: 10.1016/j.jnoncrysol.2005.08.019.

[59] P. G. Yot and F. O. Méar, "Characterization of lead, barium and strontium leachability from foam glasses elaborated using waste cathode ray-tube glasses," *J Hazard Mater*, vol. 185, no. 1, pp. 236–241, 2011, doi: 10.1016/j.jhazmat.2010.09.023.

[60] J. C. Soares, J. S. de Azevedo, and D. P. Dias, "Effect of temperature on metakaolin-quartz powder geopolymer binder with different combinations of silicates and hydroxides," *Case

Studies in Construction Materials, vol. 16, no. August 2021, p. e00813, 2022, doi: 10.1016/j.cscm.2021.e00813.

[61] V. F. F. Barbosa, K. J. D. MacKenzie, and C. Thaumaturgo, "Synthesis and characterisation of materials based on inorganic polymers of alumina and silica: Sodium polysialate polymers," *International Journal of Inorganic Materials*, vol. 2, no. 4, pp. 309–317, 2000, doi: 10.1016/S1466-6049(00)00041-6.

[62] T. Bezabih, C. Kanali, and J. Thuo, "Effects of teff straw ash on the mechanical and microstructural properties of ambient cured fly ash-based geopolymer mortar for onsite applications," *Results in Engineering*, vol. 18, no. March, p. 101123, 2023, doi: 10.1016/j.rineng.2023.101123.

[63] O. Agboola, D. E. Babatundea, O. S. I. Fayomi, *et al.*, "A review on the impact of mining operation: Monitoring, assessment and management," *Results in Engineering*, vol. 8, no. October, p. 100181, 2020, doi: 10.1016/j.rineng.2020.100181.

[64] N. Shehata, E. T. Sayed, and M. A. Abdelkareem, "Recent progress in environmentally friendly geopolymers: A review," *Science of the Total Environment*, vol. 762, 2021, doi:10.1016/j.scitotenv.2020.143166.

[65] M. Kheimi, I. H. Aziz, M. M. A. B. Abdullah, M. Almadani, and R. A. Razak, "Waste Material via Geopolymerization for Heavy-Duty Application: A Review," *Materials*, vol. 15, 2022, doi:10.3390/ma15093205.

[66] J. Matsimbe, M. Dinka, D. Olukanni, and I. Musonda, "Geopolymer: A Systematic Review of Methodologies," *Materials*, vol. 15, 2022, doi: 10.3390/ma15196852.

[67] M. A. Faris, M.M. A. Abdullah, A. Sansu, *et al.*, "Assessment of Alkali Activated Geopolymer Binders as an Alternative of Portland Cement." *Materiale Plastice* vol. 54, pp.145-154, 2017.

[68] J. Davidovits, "Geopolymer chemistry and sustainable development," *Conference: Geopolymer Green Chemistry and Sustainable Development Solutions, Geopolymer*, France. vol. 1, pp. 9-17, 2005.

[69] V. Shikuku and T. Sylvain, "Application of Geopolymer Composites in Wastewater Treatment: Trends, Opportunities, and Challenges," Research and Development Institute of Industry and Defense Technologies, Algeria & Harbin Engineering University, China, 2019.

[70] J. G. S. Van Jaarsveld, J. S. J. Van Deventer, and L. Lorenzen, "Factors affecting the immobilization of metals in geopolymerized flyash," *Metallurgical and Materials Transactions B: Process Metallurgy and Materials Processing Science*, vol. 29, no. 1, pp. 283–291, 1998, doi: 10.1007/s11663-998-0032-z.

[71] S. Mabroum, S. Moukannaa, A. El Machi, Y. Taha, M. Benzaazoua, and R. Hakkou, "Mine wastes based geopolymers: A critical review," *Clean Eng Technol*, vol. 1, no. June, p. 100014, 2020, doi: 10.1016/j.clet.2020.100014.

[72] M. M. A. B. Abdullah, L. Y. Ming, H. C. Yong, and M. F. M. Tahir, "Clay-Based Materials in Geopolymer Technology," in *Cement-Based Materials*, InTech, 2018. doi:10.5772/intechopen.74438.

[73] K. Komnitsas and D. Zaharaki, "Geopolymerisation: A review and prospects for the minerals industry," *Minerals Engineering,* vol.20, pp.1261-1271, 2007, doi:10.1016/j.mineng.2007.07.011.

[74] J. S. J. Van Deventer, J. L. Provis, and P. Duxson, "Technical and commercial progress in the adoption of geopolymer cement," *Miner Eng*, vol. 29, pp. 89–104, 2012, doi:10.1016/j.mineng.2011.09.009.

[75] Z. H. Zhang, H. J. Zhu, C. H. Zhou, and H. Wang, "Geopolymer from kaolin in China: An overview," *Appl Clay Sci*, vol. 119, pp. 31–41, 2016, doi: 10.1016/j.clay.2015.04.023.

[76] B. Kim, S. Lee, C. M. Chon, and S. Cho, "Setting Behavior and Phase Evolution on Heat Treatment of Metakaolin-Based Geopolymers Containing Calcium Hydroxide," *Materials*, vol. 15, no. 1, 2022, doi: 10.3390/ma15010194.

[77] E. G. Nawy, "Concrete Construction Engineering Handbook," *Concrete Construction Engineering Handbook*, 2008, doi: 10.1201/9781420007657.

[78] H. Peng, T. Qi, J. Vogrin, Q. Huang, W. Wu, and J. Vaughan, "The effect of leaching temperature on kaolinite and meta-kaolin dissolution and zeolite re-precipitation," *Miner Eng*, vol. 170, 2021, doi: 10.1016/j.mineng.2021.107071.

[79] Z. Zhang, H. Wang, X. Yao, and Y. Zhu, "Effects of halloysite in kaolin on the formation and properties of geopolymers," *Cem Concr Compos*, vol. 34, no. 5, pp. 709–715, 2012, doi:10.1016/j.cemconcomp.2012.02.003.

[80] A. M. M. Al. Bakri, A. K. A. A. K. Omar, and S. Myint, "Study on the effect of the alkaline activators ratio in preparation of fly ash-based geopolymer," Conference: RAMM & ASMP, 2009.

[81] A. Fernández-Jiménez and A. Palomo, "Characterisation of fly ashes. Potential reactivity as alkaline cements," *Fuel*, vol. 82, no. 18, pp. 2259–2265, 2003, doi: 10.1016/S0016-2361(03)00194-7.

[82] B. V. Rangan, "Fly Ash-based geopolymer concrete," *Engineering Faculty Curtin University of Technology Perth, Australia*, pp. 3124–3130, 2008.

[83] A. Palomo, M. W. Grutzeck, and M. T. Blanco, "Alkali-activated fly ashes: A cement for the future," *Cem Concr Res*, vol. 29, no. 8, pp. 1323–1329, 1999, doi:10.1016/S00088846(98)00243-9.

[84] F. Bowen, L. Jiesheng, W. Jing, C. Yaohu, Z. Tongtong, T. Xiaoming, and S. Zhengguang, "Investigation on the impact of different activators to solid ratio on properties and micro-structure of metakaolin geopolymer," *Case Studies in Construction Materials*, vol. 16, no. May, p. e01127, 2022, doi: 10.1016/j.cscm.2022.e01127.

[85] N. A. Mohd, M.M. Abdullah, R. A. Razak, S. Z. Abd Rahim, I. H. Aziz, M. Nabiałek, R. P. Jaya, A. Semenescu, R. Mohamed, and M. F. Ghazali, "Geopolymer Ceramic Application: A Review on Mix Design, Properties and Reinforcement Enhancement," *Materials*, vol. 15, no. 21, pp. 6–8, 2022, doi: 10.3390/ma15217567.

[86] Y. C. Chen, W. H. Lee, T. W. Cheng, and Y. F. Li, "A Study on the Shrinkage and Compressive Strength of GGBFS and Metakaolin Base Geopolymer under Different NaOH Concentrations," *Materials*, vol. 17, 2024, doi: 10.3390/ma17051181.

[87] A. Lopes, S. Lopes, and I. Pinto, "Influence of Curing Temperature on the Strength of a Metakaolin-Based Geopolymer," *Materials*, vol. 16, 2023, doi: 10.3390/ma16237460.

[88] C. a. Strydom and J. C. Swanepoel, "Utilisation of fly ash in a geopolymeric material," *Applied Geochemistry*, vol. 17, pp. 1143–1148, 2002.

[89]   S. E. Wallah and B. V. Rangan, "Low-calcium fly ash-based geopolymer concrete: Long-term properties," *Research report GC*, 2006.

[90]   P. Chindaprasirt, T. Chareerat, and V. Sirivivatnanon, "Workability and strength of coarse high calcium fly ash geopolymer," *Cem Concr Compos*, vol. 29, no. 3, pp. 224–229, 2007, doi: 10.1016/j.cemconcomp.2006.11.002.

[91]   T. Y. Yi, H. Awang, and N. H. M. Kaus, " Strength Characteristics of Geopolymer Mortar Formulated with Fly Ash and Ground Granulated Blast Furnace Slag Activated using Wood Ash Lye", *Journal of Advanced Research in Applied Mechanics*, vol. 131, 2025, doi:10.37934/aram.131.1.143

[92]   P. Duxson, S. W. Mallicoat, G. C. Lukey, W. M. Kriven, and J. S. J. van Deventer, "The effect of alkali and Si/Al ratio on the development of mechanical properties of metakaolin-based geopolymers," *Colloids Surf A Physicochem Eng Asp*, vol. 292, no. 1, pp. 8–20, 2007, doi:10.1016/j.colsurfa.2006.05.044.

[93]   N. A. Jaya, Y. M. Liew, C. Y. Heah, and M. M. A. B. Abdullah, "Effect of solid-to-liquid ratios on metakaolin geopolymers," in *AIP Conference Proceedings*, American Institute of Physics Inc., 2018. doi: 10.1063/1.5080912.

[94]   S. K. Mohammed, and R. Géber, "Production of lightweight geopolymer concrete with foam glass aggregate derived from cathode-ray glass waste", Case Studies in Construction Materials, vol. 21, 2024. doi:10.1016/j.cscm.2024.e03888

[95]   O. Youssf, J. E. Mills, M. Elchalakani, F. Alanazi, and A. M. Yosri, "Geopolymer Concrete with Lightweight Fine Aggregate: Material Performance and Structural Application," *Polymers (Basel)*, vol. 15, no. 1, 2023, doi: 10.3390/polym15010171.

[96]   A. Niş, and T. S. W. Al-Antaki, "Pumice aggregate based lightweight concretes under sulfuric acid environment," *Revista Română de Materiale / Romanian Journal of Materials*, vol. 52 , pp. 194 – 202,2022.

[97]   K. Kalinowska-Wichrowska, E. Pawluczuk, M. Bołtryk, and A. Nietupski, "Geopolymer Concrete with Lightweight Artificial Aggregates," *Materials*, vol. 15, no. 9, 2022, doi:10.3390/ma15093012.

[98]   B. A. Tayeh A. M. Zeyad, I. S. Agwa, and M. Amin, "Effect of elevated temperatures on mechanical properties of lightweight geopolymer concrete," *Case Studies in Construction Materials*, vol. 15, Dec. 2021, doi: 10.1016/j.cscm.2021.e00673.

[99]   F. Kristály, R. Szabó, F. Mádai, Á. Debreczeni, and G. Mucsi, "Lightweight composite from fly ash geopolymer and glass foam," *J Sustain Cem Based Mater*, vol. 10, no. 1, pp. 1–22, 2021, doi: 10.1080/21650373.2020.1742246.

[100]   M. Sarıdemir and S. Çelikten , "Investigation of fire and chemical effects on the properties of alkali-activated lightweight concretes produced with basaltic pumice aggregate," *Constr Build Mater*, vol. 260, 2020, doi: 10.1016/j.conbuildmat.2020.119969.

[101]   M. Priyanka, M. Karthikeyan, and M. S. R. Chand, "Development of mix proportions of geopolymer lightweight aggregate concrete with LECA," in *Materials Today: Proceedings*, Elsevier Ltd, Jan. 2020, pp. 958–962. doi: 10.1016/j.matpr.2020.01.271.

[102]   F. Aslani, A. Deghani, and Z. Asif, "Development of Lightweight Rubberized Geopolymer Concrete by Using Polystyrene and Recycled Crumb-Rubber Aggregates," *Journal of Materials in Civil Engineering*, vol. 32, no. 2, 2020, doi: 10.1061/(asce)mt.19435533.0003008.

[103] S. Top and H. Vapur, "Effect of basaltic pumice aggregate addition on the material properties of fly ash based lightweight geopolymer concrete," *J Mol Struct*, vol. 1163, pp. 10–17, 2018, doi: 10.1016/j.molstruc.2018.02.114.

[104] W. Abbas, W. Khalil, and I. Nasser, "Production of lightweight Geopolymer concrete using artificial local lightweight aggregate," in *MATEC Web of Conferences*, EDP Sciences, 2018. doi: 10.1051/matecconf/201816202024.

[105] S. N. Sarmin, S. F. Mhd Ramle, M. H. Mohamad Amini, and N. Salim, "The Influence of Curing Conditions on the Compressive Strength of Lightweight Geopolymer Composite Containing Wood Aggregates," in *Regional Conference on Science, Technology and Social Sciences (RCSTSS 2016)*, Springer Singapore, pp. 727–737, 2018.

[106] D. M. A. Huiskes, A. Keulen, Q. L. Yu, and H. J. H. Brouwers, "Design and performance evaluation of ultra-lightweight geopolymer concrete," *Mater Des*, vol. 89, pp. 516–526, Jan. 2016, doi: 10.1016/j.matdes.2015.09.167.

[107] M. Y. J. Liu, U. J. Alengaram, M. Z. Jumaat, and K. H. Mo, "Evaluation of thermal conductivity, mechanical and transport properties of lightweight aggregate foamed geopolymer concrete," *Energy Build*, vol. 72, pp. 238–245, 2014, doi: 10.1016/j.enbuild.2013.12.029.

[108] H. Shu-guan, W. Jing, Y. Wen, H. Yong-jia, W. Fa-zhou, D. Qing-jun, "Preparation and properties of geopolymer-lightweight aggregate refractory concrete," *J. Cent. South Univ. Technol*, vol. 16, 2009, doi: 10.1007/s11771−009−0152−x.

[109] Y. Liao and C. Huang, "Effects of heat treatment on the physical properties of lightweight aggregate from water reservoir sediment," vol. 37, pp. 3723–3730, 2011, doi:10.1016/j.ceramint.2011.04.122.

[110] C. Yang, C. Cui, and J. Qin, "Recycling of low-silicon iron tailings in the production of lightweight aggregates," *Ceram Int*, vol. 41, no. 1, pp. 1213–1221, 2015, doi:10.1016/j.ceramint.2014.09.050.

[111] Y. Li, D. Wu, J. Zhang, L. Chang, and D. Wu, "Measurement and statistics of single pellet mechanical strength of differently shaped catalysts," *Powder Technology*, vol. 133, pp. 176–184, 2000.

[112] Y. Hiramatsu, Y. Oka, "Determination of the tensile strength of rock by a compression test of an irregular test piece," *International Journal of Rock Mechanics and Mining Sciences & Geomechanics Abstracts,* vol. 3, pp 89-90,1966, doi:10.1016/0148-9062(66)90002-7

[113] EN 12457 -3, "Standard test for characterization of waste leaching compliance test for leaching of granular waste materials and sludges",2004.

[114] ASTM D7984-16, "Standard Test Method for Measurement of Thermal Effusivity of Fabrics Using a Modified Transient Plane Source (MTPS) Instrument 1", doi: 10.1520/D7984-16.

[115] J. E. Martínez-Martínez, F. P. Álvarez Rabanal, M. Lázaro, M. Alonso-Martínez, D. Alvear, and J. J. Del Coz-Díaz, "Assessment of lightweight concrete thermal properties at elevated temperatures," *Applied Sciences (Switzerland)*, vol. 11, no. 21, Nov. 2021, doi:10.3390/app112110023.

[116] A. S. Sarah, R. Géber, A. Simon, E. Kurovics, and A. Hamza, "Comparative study of metakaolin-based geopolymer characteristics utilizing different dosages of water glass in the activator solution," *Results in Engineering*, vol. 20, no. September, 2023, doi:10.1016/j.rineng.2023.101469.

[117]   ASTM C642-06, "Standard test method for density, absorption, and voids in hardened concrete," *ASTM International*, no. March, pp. 11–13, 2006, doi: 10.1520/C0642-13.5.

[118]   ASTM C1241-14, "Standard Test Method for Volume Shrinkage of Latex Sealants During Cure 1," *ASTM International,*2022.

[119]   ASTM C109/C109M-02, "Standard Test Method for Compressive Strength of Hydraulic Cement Mortars," *Annual Book of ASTM Standards*, vol. 04, p. 9, 2020.

[120]   Y. Wang Y. Wang, X. Liu, W. Zhang, Z. Li, Y. Zhang, Y. Li, and Y. Ren, "Effects of Si/Al ratio on the efflorescence and properties of fly ash based geopolymer," *J Clean Prod*, vol. 244, 2020, doi: 10.1016/j.jclepro.2019.118852.

[121]   X. Xue, Y. L. Liu, J. G. Dai, C. S. Poon, W. D. Zhang, and P. Zhang, "Inhibiting efflorescence formation on fly ash–based geopolymer via silane surface modification," *Cem Concr Compos*, vol. 94 , pp. 43–52, 2018, doi: 10.1016/j.cemconcomp.2018.08.013.

[122]   EN 196-3:2005, Methods of Testing Cement – Part 3: Determination of Setting Times and Soundness, CEN, 2005.

[123]   J. Frost, "Regression Analysis: An Intuitive Guide for Using and Interpreting Linear Models," 2019.

[124]   S. Pilehvar*,* A.M. Szczotok, J. F. Rodríguez, L.Valentini, M. Lanzón, R. Pamies, and A. Kjøniksen, "Effect of freeze-thaw cycles on the mechanical behavior of geopolymer concrete and Portland cement concrete containing micro-encapsulated phase change materials," *Constr Build Mater*, vol. 200, pp. 94–103, 2019, doi: 10.1016/j.conbuildmat.2018.12.057.

[125]   Y. Min, J. Wu, B. Li, M. Zhang, and J. Zhang, "Experimental study of freeze–thaw resistance of a one-part geopolymer paste," *Case Studies in Construction Materials*, vol. 17, 2022, doi:10.1016/j.cscm.2022.e01269.

[126]   B. M. Taheri, A. M. Ramezanianpour, S. Sabokpa, and M. Gapele, "Experimental evaluation of freeze-thaw durability of pervious concrete," *Journal of Building Engineering*, vol. 33, Jan. 2021, doi: 10.1016/j.jobe.2020.101617.

[127]   H. Nazarpour and M. Jamali, "Mechanical and freezing cycles properties of geopolymer concrete with recycled aggregate", *Structural Concrete: Journal of the fib*, Vol. 21, No. 3, pp 1004-1012, 2020, doi.org/10.1002/suco.201900317.

[128]   B. Girts, D. Bajare, A. Korjakins, and D. Vaičiukynienė, "Sulfate and Freeze-Thaw Resistance of Porous Geopolymer Based on Waste Clay and Aluminium Salt Slag", *Minerals,* vol. 12, 2022, doi.org/10.3390/min12091140

[129]   J. T. Ding and Z. Li, "Effects of metakaolin and silica fume on properties of concrete," *ACI Mater J*, vol. 99, no. 4, pp. 393–398, 2002, doi: 10.14359/12222.

[130]   V. Guder and S. Senturk Dalgic, "Thermodynamic properties of potassium oxide (K2O) nanoparticles by molecular dynamics simulations," *Acta Phys Pol A*, vol. 131, no. 3, pp. 490–494, 2017, doi: 10.12693/APhysPolA.131.490.

[131]   M. M. Abdelfattah, R. Géber, and I. Kocserha, "Enhancing the properties of lightweight aggregates using volcanic rock additive materials", *Journal of Building Engineering,* vol. 63, 2023, doi: 10.1016/j.jobe.2022.105426.

[132]   A. Baba and A. Kaya, "Leaching characteristics of solid wastes from thermal power plants of western Turkey and comparison of toxicity methodologies," *J Environ Manage*, vol. 73, no. 3, pp. 199–207, 2004, doi: 10.1016/j.jenvman.2004.06.005.

[133] M. U. Kankia, L. Baloo, B. S. Mohammed, S. B. Hassan, E. A. Ishak, and Z. U. Zango, "Review of petroleum sludge thermal treatment and utilization of ash as a construction material, a way to environmental sustainability," *International Journal of Advanced and Applied Sciences*, vol. 7, no. 12, pp. 68–81, 2020, doi: 10.21833/ijaas.2020.12.008.

[134] B. Hu, S. Zhao, and S. Zhang, "Removal of Lead from Cathode Ray Tube Funnel Glass by Generating Sodium Silicate." *Journal of the Air & Waste Management Association*, vol. 1,pp. 106–14, 2014, doi:10.1080/10962247.2014.976721.

[135] T. Bristogianni, F. Oikonomopoulou, C. J. De Lima, F. A. Veer, and R. Nijsse, "Structural cast glass components manufactured from waste glass: Diverting everyday discarded glass from the landfill to the building industry," *Heron*, vol. 63, no. 1–2, pp. 57–102, 2018.

[136] M. Sassi, A. Simon, S. Fuhrmann, S. A. H. Sander, and R. Szabó, "Effect of microstructure on the physicochemical characteristics of foam glass made by soda lime -CRT glasses and aluminium dross," *Ceram Int*, vol. 51, pp. 37085-37095, 2024, doi:10.1016/j.ceramint.2024.07.098.

[137] A.-S. S. K. Mohammed, A. Simon, and R. Géber, "Preparation and characterization of foam glass from soda lime silicate glass waste by using different dosages of limestone," *Multidiszciplináris tudományok*, vol. 12, no. 4, pp. 189–197, 2022, doi:10.35925/j.multi.2022.4.20.

[138] M. Sassi and A. Simon, "Waste-to-reuse foam glasses produced from soda-lime-silicate glass, cathode ray tube glass, and aluminium dross," *Inorganics (Basel)*, vol. 10, no. 1, 2022, doi:10.3390/inorganics10010001.

[139] M. Osfouri and A. Simon, "Study on the thermal conductivity and density of foam glass," *Pollack Periodica*, vol. 18, no. 1, pp. 126–131, Mar. 2023, doi: 10.1556/606.2022.00591.

[140] Z. Chen, H. Wang, R. Ji, L. Liu, C. Cheeseman, and X. Wang, "Reuse of mineral wool waste and recycled glass in ceramic foams," *Ceram Int*, vol. 45, no. 12, pp. 15057–15064, 2019, doi:10.1016/j.ceramint.2019.04.242.

[141] D. Wattanasiriwech, S. Nontachit, P. Manomaivibool, and S. Wattanasiriwech, "Foam glass from municipal waste as a lightweight aggregate for cement mortar," in *IOP Conference Series: Earth and Environmental Science*, Institute of Physics Publishing, 2019. doi: 10.1088/1755-1315/351/1/012008.

[142] M. Zhu, R. Ji, Z. Li, H. Wang, L. L. Liu, and Z. Zhang, "Preparation of glass ceramic foams for thermal insulation applications from coal fly ash and waste glass," *Constr Build Mater*, vol. 112, pp. 398–405, 2016, doi: 10.1016/j.conbuildmat.2016.02.183.

[143] A. Lopes, S. Lopes, and I. Pinto, "Influence of Curing Temperature on the Strength of a Metakaolin-Based Geopolymer" *Materials* 16, no. 23: 7460, 2023, doi:10.3390/ma16237460.

[144] Z. Yunsheng, J. Yantao, W. Sun, and L. Zongjin, "Study of ion cluster reorientation process of geopolymerisation reaction using semi-empirical AM1 calculations," *Cem Concr Res*, vol. 39, no. 12, pp. 1174–1179, 2009, doi: 10.1016/j.cemconres.2009.07.022.

[145] P. Rovnaník, "Effect of curing temperature on the development of hard structure of metakaolin-based geopolymer," *Constr Build Mater*, vol. 24, no. 7, pp. 1176–1183, 2010, doi:10.1016/j.conbuildmat.2009.12.023.

[146] I. Elkhadiri, M. Elkhadiri, and F. Puertas, "Effect of curing temperature on cement hydration," *Ceramics - Silikaty*, vol. 53, no. 2, pp. 65–75, 2009.

[147] H. Xu and J. S. J. Van Deventer, "The geopolymerisation of alumino-silicate minerals," *Int J Miner Process*, vol. 59, no. 3, pp. 247–266, 2000, doi: 10.1016/S0301-7516(99)00074-5.

[148] H. Castillo, H. Collado, T. Droguett, S. Sánchez, M. Vesely, P. Garrido, and S. Palma, "Factors affecting the compressive strength of geopolymers: A review," *Minerals*, vol. 11, 2021, doi:10.3390/min11121317.

[149] Z. Li, S. Zhang, Y. Zuo, W. Chen, and G. Ye, "Chemical deformation of metakaolin based geopolymer," *Cem Concr Res*, vol. 120, no. March, pp. 108–118, 2019, doi:10.1016/j.cemconres.2019.03.017.

[150] A. M. Mustafa Al Bakria, H. Kamarudin, M. Bin Hussain, I. Khairul Nizar, Y. Zarina, and A. R. Rafiza, "The effect of curing temperature on physical and chemical properties of geopolymers," *Phys Procedia*, vol. 22, pp. 286–291, 2011, doi: 10.1016/j.phpro.2011.11.045.

[151] A. Kar, "Characterizations of concretes with alkali-activated binder and correlating their properties from micro- to specimen level," *Graduate Theses, Dissertations, and Problem Reports*, 2013.

[152] M. Ivanović, S. Nenadović, V. P. Pavlović, I. Radović, M.Kijevčanin, V. B. Pavlović, and L. Kljajević1, "The Influence Of Thermodynamic Parameters On Alkaline Activators Of Geopolymers And The Structure Of Geopolymers," *Macedonian Journal of Chemistry and Chemical Engineering*, vol. 40, no. 1, pp. 107–117, 2021, doi: 10.20450/MJCCE.2021.2127.

[153] C. Karlsson, E. Zanghellini, J. Swenson, B. Roling, D. T. Bowron, and L. Börjesson, "Structure of mixed alkali/alkaline-earth silicate glasses from neutron diffraction and vibrational spectroscopy," *Phys Rev B Condens Matter Mater Phys*, vol. 72, no. 6, 2005, doi:10.1103/PhysRevB.72.064206.

[154] A. Fernández-Jiménez and A. Palomo, "Mid-infrared spectroscopic studies of alkali-activated fly ash structure," *Microporous and Mesoporous Materials*, vol. 86, no. 1–3, pp. 207–214, 2005, doi: 10.1016/j.micromeso.2005.05.057.

[155] H. Ashfaq, M. B. Sharif, M. I. Hassan, U. Sahar, U. Akmal, and A. Mohamed, "Up-scaling of fly ash-based geopolymer concrete to investigate the binary effect of locally available metakaolin with fly ash" , *Heliyon*, vol. 10, 2024, doi:10.1016/j.heliyon.2024.e26331

[156] M. Kaya, "The effect of micro-SiO_2 and micro-Al_2O_3 additive on the strength properties of ceramic powder-based geopolymer pastes," *J Mater Cycles Waste Manag*, vol. 24, no. 1, pp. 333–350, 2022, doi: 10.1007/s10163-021-01323-3.

[157] B. Kim and S. Lee, "Review on characteristics of metakaolin-based geopolymer and fast setting," *Journal of the Korean Ceramic Society*, vol. 57, no. 4, pp. 368–377, 2020, doi:10.1007/s43207-020-00043-y.

[158] S. Chandrasekhar and P. N. Pramada, "Microwave assisted synthesis of zeolite A from metakaolin," *Microporous and Mesoporous Materials*, vol. 108, no. 1–3, pp. 152–161, 2008, doi: 10.1016/j.micromeso.2007.04.003.

[159] A.M. Neville, "Concrete Technology," 2nd Edition, Pearson Education Ltd., London, 2010.

[160] P. J. Wibawa, M. Nur, M. Asy'Ari, H. Nur, M. A. Agam, and H. Saim, "Study on the ion-exchange properties of the activated carbon black nanoparticles of ACBNPs20-17 code using sodium hydroxide solution," *AIP Conf Proc*, vol. 2237, 2020, doi: 10.1063/5.0005234.

[161] N. A. Jaya, L. Yun-Ming, M. M. A. B. Abdullah, H. Cheng-Yong, and K. Hussin, "Effect of Sodium Hydroxide Molarity on Physical, Mechanical and Thermal Conductivity of Metakaolin

Geopolymers," *IOP Conf Ser Mater Sci Eng*, vol. 343, no. 1, 2018, doi: 10.1088/1757-899X/343/1/012015.

[162] W. Wongkeo, S. Seekaew, and O. Kaewrahan, "Properties of high calcium fly ash geopolymer lightweight concrete," *Mater Today Proc*, vol. 17, pp. 1423–1430, 2019, doi: 10.1016/j.matpr.2019.06.163.

[163] L. Jamaludin, R. A. Razak, M. M. Abdullah, P. Vizureanu, A. V. Sandu, S. Z. Abd Rahim, and R. Ahmad "Solid-to-Liquid Ratio Influenced on Adhesion Strength of Metakaolin Geopolymer Coating Paste Added Photocatalyst Materials," *Coatings*, vol. 13, no. 2, 2023, doi: 10.3390/coatings13020236.

[164] W. M. W. Ibrahim, R. Ahmad, B. T. Coman, M. M. A. B. Abdullah, A. Puskas, and V. S. Jaganathan, "The Effects of Solid to Liquid Ratio on Fly Ash Based Lightweight Geopolymer," *IOP Conf Ser Mater Sci Eng*, vol. 877, no. 1, 2020, doi: 10.1088/1757-899X/877/1/012013.

[165] R. Mohamed, R. Abd Razak, M. Mustafa Al Bakri Abdullah, R. Khimi Shuib, N. Aida Mohd Mortar, and W. Wazien Ahmad Zailani, "Investigation of Heat Released during Geopolymerization with Fly Ash based Geopolymer," *IOP Conf Ser Mater Sci Eng*, vol. 551, no. 1, 2019, doi: 10.1088/1757-899X/551/1/012093.

[166] B. B. Kenne Diffo, A. Elimbi, M. Cyr, J. Dika Manga, and H. Tchakoute Kouamo, "Effect of the rate of calcination of kaolin on the properties of metakaolin-based geopolymers," *Journal of Asian Ceramic Societies*, vol. 3, no. 1, pp. 130–138, 2015, doi: 10.1016/j.jascer.2014.12.003.

[167] A. M. Rashad and M. Gharieb, "Valorization of sugar beet waste as an additive for fly ash geopolymer cement cured at room temperature," *Journal of Building Engineering*, vol. 44, no. July, p. 102989, 2021, doi: 10.1016/j.jobe.2021.102989.

[168] T. S. B. A. Manan, N. L. M. Kamal, S. Beddu, T. Khan, *et al.*, "Strength enhancement of concrete using incinerated agricultural waste as supplementary cement materials," *Sci Rep*, vol. 11, no. 1, Dec. 2021, doi: 10.1038/s41598-021-92017-1.

[169] F. Li, Q. Zhao, L. Chen, and G. Shao, "Experimental and theoretical research on the compression performance of CFRP sheet confined GFRP short pipe," *The Scientific World Journal*, 2014, doi: 10.1155/2014/109692.

[170] ASTM C330-04, "Standard Specification for Lightweight Aggregates for Structural Concrete," *ASTM International*, vol. 552, no. 18, p. 4, 2009.

[171] S. Fatimah Azzahran Abdullah, L. Yun-Ming, M. Mustafa Al Bakri Abdullah, H. Cheng-Yong, and K. Zulkifly, "Mechanical Properties and Thermal Conductivity of Lightweight Foamed Geopolymer Concretes," in *IOP Conference Series: Materials Science and Engineering*, Institute of Physics Publishing, 2019. doi: 10.1088/1757-899X/551/1/012089.

[172] S. Tiyasangthong, P. Yoosuk, K. Krosoongnern, B. Krittacom, P. Nachaisit, and C. Suksiripattanapong, "Unit Weight, Strengths and Thermal Conductivity of Cellular Lightweight Fly Ash Geopolymer Mortar Reinforced with Polyvinyl Alcohol," *Civil Engineering and Architecture*, vol. 10, no. 7, pp. 2943–2952, 2022, doi:10.13189/cea.2022.100713.

[173] T. Tracz and Ś. Jacek, "Effect of cement paste content and w/c ratio on concrete water Absorption," *Cement Wapno Beton*, vol .17(3), pp. 131-137, 2012.

[174] G. L. Golewski, "Assessing of water absorption on concrete composites containing fly ash up to 30 % in regards to structures completely immersed in water," *Case Studies in Construction Materials*, vol. 19, 2023, doi: 10.1016/j.cscm.2023.e02337.

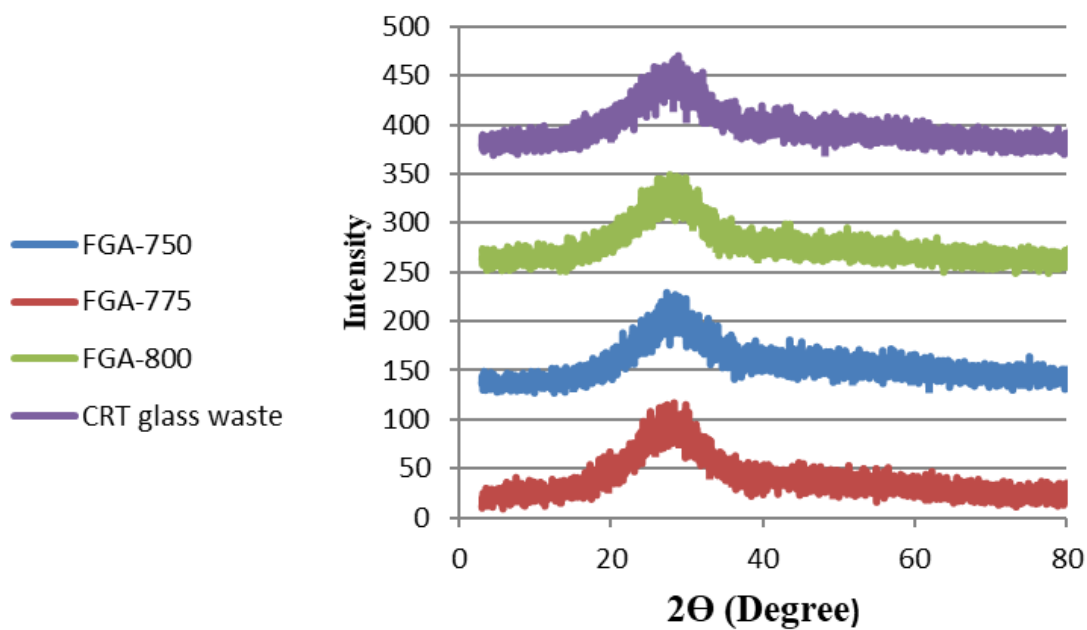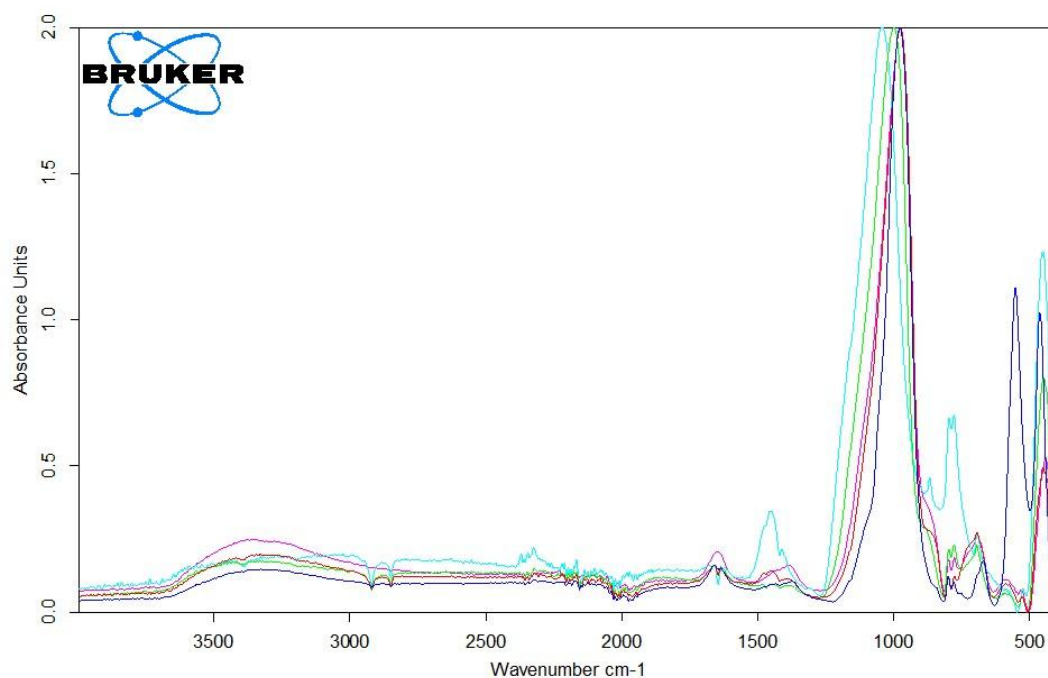**Figure.** X-ray diffraction of CRT glass waste and foam glass aggregate sintered at temperatures 750° C, 775° C, and 800° C.

D:\ftir_ADATOK\Sarah\2023marcius\0waterglass.0	0waterglass	Instrument type and / or accessory	2023.03.13
D:\ftir_ADATOK\Sarah\2023marcius\25waterglass.0	25waterglass	Instrument type and / or accessory	2023.03.13
D:\ftir_ADATOK\Sarah\2023marcius\75waterglass.0	75waterglass	Instrument type and / or accessory	2023.03.13
D:\ftir_ADATOK\Sarah\2023marcius\100waterglass.0	100waterglass	Instrument type and / or accessory	2023.03.13
D:\ftir_ADATOK\Sarah\MKGP60.0	MKGP60	Instrument type and / or accessory	2022.11.30

Figure. FTIR spectra of MK-GP cured at 60 °C with different water glass dosages of activator solution

Particle Size Measurement

CILAS 715

QUANTACHROME CILAS

Material : #1
Comment : MEKA metakaolin milled
Suspension fluid : water
Wetting agent : sodium-tripoliphosphate
Ultrasonic : 60 sec
Concentration : 72
Operator : GR
Company : Quantachrome GmbH
City : D-85235 Odelzhausen
Date : 05.03.2023 10:30:48
File name : C:\CILAS\MEKAMK1
Surface area : 1.61 m2/cm3
(spherical shape assumed)

C/%	10.00	50.00	90.00
D/µm	1.60	5.46	70.85

D/µm	0.70	0.90	1.00	1.40	1.70	2.00	2.60	3.20
C/%	4.21	5.21	5.70	8.00	11.43	16.30	26.10	31.73
H/%	4.21	1.01	0.49	2.30	3.43	4.87	9.80	5.62

D/µm	4.00	5.00	6.00	8.00	10.00	12.00	15.00	18.00
C/%	36.50	46.25	52.70	56.20	64.18	68.20	68.20	69.61
H/%	4.77	9.75	6.45	3.50	7.98	4.02	0.00	1.41

D/µm	23.00	30.00	36.00	45.00	56.00	70.00	90.00	110.00
C/%	74.77	75.00	76.40	82.28	84.80	89.38	99.76	100.00
H/%	5.16	0.23	1.40	5.89	2.51	4.58	10.38	0.24

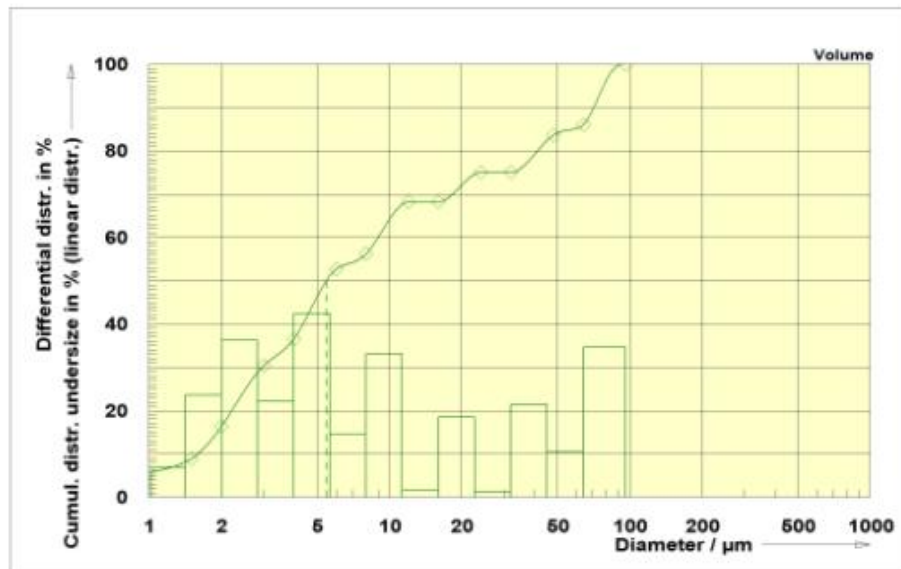| D/µm	135.00	165.00	210.00	260.00	320.00	400.00
C/%	100.00	100.00	100.00	100.00	100.00	100.00
H/%	0.00	0.00	0.00	0.00	0.00	0.00

C: Cumulative, H: Histogram

Figure. Particle size distribution results of metakaolin.

Material	: waste glass powder average
Comment	: waste glass powder average
Suspension fluid	: water
Wetting agent	: Sodium-tripolyphosphate
Ultrasonic	: 120 sec
Concentration	: 27
Operator	: GR
Company	: Quantachrome GmbH
City	: D-85235 Odelzhausen
Date	: 06.04.2022 10:17:29
File name	: C:\CILAS\WAGLASSA
Surface area	: 0.62 m2/cm3
(spherical shape assumed)	

C/%	10.00	50.00	90.00
D/µm	3.85	34.32	78.15

D/µm	0.70	0.90	1.00	1.40	1.70	2.00	2.60	3.20
C/%	1.25	1.52	1.65	2.42	3.58	5.05	7.85	9.32
H/%	1.25	0.27	0.13	0.77	1.16	1.47	2.80	1.46

D/µm	4.00	5.00	6.00	8.00	10.00	12.00	15.00	18.00
C/%	10.25	13.28	15.85	17.55	21.47	24.90	26.79	31.06
H/%	0.93	3.03	2.57	1.70	3.92	3.43	1.89	4.27

D/µm	23.00	30.00	36.00	45.00	56.00	70.00	90.00	110.00
C/%	40.68	45.15	53.00	67.73	70.72	77.99	99.49	100.00
H/%	9.63	4.46	7.85	14.73	2.99	7.28	21.50	0.51

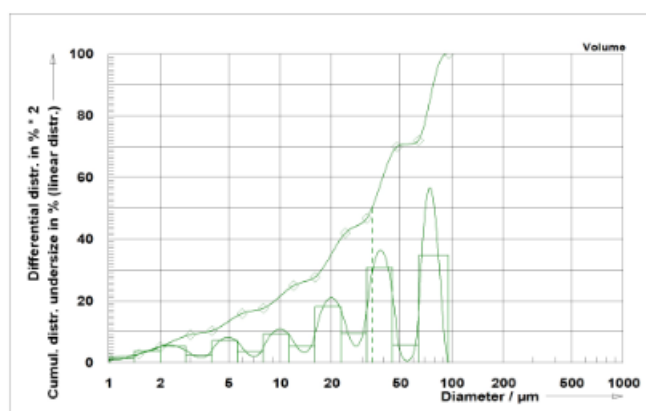| D/µm	135.00	165.00	210.00	260.00	320.00	400.00
C/%	100.00	100.00	100.00	100.00	100.00	100.00
H/%	0.00	0.00	0.00	0.00	0.00	0.00

C: Cumulative, H: Histogram

Figure. Particle size distribution results of CRT glass waste.